Towards an Understanding behind Adsorptive and Extractive Desulfurization of Liquid Fuels with Carbon-Based Adsorbents and Deep Eutectic Solvents

Thesis submitted in partial fulfilment

for the Award of Degree

Doctor of Philosophy

by

Divyam Jha

Chemical Engineering & Engineering Sciences

RAJIV GANDHI INSTITUTE OF PETROLEUM TECHNOLOGY

JAIS – 229304

PCH15001 2020

CERTIFICATE

It is certified that the work contained in the thesis titled "**Towards an understanding behind adsorptive and extractive desulfurization of liquid fuels with carbon-based adsorbents and Deep Eutectic Solvents**" by **Divyam Jha** has been carried out under my supervision and this work has not been submitted elsewhere for a degree.

It is further certified that the student has fulfilled all the requirements of Comprehensive, Candidacy and SOTA.

Dr. M.S. Balathanigaimani

Signature: Supervisor

DECLARATION BY THE CANDIDATE

I, **Divyam Jha**, certify that the work embodied in this thesis is my own bona-fidework and carried out by me under the supervision of "**Dr. M.S. Balathanigaimani**" from August 2015 to October 2020 at the "Department of Chemical Engineering & Engineering Sciences", Rajiv Gandhi Institute of Petroleum Technology, Jais. The matter embodied in this thesis has not been submitted for the award of any other degree. I declare that I have faithfully acknowledged and given credits to the research workers wherever their works have been cited in my work in this thesis. I further declare that I have not wilfully copied any other's work, paragraphs, text, data, results, etc., reported in journals, books, magazines, reports dissertations, theses, etc., or available at websites and have not included them in this thesis and have not cited as my own work.

Divyam Jha

Date:

Place:

CERTIFICATE BY THE SUPERVISOR

It is certified that the above statement made by the student is correct to the best of my/our knowledge.

Dr. M.S. Balathanigaimani

Supervisor

Dr. Amit Ranjan

Head of Department

Chemical Engineering & Engineering Sciences

CERTIFICATE

It is to certify that the work contained in the thesis titled "**Towards an understanding behind adsorptive and extractive desulfurization of liquid fuels with carbon-based adsorbents and Deep Eutectic Solvents**" by Ms. **Divyam Jha** has been carried out under my supervision. It is also certified that he fulfilled the mandatory requirement of TWO quality publications arose out of his/her thesis work.

It is further certified that the publications (copies enclosed) of the aforesaid Ms. Divyam Jha have been published in the Journals indexed by –

(a) SCI

(b) SCI Extended

(c) SCOPUS

Supervisor	**Head of Department**	**Convenor, DPGC**
Dr. M.S. Balathanigaimani	Dr. Amit Ranjan	Dr. Milan Kumar

COPYRIGHT TRANSFER CERTIFICATE

Title of the Thesis: Towards an understanding behind adsorptive and extractive desulfurization of liquid fuels with carbon-based adsorbents and Deep Eutectic Solvents.

Name of the Student: Divyam Jha

Copyright Transfer

The undersigned hereby assigns to the Rajiv Gandhi Institute of Petroleum Technology Jais all rights under copyright that may exist in and for the above thesis submitted for the award of the "Doctor of Philosophy ".

Note: However, the author may reproduce or authorize others to reproduce material extracted verbatim from the thesis or derivative of the thesis for the author's personal use provided that the source and the Institute's copyright notice are indicated.

Divyam Jha

Date:

Place:

Acknowledgment

Creating a Ph.D. is not an individual experience rather it takes place in a social context and includes several, whom I would like to thank sincerely.

First and foremost I would like to express my profound gratitude to my Ph.D. advisor Dr. M.S. Balathanigaimani. It has been an honour to be his first Ph.D. student. I appreciate all his contributions of time, ideas, and funding to make my Ph.D. experience productive and stimulating. He has supported me not only by providing a research assistantship over years, but also academically and emotionally through the rough road to finish this thesis.

I would like to express my heartfelt gratitude to Dr. Rakesh Kumar. He has always been needful support for me to complete my Ph.D. He was there when there was the requirement of apparatus, funds and every possible effort he could have lend to me. He has always been a great mentor in many ways.

I will forever be thankful to Dr. U. P. Ojha. He has always shown the path for productive research. He guided me to differentiate between hard and smart work. He always put up valuable comments on my work and was always ready to clear my doubts. The joy and enthusiasm he has for his research were contagious and motivational for me, even during tough times in the Ph.D. pursuit.

I extend my heartfelt thanks to Dr. Amit Ranjan and Dr. Milan Kumar for supporting my work and improving my thermodynamics and process optimization history and being part of my Generals committee, a thesis reader, and an inspiration in many ways.

A Special mention goes Dr. U.P Ojha's group (Suman, Shubhankar, and Dr. Ujjwal), who helped me in the FTIR and HNMR analysis. I thank Dr. Tushar Sharma and his team (Ravi

Shankar, Ramesh Narukulla, and Krishna R Chaturvedi) for helping me to examine the viscosity and insightful discussion.

The members of the Green Separation lab have contributed immensely to my personal and professional time at Rajiv Gandhi Institute of Petroleum Technology. The group has been a source of friendships as well as good advice and collaboration. I am especially grateful for the fun group of original Green lab group members Belal, Komal, Uttam, Matamani, Manas, Vikrant who stuck it out in graduate school with me.

Besides, I would also like to thank Md. Belal Haider, who has extended the full help and co-operation. I am indebted to him who did his best to bring improvements through his helpful discussion and valuable suggestions during my research work.

The best outcome of the journey is finding new friends Somendra, Praveen, Mukkarum, Vivek, Bijoy,and Ankit for providing support. The small talks over the food table and on tea break after exhausting work are always memorable. The small breaks and discussion really charged me to work further efficiently. I am grateful to Dr. Shama Perveen and Dr. R.R. Ujjwal, my seniors, who are constantly supporting me with their motivation and guidance.

Without the company and assistance provided by Mr. Sudhir Arrora, Mr. Amit Bajpai, and Rakesh Singh, who regularly supported me in getting timely chemicals, instruments, and equipment for my research work, the PhD thesis would not have been possible. I would also like to thank Mr. T. P. Joshi, for getting academic assistance. I highly appreciate the support that Mr. Anil Verma, Lokesh Bhatnagar, and Ashwini Chaudhary have earned.

I also thank the outstanding workers Arun Kumar, Ashok Kumar in the Department of Chemical engineering as well as in other Departments for being so supportive and polite at all times.

My time at RGIPT was made enjoyable in large part due to the many friends and groups that became a part of my life. I am grateful for the time spent with roommates and friends, I finished up my degree, and collected many other people and memories.

Also, I would like to thank God and my family for all their love and encouragement. For my parents who raised me with love and supported me in all my pursuits. And most of all for my loving, supportive, encouraging, and patient husband Piyush whose faithful support and calmness during the entire journey and final stages of this Ph.D. is so appreciated. Thank you.

Divyam Jha

Rajiv Gandhi Institute of Petroleum Technology,

December 2020

Contents

List of Tables

List of Figures

Preface

The drive to reduce refractory sulfur compounds from liquid fuels as well as increased awareness of the environmental impacts of gas emissions, has led the chemicals industry to seek to find the alternatives for desulfurization apart from Hydrodesulphurization (HDS) and improve energy efficiency. The thesis work presents the desulfurization of refractory sulfur compounds in liquid fuels in general, and to investigate the desulfurization of Dibenzothiophene (DBT), 2- Methylthiophene, and Thiophene in diesel by batch adsorption, continuous adsorption, and extraction in particular. In addition, the strict implementations of the European emission standard due to the increasing effect of sulfur emission on our environment and human health has been presented.

Hydrodesulphurization (HDS) is widely used for removal of carcinogenic compounds from the fuel oil. However, less reactive refractory compounds such as Dibenzothiophene (DBT) and some alkyl DBTs as 4, 6-Dimethyldibenzothiophene (4, 6-DMDBT) are not easily removable by hydrodesulphurization (HDS) process due to steric hindrance, which causes sulfur reduction up to a certain limit. The production of ultra-low sulfur diesel (ULSD) consumes large quantity of hydrogen and requires severe operating condition. Therefore, several other methodologies have been employed such as Adsorption, bio desulfurization and Extraction etc.

The desulfurization process widely utilizes carbon material as an efficient adsorbent. For the same Microwave synthesized carbon nanotube (M-CNT), and carbon nanofiber (M-CNF) were tested for removal of Dibenzothiophene (DBT) from a model diesel fuel (MDF) by adsorption process. M-CNT showed relatively higher DBT removal capacity over M-CNF and followed Sips isotherm models in the adsorption equilibrium experimental of DBT on M-CNT and M-

CNF. The adsorption process was found out to be spontaneous, exothermic nature, and showed non-random behavior of DBT molecule on M-CNT.

The different carbon material shows different physical behavior and also, the textural properties. These properties of the carbon material highly dominate the behavior of the adsorption process. Thus carbon adsorbents like Mongolian anthracite-based porous activated carbons (PMACs) that possess much higher surface area and pore volume than M-CNT and M-CNF have been considered for further study. The maximum DBT adsorption by PMAC 1/3 and PMAC 1/4 was 99.7% and 95.7 % by varying the adsorbent dosage. The experimental adsorption isotherm results were well represented by the Sips isotherm for PMAC 1/3 and the Dual Site Langmuir isotherm for PMAC 1/4, respectively. The kinetics for the adsorption of DBT on PMACs follows the pseudo-second-order behavior and both surface and pore diffusions control the adsorption .The studied process is spontaneous, exothermic, and possess less randomness at the interface and the designing of the batch-adsorber was done for the adsorption of DBT onto PMAC 1/3.

In previous chapters, four carbon materials named as M-CNT, M-CNF, PMAC 1/3, and PMAC 1/4 have been studied in the batch process. Therefore, due to the significant and comparable adsorption capacity of GNP and PMACs, GNP has been further used to see the adsorption behavior of the system in continuous experiments for multicomponent feed. The single component adsorption isothermal experimental results for batch process were well represented by the Freundlich isotherm (Thiophene (T), 2-Methylthiophene (2-MT)) and the Langmuir isotherm (Dibenzothiophene (DBT)) models. The adsorption process kinetics fits with the pseudo second order model for T, 2-MT and DBT on GNP. A process design of single-stage batch-adsorber for the adsorption of T, 2-MT & DBT onto GNP was also studied using the

calculated adsorption isotherm parameters. In addition, a fixed-bed adsorber was used for studying the continuous system at ambient conditions for multicomponent MDFs. The effect of flow rate, bed height, and initial sulfur concentration on the adsorptive capacity of the adsorbent for T, 2-MT, and DBT were evaluated. The Adam-Bohart model was used to check the performance of the adsorption breakthrough curves.

Further to achieve the thio-selectivity in the process the extractive desulfurization (EDS) has been adopted for further studies. Although, Adsorptive desulfurization has shown prominent potential for significant desulfurization of liquid fuels. The Deep Eutectic Solvents (DESs) have been utilized for sulfur extraction of organo-sulfur compounds and for the same three different DESs were prepared using a common hydrogen bond donor (HBDs), Diglycol, and different hydrogen bond acceptors (HBAs). The sulfur removal varies by changing the experiment variables such as temperature, DESs/feed ratio, and the time on desulfurization efficiency. The DBT has higher extraction efficiency as compare to 2-MT and T. Further, a non-random two liquids (NRTL) thermodynamic model was employed to model liquid-liquid equilibrium.

Chapter 1

Introduction

1.1 Desulfurization of liquid fuels

It has been recognized that petroleum products must meet lower limits of contaminants such as sulfur and nitrogen due to environmental concerns and human health effects [1,2]. Very stringent regulations are required essentially for the complete removal of sulfur from liquid hydrocarbons that are used in transportation fuels, such as gasoline and diesel. European emission standards have been made and followed to control the various pollutants in general [3,4].

All Emission Standards have been proposed and implemented to protect environmental and human living conditions. Due to increasing toxic components in the environment by burning of carcinogenic compounds like sulfur, nitrogen, metals and some aromatic and refractory components from automobile and industrial factories which cause the acid rain when coming in the contact and react with present air near ozone layer. Sulfur 'S' present in the petroleum liquid fuels reacts with oxygen, forming SOx after reacting with water, ultrafine droplets of H_2SO_4 form that can easily penetrate in the lungs of the human body[5]. Second-hand pollution is becoming a detrimental reason for human health, including mortality, exacerbation of asthma, cardiovascular effects, chronic bronchitis, respiratory tract infections, ischemic heart disease, and stroke are the severe results. Recently it has been found that the ultrafine particle (UFP) in second hand smoke (SHS) and traffic related air pollution may elicit the chronic

effects on human health and concluded the rate of being asthmatic was 24.4% and 14.2% respectively for overweight and normal-weight children. Urbanization is found the reason for increasing pollution as the rural area people migrate from rural to the urban area, therefore increasing transportation facilities and fuel consumption and more pollution production.

Diesel is the most consumed fuel nowadays and it is the main reason for the highest particulate emission in the environment. The complete combustion of diesel produces water and carbon dioxide, but in the engine due to incomplete combustion, many gases are produced as oxides and aldehydes and submicron soot particles (black carbon) that adversely affect the respiratory system of the human body [6–9].

Hydrodesulfurization process is a conventional process used for the desulfurization of heavy refractory sulfur compounds but requires severe conditions such as high pressure (3–7 MPa), high temperature (320–380°C), and hydrogen. Also, HDS is not very effective in removing heavy refractory compounds such as sulfur species (benzothiophene) and their derivatives due to steric hindrance[10]**.** In most cases, the conventional HDS process is not the only method to decrease the sulfur content in the liquid fuels to less than the Euro 6 regulatory limit, which is less than 10 ppm. Various alternative methods need to be explored[11] due to few limitations of HDS, such as oxidative desulfurization (ODS)[12–15]**,** bio desulfurization (BDS)[16–18]**,** extractive desulfurization (EDS)[19–22] and adsorption desulfurization (ADS)[23–25]**,** etc.

1.2 Scope of the thesis

This thesis work covers the desulfurization of refractory sulfur compounds in liquid fuels in general, and to investigate the desulfurization of Dibenzothiophene (DBT), 2-Methylthiophene, and Thiophene in diesel by batch adsorption, continuous adsorption, and

extraction in particular. The effect of sulfur emission on our environment and human health are discussed in chapter 1. It is followed by a brief description of European standards adopted to regulate environmental pollution.

In chapter 2, the various desulfurization processes such as commercialized Hydrodesulphurization, Bio-desulfurization, adsorptive and extractive desulfurization is discussed.

Carbon-based materials are considered to be efficient adsorbents for the application of desulfurization. In chapter 3, Microwave synthesized carbon nanotube (M-CNT), and carbon nanofiber (M-CNF) were tested for removal of Dibenzothiophene (DBT) from a model diesel fuel (MDF) by adsorption process. M-CNT showed relatively higher DBT removal capacity over M-CNF. The Sips and Freundlich adsorption isotherm models were used to correlate the adsorption equilibrium experimental results of DBT on M-CNT and M-CNF. The negative values of $\Delta G°$, $\Delta H°$, and $\Delta S°$ from the thermodynamic studies confirm the spontaneity and feasibility of the system, exothermic nature, and non-random behavior of DBT molecule on M-CNT respectively.

The adsorption capacity is mainly dependent on the physical behavior of the adsorbents. Also, the textural properties of the carbon material highly dominate the behavior of the adsorption process. Thus carbon adsorbents like Mongolian anthracite-based porous activated carbons (PMACs) that possess much higher surface area and pore volume than M-CNT and M-CNF have been considered for further study. In chapter 4 the usage of PMACs namely PMAC 1/3 and PMAC 1/4 for model diesel fuel desulfurization, having 500 ppmw of Dibenzothiophene (DBT) in n-heptane has been investigated. Further, the effects of adsorbent dosage, contact time, and temperature on the adsorption capacity were studied systematically. The

experimental adsorption isotherm results were well represented by the Sips isotherm for PMAC 1/3 and the Dual Site Langmuir isotherm for PMAC 1/4, respectively. The maximum DBT adsorption by PMAC 1/3 and PMAC 1/4 was 99.7% and 95.7 %, respectively. The kinetics for the adsorption of DBT on PMACs follows the pseudo-second-order behavior. The Weber- Morris plot shows the multi-linearity over the entire time range, suggesting that by both surface and pore diffusions control the adsorption. The change in Gibbs free energy (ΔG°), enthalpy (ΔH°), and entropy (ΔS°) are negative that confirm that the studied process is spontaneous, exothermic, and possess less randomness at the interface. Based on sips isotherm single-stage batch-adsorber design was done for the adsorption of DBT onto PMAC 1/3.

In previous chapters, the adsorption behavior of carbon materials named M-CNT, M-CNF, PMAC 1/3, and PMAC 1/4 have been studied in the batch process. Further, Graphene Nanoplatelets (GNP) has also been employed in the adsorptive desulfurization study. Consequently, due to the significant and comparable adsorption capacity of GNP and PMACs, GNP has been further used to see the adsorption behavior of the system in continuous experiments for multicomponent feed. Therefore, in chapter 5, an experimental investigation on adsorptive desulfurization for model diesel fuels (MDFs) is described using GNP as an adsorbent. The batch experiments for the single component as well as a multi-component system were conducted. The single component adsorption isothermal experimental results for batch process were well represented by the Freundlich isotherm (Thiophene (T), 2-Methylthiophene (2-MT)) and the Langmuir isotherm (Dibenzothiophene (DBT)) models. The adsorption process kinetics fits with the pseudo second order model for T, 2-MT and DBT on GNP. A process design of single-stage batch-adsorber for the adsorption of T, 2-MT & DBT onto GNP was also studied using the calculated adsorption isotherm parameters. In addition, a

fixed-bed adsorber was used for studying the continuous system at ambient conditions for multicomponent MDFs. The main objective of continuous studies was to investigate the process variables that affect desulfurization. The effect of flow rate, bed height, and initial sulfur concentration on the adsorptive capacity of the adsorbent for T, 2-MT, and DBT were evaluated. The Adam-Bohart model was used to check the performance of the adsorption breakthrough curves.

Adsorptive desulfurization has shown prominent potential for significant desulfurization of liquid fuels. However, to achieve additional thio-selectivity, the extractive desulfurization (EDS) has been adopted for further studies. Also, EDS is an attractive process because it can also can be carried out at ambient conditions. Thus, in chapter 6, the effect of Deep Eutectic Solvents (DESs) on sulfur extraction of organo-sulfur compounds was investigated. Different DESs were prepared using a common hydrogen bond donor, Diglycol, and different hydrogen bond acceptors. The effects of experiment variables such as temperature, DESs/feed ratio, and the time on desulfurization efficiency of different organo-sulfur compounds were also studied. Also, all DESs have higher DBT extraction efficiency followed by 2-MT and T. Further, a non-random two liquids (NRTL) thermodynamic model was employed to model liquid-liquid equilibrium.

Finally, the conclusions and recommendations for future research were highlighted.

Chapter 2

Literature Review

The content of this work is based on the publications,

Divyam Jha, Mohd. Belal Haider, Rakesh Kumar, M.S. Balathanigaimani, "Recent Advancements in Extractive Desulfurization using Ionic Liquids & Deep Eutectic Solvents: A Short Review", ***Fluid Phase Equilibria, 2020***. (Under-revision).

Divyam Jha, Md. Belal Haider, Rakesh Kumar, M. S. Balathanigaimani, J. N. Sahu, "A Review on Role of Nanocomposites for Desulfurization of Liquid Transportation Fuels", (*In Submission Process*)

2.1 Problem statement and motivation

It has been made mandatory that the petroleum products must meet a specified low limit of contaminants such as sulfur and nitrogen in response to environmental concerns and to mitigate its effects on human health[1,2]. Sulfur present in liquid fuels reacts with oxygen to form SO_x which in contact with water produce ultrafine droplets of H_2SO_4 that can easily penetrate the lungs and initiate medical complications[3]. The sulfur and nitrogen compounds that are typically found in transportation fuels are shown in **Figure 2.1**. Emitted sulfur also results in second-hand pollution, which leads to a health problem such as aggravated asthma, cardiovascular effects, chronic bronchitis, emphysema, lung damage, heart disease, stroke, and many

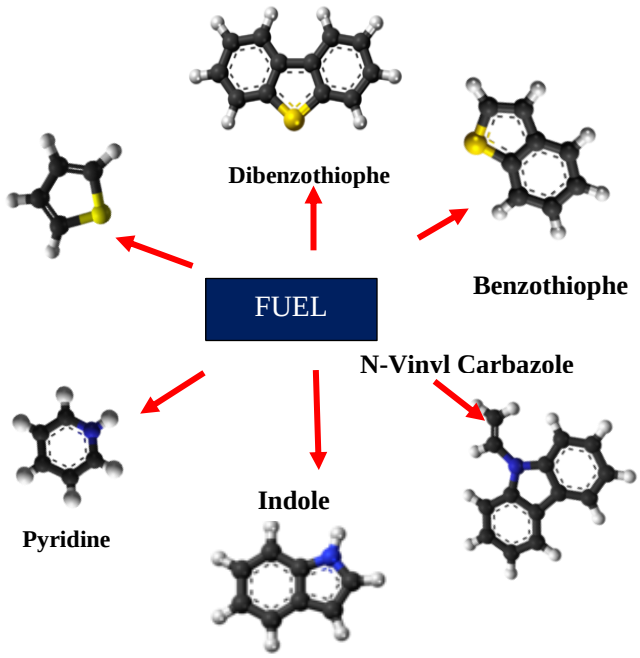

Figure 2.1. Refractory sulfur and nitrogen compounds present in fuel.

more[4,5].

The European Union emission standards have been trying to lower permissible sulfur composition in transportation fuels, such as gasoline and diesel by implementing emission standards, respectively. The Euro emission standards related to sulfur emissions are listed in **Table 2.1.**

Table 2.1 EURO emission standards for diesel.

Properties	**Fuel**	**EURO VI (2014)**	**EURO V (2009)**	**EURO IV (2005)**	**EURO III (2000)**	**EURO II (1998)**	**EURO I (1994)**
Density, kg/m^3(15°C)	Diesel	Max 845	Max 825	-	Max 845	Max 860	Max 860
	Gasoline		-	-	-	-	---
S,ppmw (mg/kg)	Diesel	10<	10	50	350	500	1000
	Gasoline	-	10	50	150	-	---
Cetane No.	Diesel	51	Min 58	Min 58	Min 51	Min 49	Min49
	Gasoline	-	-	-	-	-	-
Polyaromatic (%Volume)	Diesel	-	-	1	6	11	-
	Gasoline	8	-	-	-	-	-

Several desulfurization techniques such as hydrodesulfurization, Bio desulfurization, adsorptive and extractive desulfurization are employed. However, each of these techniques suffers from one or more drawbacks which limit their use in industries.

2.2 Desulfurization processes

Hydrodesulfurization (HDS) is a hydro-catalytic chemical process, widely applied to eliminate sulfur from premium fuel products such as ATF (Aviation Turbine Fuel), diesel fuel, and fuel oils[26]. The presence of refractory components such as dibenzothiophene and alkyl dibenzothiophene makes the process more difficult due to steric hindrance and difficult

scission of C-S bond. In general, two routes are adopted for HDS of alkyl dibenzothiophene compounds. The first route involves direct hydrogenolysis which produces biphenyl compounds and the other one consists of hydrogenation followed by hydrogenolysis produces cyclohexyl compounds as shown in **Figure 2.2**[11,27].

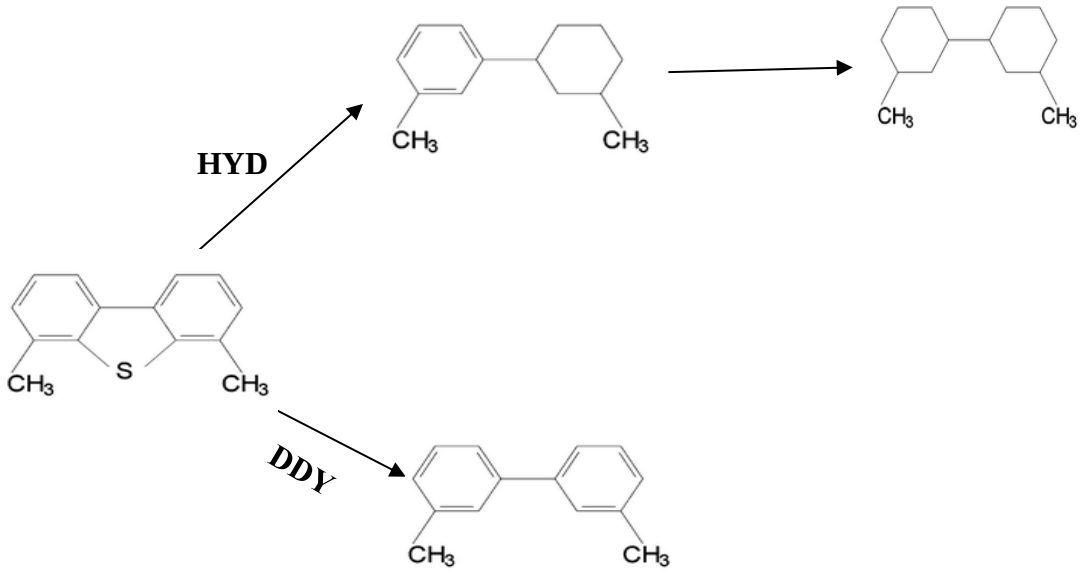

Figure 2.2. HDS of dibenzothiophene **(a)** Hydrogenation, hydrogenation followed by hydrogenolysis, route **(b)** direct hydrogenolysis route

Bio-desulfurization (BDS) was first identified for *Rhodococcus rhodochrous* strain IGTS8 [28]. *Rhodococcus erythropolis* IGTS8 is repressed in the presence of sulfate and intermediate compounds are accumulated in the cells which reduce the yield of desulfurized oil. To overcome these problems, the use of genetically modified organisms (GMO) like *Pseudomonas putida* CECT5279 [17] is suggested. Previous studies on the *P. putida* CECT5279 shows that BDS capacity depends on the growth time of microorganism[29,30]. Recently studies show that the newly isolated strain *R. erythropolis* SHT87 can be also used for desulfurization purpose[31–34]. Higher associated energy and cost make this process

difficult to execute in refineries[35,36]. Also, in the adsorption process, these refractory compounds get adsorbed on the surface of solid adsorbents. Here, Adsorbent interaction with the organometallic sulfur compound is the major factor that decides sulfur dismissal[37,38]. Concerning, selectivity and adsorption, polymer derived adsorbent have shown better results compared to commercial carbon. In addition to adsorption capacity, presence of acidic group enhances sulfur compounds removal and as well as facilitates selective adsorption of DBT and 4, 6-DMDBT [39]. In desulfurization through reactive adsorption, wherein present sulfur compounds are first reacted to H_2S and subsequently the same is adsorbed at the adsorbent site. Various adsorbent–catalyst combinations such as Ni–Al_2O_3, Cu–ZnO, Ni/Al–SiO_2, Ni–ZnO, Ni–SBA-15, Ni–SiO_2, NiP/SiO_2 and among all Ni–ZnO system [40,41] shows better performance.

2.2.1 Adsorptive Desulfurization

The adsorption process is adopted to desulphurize the most refractory compounds of sulfur which is difficult to remove by HDS from the fuel. In this process, these refractory compounds are adsorbed on the surface of solid adsorbents by physical or reactive adsorptive desulphurization. Adsorbent interaction with the organometallic sulfur compound is the major factor to decide the removal of sulfur by adsorption. The adsorptive desulphurization occurs if the organometallic sulfur compound physically interacts with the active site of sorbent and the reactive adsorption desulfurization occurs if chemical interaction between adsorbent and adsorbate usually takes part leaving some conversion with the medium of hydrogen gas[38].

2.2.1.1 Adsorbents

An adsorbent with a large surface area, large pore volume, and small pore size is an effective adsorbent to adsorb compounds come in the range of its diameter range. Hence a large number of pores provides a huge surface area for better adsorption. The textural as well as surface properties are equally important for selective and effective adsorption of DBT [42].

In recent years, the use of nanocomposites for desulfurization has marked presence through its remarkable output. Generally, nanocomposites can be classified as Polymer-based Nanocomposites and Non-polymer Nanocomposites. The structure of Polymer- silica Nano composites is shown in **Figure 2.3.** Carbon nanotubes and silicate layered polymer nanocomposites are among the areas where new materials with favorable chemical and structural properties are seen to be synthesized.

Carbon nanofibers were invented more than a century ago in 1889 [43]**.** Carbon nanofiber (CNF) possesses superior electrical, electromagnetic interference (EMI) shielding effectiveness (SE) and thermal properties compared to conventional conductive polymer composites. Generally, CNF has a diameter under 200 nm dimensions and are conically and plate-shaped graphene structure. When graphene structure is found in cylindrical form thus convert into CNT (Carbon nanotubes) and can efficiently involve in the process for desulfurization [44–46]**.**

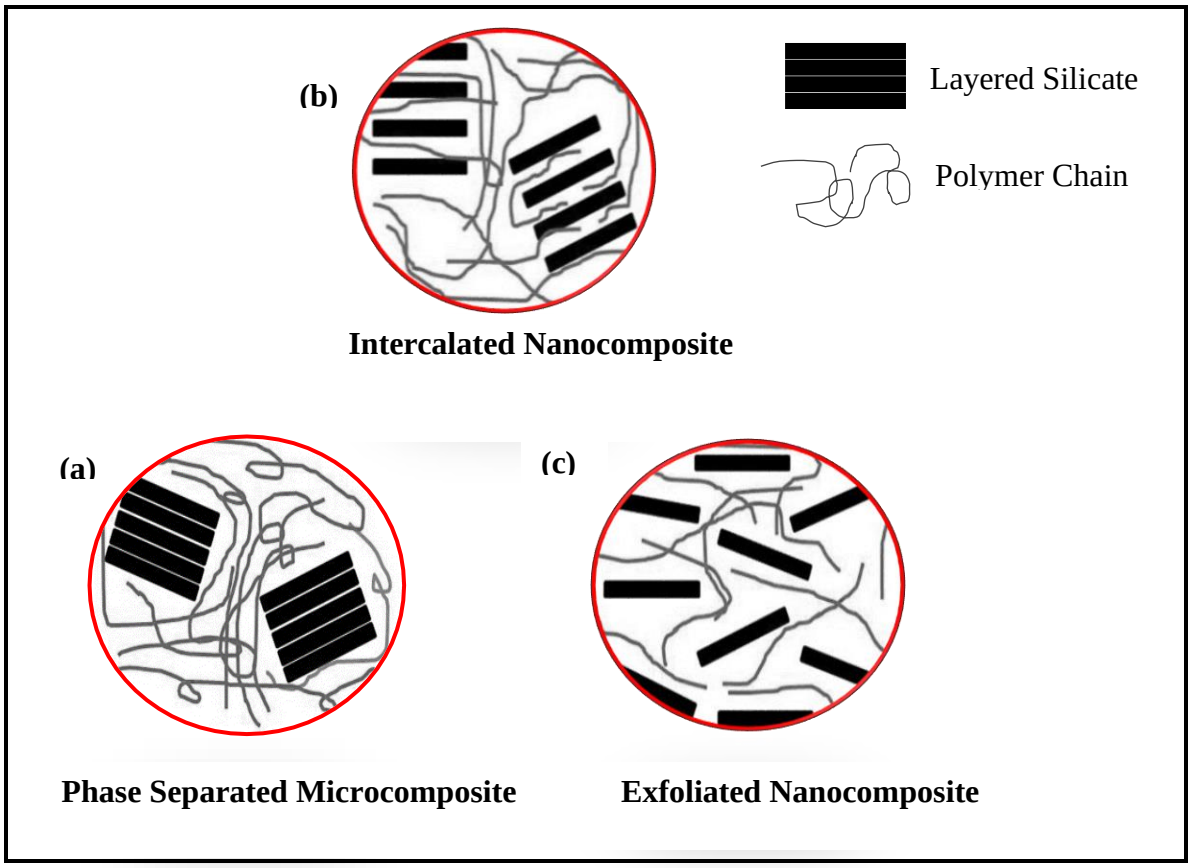

Figure 2.3. Structure Detail of Nanocomposites **(a)** Phase Separated Microcomposite **(b)**Intercalated Nanocomposite**(c)** Exfoliated Nanocomposite.

Carbon nanotubes (CNTs) are tube-shaped carbon material and diameter in the range of nanoscale. Most commonly CNTs have dimensions <1nm -50nm diameter. CNTs have continuous hexagonal links. These materials are first invented by Radushkevich and Lukyanovich in 1952. The mechanical and physical properties of CNTs makes these are valuable material for research purpose. CNTs show multiple effective properties as stiffness, strength, tenacious. Thermal and electrical conductivity are also very high as compared to other materials. CNTs have been effectively used for the purpose of desulfurization [47,48]**.** The

single walled carbon nanotube (SWNT) has unique electronic and mechanical properties that can be used in numerous applications, such as field-emission displays, nanocomposite materials, nanosensors, and logic elements. These materials are on the leading-edge of electronic fabrication, and are expected to play a major role in the next generation of miniaturized electronics[49].

Multi-walled nanotubes (MWNTs) are arranged in the coaxial assembly of SWNTs .The diameters of MWNT are typically in the range of 5 nm to 50 nm. The interlayer distance in MWNT is close to the distance between graphene layers in graphite. MWNT are easier to produce in high volume quantities than SWNT. However, the structure of MWNT is ~~less~~ not well understood because of its greater complexity and variety. Regions of structural imperfection may diminish its desirable material properties. MWNT, however, have a performance of up to ten times better and is outstanding for very specific applications and one of the most promising applications of MWCNT is desulfurization [50].

In addition, Mongolian Anthracite based activated carbon and Graphene Nanoplateletes also have been incorporated for the adsorptive desulfurization of model diesel fuel.

2.2.2 Extractive Desulfurization

Extractive desulfurization and the combination of extractive/oxidative desulfurization are found to be the most economical approach among the different processes tested. This method can be operated at mild operational conditions and the extracted sulfur compound can be utilized as another raw material due to the unaltered structure of S-compound. Several solvents have been used for the extraction process. However, the high vapor pressure and impossible regeneration of the solvents prevent its utilization in the industries[51–53].

The EDS process is based on the difference in the partitioning coefficient of organosulfur compounds between the extractant and the oil phase. Therefore, the selection of extractant very is important for the EDS process. Solvents, such as imidazolidinone, polyalkylene glycol, dimethyl sulfoxide, and pyrimidinone have been previously reported for their capabilities in sulfur removal however because of their volatile nature they are not considered as an effective choice for EDS. The choice of the solvent depends on its extraction efficiency, reusability, and recyclability. Therefore, researchers are more focused on the techniques to substitute volatile solvents with new green solvents. The neoteric solvents such as DESs and ILs have gained attention due to their potential application in separation and purification processes. Owing to this, ILs and DESs have also been investigated for the EDS process given in **Table 2.2 and 2.3** [52,54–57]**.**

Ionic liquids (ILs) widely regarded as green solvents have been used for extractive desulfurization. The remarkable advantages of ILs over volatile solvents lead to involve them as efficient extractants with a melting point below 100 °C. ILs comprises anions and cations that have negligible vapor pressure, high thermal stability, and are non-flammable[58–65]**.**

Extractive desulfurization with ILs and DESs shares many of the advantages. However, this technique also has a shortcoming when coming to large feedstock of heavy oil, the high cost and water sensitivity of some DESs and ionic liquids detract from its large-scale industrial application. Also, the need of large quantities of organic solvents as extractant is itself imposes important health and environmental concerns

Table 2.2 Ionic Liquids for extractive desulfurization.

S.No.	Ionic Liquid	Sulfur Compounds	Solvent for model fuel	Reaction temp (°C)	Time (min)	Reference
1.	$C_5H_9NO.0.3FeCl_3$	DBT	n-Octane	30	10	[66]
2.	$[C_1p_i][Lac]$	TS,DBT,BT, 4-MDBT	n-heptane, n-nonane, n-dodacane	30	30	[67]
3.	$C_{48}H_{10}2O_2P_2$	T,DBT,BT,4-MDBT,4,6-DMDBT	n-dodecane	30	5-30	[68]
4.	$[C_4mpyr][OTf]$	2-MT,BT	n-octane	10-30	50	[69]
5.	$[C_4mpip]FeCl_4$	DBT, BT and 4,6-DMDBT 124	n-octane	45	10	[70]
6.	[BMTH]SCN	BT, 4-MDBT, 4,6-DMDBT, T, and 3-MT	n-octane	30	5-30	[71]
7.	$[C_4P_y][SCN]$	BT, DBT,4,6-DMDBT,	n-octane	25	15	[72]
8.	$[Bmim]Cl/ZnCl_2$	TS, DBT	n-hexane& n-octane	25	30	[73]
9.	$[C_6mim]Cl/FeCl_3$	BT, DBT, 4,6-DMDBT	n-octane	25	5	[74]
10.	[TBCMP][Br]	BT, DBT or DMDBT	n-heptane	RT	10	[75]

The ILs are known as designer solvents because their properties, such as miscibility and polarity, can be altered by changing the choice of cation and/or anion.

Table 2.3 Deep Eutectic Solvents for Extractive Desulfurization

DES combinations (HBA:HBD)	**Molar ratio(HBA:HBD) (mol:mol)**	**References**
TBAC:MA	1:1 &1:2	[76]
TBAC:PEG	1:1 &1:2	[76,77]
ChCl:MA	1:1 &1:2	[70,76]
$ZnCl_2$:$HOCH_2CH_2OH$	1:3,1:4,1:5 &1:6	[78]
(Alcl3:Paraffins-52):o-xylene	--	[79]
Chloride-Glycerol	--	[80,81]
$FeCl_3$:$[CH_3(CH_2)_3]_4PBr$	1:2 &1:1.5	[82]
ChCl:OXA	1:2	[83]
ChCl:PAS	1:2	[84]

However, due to the complex preparation method of ILs and the expensive solvent regeneration step, the use of ionic liquids for industrial EDS is unfeasible[85–89]**.**

Recently, Deep Eutectic Solvents (DESs) analogous to ILs have been developed[90–98]**.** DES possesses properties similar to ionic liquids like low volatility high and thermal stability due to which they also fall into the category of green solvents. The DES is a combination of two compounds and possesses a lower melting point than the constituting compounds[99]**.** The DESs require no complex purification step for synthesis[78]**.** In addition, DESs are biodegradable, non-toxic, and cheaper than ILs making DESs more favourable than ILs[76,100]**.**Deep Eutectic Solvents are composed of hydrogen bond donor(HBD) and

hydrogen bond Acceptor(HBA) in a fixed molar ratio. The formed DESs have melting point lower than the either of HBA or HBD due to hydrogen bonding. It should be noted that the term eutectic is not new in the literature. However due to hydrogen bond formation the melting point of formed DES is "Deep" compared to other mixtures.

2.2.2.1 EDS using ILs and DESs

Ionic liquids are molten salts having melting points below room temperature and are composed of ions only. The cations and anions in the ILs are bounded by weak interactions due to the presence of large cations and delocalized charged anions. This weak interaction, which arises due to the flexibility (anion) and dissymmetry (cation), makes it difficult for ILs to form a crystal. ILs have attracted researchers' attention due to its non-volatility, non-inflammability, high thermal stability, and non-corrosive properties [101–103]**.**

ILs can be tailored depending upon various combinations of anions and cations and therefore can be specifically designed for particular applications[103–111]**.** Rashid et al. have described all possible aspects and factors affecting EDS using ILs [103]**.** Further, various developments and alternate ways have been explored for desulfurization using DES.

The EDS process which formerly used molecular solvents like polyalkylene glycol, imidazolidone, pyrimidinone, and dimethyl sulfoxide, has recently shifted to use ILs/DESs instead**.** There are several factors affecting the entire process of EDS as shown in **Figure 2.4.**

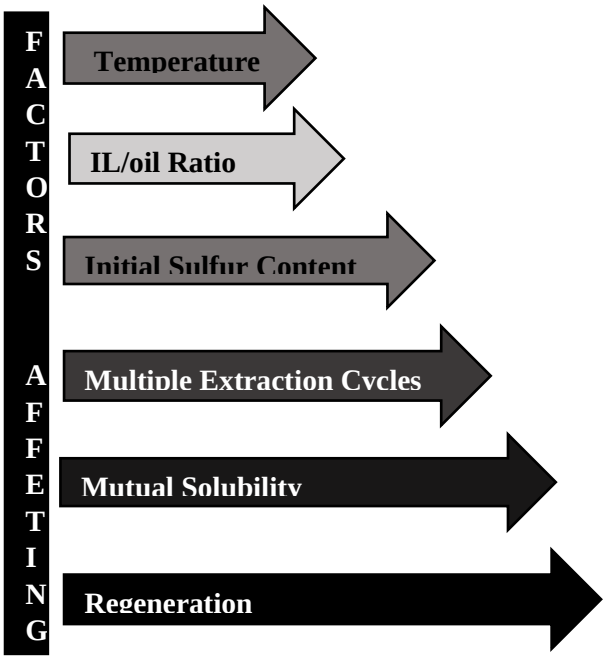

Figure 2.4. Factors affecting EDS using ILs and DESs.

The operating temperature, the time involved, the ratio of IL-DES / oil, and the initial sulfur content significantly change the yield as well as the S-removal efficiency of the process There have been studies related to the miscibility of oil and ILs because dissolution leads to loss of the solvent and contamination of oil [112]**.** Furthermore, solvent regeneration and the ability to get recycled can also reduce the process cost.

Chapter 3

Adsorptive Removal of Dibenzothiophene from Diesel Fuel Using Microwave Synthesized Carbon Nanomaterials

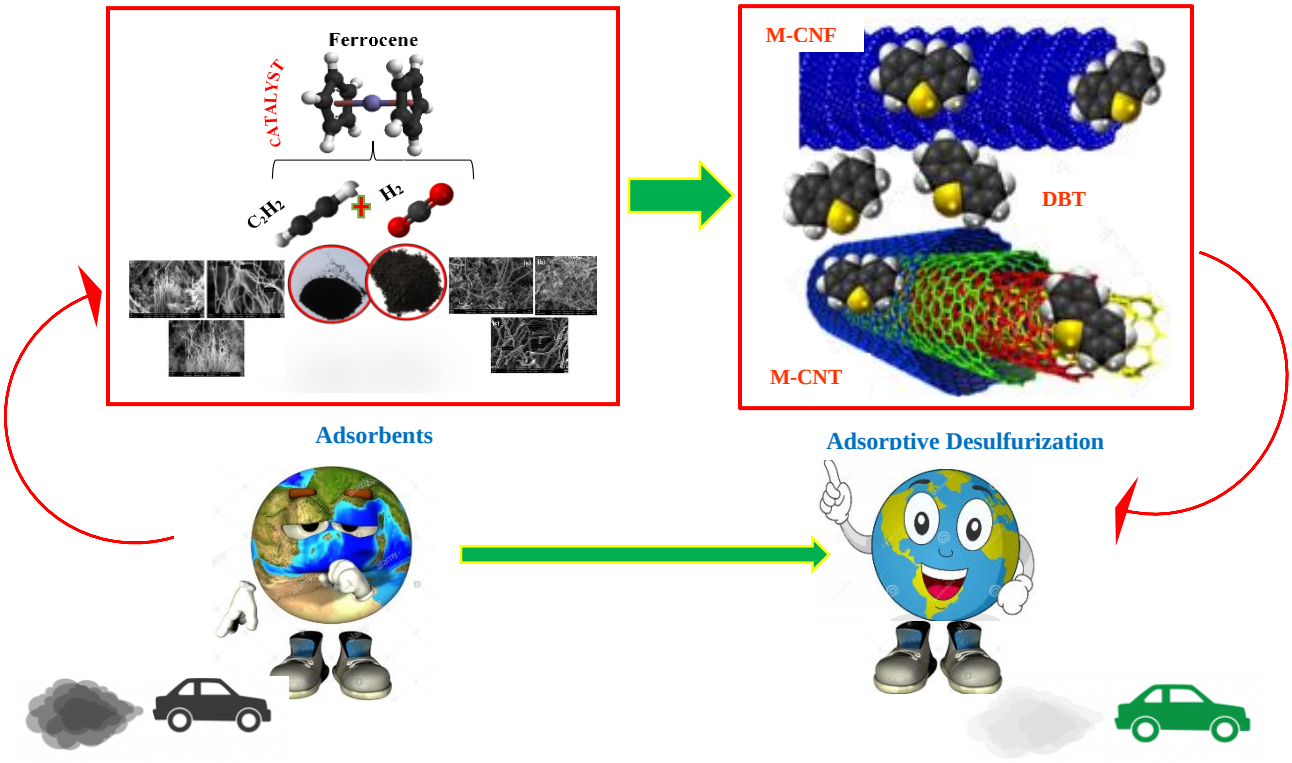

The content of this chapter is published in

Divyam Jha, N.M. Mubarak, Mohd Belal Haider, M. S. Balathanigaimani, J.N.Sahu. "Adsorptive Removal of Dibenzothiophene from Model Diesel Fuel using Microwave synthesized Carbon Nanotube (M-CNT) and Carbon Nanofiber(M-CNF)",***Fuel*,*2019***,*244,132-139. https://doi.org/10.1016/j.fuel.2019.01.006.*

3.1 Introduction

The sulfur compounds separation from liquid fuel is getting more and more attention of petroleum refineries and researchers as the combustion of these compounds affects the environment as well as human health by emitting SO_x [11,27]. Various stringent norms have been proposed and implemented by the European Union (EU) to control sulfur emission.EU has implemented the production of diesel with less than 10 mg/l, as referred to by EURO VI [5,113]. Hence, the development of an economically more viable new process is currently needed to tighten the sulfur level in diesel to produce ultra-low sulfur diesel (ULSD).

Reducing sulfur from a raw diesel, especially from a high level to a low level is highly complicated. The well-known and commercialized process is Hydrodesulphurization (HDS). However, the process has some limitations as many factors such as the surface chemistry of catalyst, process parameters, feed quality, and inhibition effect of H_2S significantly influence this process [11]. Especially, the sulfur compounds attached with alkyl groups like 4,6-dibenzothiophene (4,6-DMDBT) or dibenzothiophene (DBT) are difficult to be desulfurized by HDS process as these compounds are least reactive to adsorb on the surface of HDS catalyst and shows no significant removal of Sulfur using HDS process. The HDS process can be effectively used up to a certain level for sulfur removal and beyond that level, the process requires a high partial pressure of hydrogen and severe operating conditions, which also makes HDS as an expensive process to produce ULSD [114]. Several processes such as Bio-desulfurization(BDS) [115], Extractive Desulfurization(EDS) using solvents and ionic liquids, Oxidative Desulfurization(ODS) and the combination of oxidative-extractive desulfurization have also been proposed and tested to remove the derivatives of DBT from diesel fuel more feasibly. Among all alternative methods, adsorptive desulfurization (ADS) has potential to

meet this limit of sulfur content. The adsorptive desulfurization process is considered as a quite reasonable alternative method for HDS, particularly for the separation of sulfur-containing aromatic compounds from diesel, as the desulfurization by adsorption happens at the ambient condition with the hydrogen free environment and also does not reduce the product yield much. Several adsorbents have been prepared and employed for desulfurization studies including metal oxides, activated carbon, silica, alumina, zeolite, metal organic frame works [6,37,116]. Adsorptive desulfurization is an effective method to remove sulfur from fuel oil, due to its low temperature and pressure conditions. However, the success of ADS process depends on the preparation of highly selective adsorbents and its further regeneration for subsequent runs. In comparison to the ADS, EDS and ODS have advantage to be more selective processes. Although ADS has its own limitations but compare to other existing desulfurization techniques it is more efficient and economic due to its lower energy consumption, broad availability of adsorbents and does not have scaling or corrosion problems.

In this study we present the preliminary results of adsorption of DBT on Microwave synthesized carbon nanotube (M-CNT) and Carbon nanofiber (M-CNF) from a model diesel fuel (MDF). The adsorption equilibrium, kinetic and heat of adsorption were studied to understand the interaction between the adsorbents and DBT.

3.2 Materials and method

3.2.1 Materials

M-CNT and M-CNF were provided by Institut Teknologi Brunei, Darussalam for this study and the horizontal tubular microwave model Synotherm-T1500, China reactor for production of M-CNT and M-CNF. It comprised a quartz tube of 55 mm OD, 50 mm ID and 615 mm

length. Ferrocene catalyst was placed at the entrance of the chamber and quartz boat size was placed in middle of the reaction chamber. The system was initially flushed with air in order to ensure an oxygen free environment. The gas flow rate of C_2H_2 and H_2 was free mixed before entering into the tubular microwave chamber using gas mixer Model KM-20-2, (Germany). The reaction was carried on for the desired time period and on completion, the total amount of M-CNTs and M-CNFs produced in the quartz boats was collected and weighed [117,118]. N-heptane (Purity >99 %), DBT (Purity >98 %) and were purchased from spectrochem Pvt. Ltd, India. Adsorbents were dried in an oven for 12 h before using them for the adsorption studies.

3.2.2 Methods

3.2.2.1 Adsorbents for desulfurization studies

The detailed experimental setup and procedure for M-CNT and M-CNF production have been given in elsewhere [117,118]. M-CNF and M-CNT were produced through Microwave assisted Chemical vapor decomposition (MA-CVD) and Tubular microwave Chemical vapor decomposition (TM-CVD), respectively. Initially, Argon was used to flush the system to ensure oxygen free environment. C_2H_2 and H_2 gases were premixed using gas mixture Model KM-20-2 before sending into the tubular microwave chamber. After the completion of the reaction, the total amount of M-CNT and M-CNF produced was collected and weighed. The physical textural characteristics of two adsorbents were determined using nitrogen adsorption/desorption (Micromeritics ASAP 2010) isotherm data measured at 77 K. The BET, BJH equations were considered for the calculation of specific surface area and meso pore volume of the adsorbents, respectively. Furthermore, the average pore size of adsorbents was obtained based on the BJH method.

3.2.2.2 Model Diesel Fuel (MDF)

n-Heptane containing 250 ppm of DBT was prepared and used as a MDF for the liquid adsorption studies.

3.2.2.3 Adsorption studies

The adsorption studies were done at 30°C and 250 rpm. The dosage amount of adsorbents were varied from 2.5 g/l to 25 g/l of MDF**.** The effect of adsorption equilibrium time was investigated for the lowest mass content (2.5 g) as well for the highest mass content (25 g) at 30°C and 250 rpm. The adsorption rate of DBT on M-CNT was measured in terms of time at constant temperature. The thermodynamic studies of DBT on M-CNT were also carried out at different temperatures for a constant adsorbent mass and initial concentration of 250 ppm of DBT in MDF. All adsorption experiments were done in an Erlenmeyer flask placed inside the isothermal chamber. In each test, the MDF and adsorbent was first mixed. The mixture was then agitated mechanically for 60 min. After each adsorption studies, the adsorbent was filtered using a what-man paper. A gas chromatograph (Perkin Elmer Claurs 580 GC-FID detector) was used for the compositional analysis of desulfurized samples.

The equation used to calculate the quantity adsorbed is given by,

$$q_e = (C_0 - C_e) \times \frac{V}{W} \qquad \textbf{(3.1)}$$

where q_e (mg-S/g-A) is sulfur adsorbed by adsorbent, C_0 and C_e (mg-S/l-MDF) are the initial and equilibrium concentration of sulfur, and W(mg) is mass of adsorbent and V(l) is volume of MDF (l) used. The percentage of sulfur removal can be calculated using the equation given below,

$$\% \text{ Sulfur Removal} = \frac{(C_0 - C_e)}{C_0} \times 100 \quad \textbf{(3.2)}$$

3.3 Gas Chromatograph analysis

GC-FID was employed for compositional analysis of desulfurized fuel. GC equipped with capillary column Elite-1 (length50m and inner diameter 200 µm) flame ionization detector was engaged in this work. Helium, as a carrier gas, with a flow rate of 1cm^3/min and split ratio of 1:85 was used for GC-FID operation. The other operational conditions of GC-FID for compositional analysis were: (i) temperature of injector: 340°C, (ii) injection volume: 1 µL and (iii) total analysis time: 45 min. The oven temperature was increased from 50°to 350°C with a heating ramp of 13 ^oC/ min.

3.4 Adsorption isotherm

The relation between equilibrium concentration C_e and equilibrium sulfur adsorbed q_e plotted to observe the heterogeneity or homogeneity of the solid surface, to calculate adsorption energy and the type of coverage and the interaction between compound from fluid bulk and the solid phase adsorbent.

3.4.1 Freundlich isotherm

The Freundlich adsorption isotherm describes heteroginity of the process and suggests every pore has the different energy of adsorption and also describes multilayer Adsorption [119,120] .$1/n_f$ factor shows the affinity between adsorbate and adsorbent to get adsorbed and strength of adsorption.

$$q_e = K_f C_e^{1/n_f} \quad \textbf{(3.3)}$$

where q_e is sulfur adsorbed by an adsorbent at equilibrium (mg-S/g-A), n_f is the Freundlich constant and K_f is the Freundlich adsorption coefficient (mg/g) $(l/mg)^{1/n_f}$. A large value of n_f shows more heterogeneity of the adsorbent.

3.4.2 Sips Isotherm

The Sips isotherm can be mathematically expressed as [121],

where q_m, b and n_s are the Sips characteristics parameters, q_m is the maximum adsorption

$$q_e = \frac{q_m \, b \, C_e^{1/n_s}}{1 + b \, C_e^{1/n_s}} \quad \textbf{(3.4)}$$

capacity in (mg-S/g-A), b is in $(l/mg)^{1/ns}$, and n_s is Sips constant. The constant n_s is the heterogeneity factor (heterogeneous >1 and homogenous < 1).

3.5 Kinetic Studies

The examination of the controlling mechanism of DBT adsorption on M-CNF and M-CNT was studied, the adsorption rates of DBT were estimated in terms of time (0, 15, 30,45,60,90 min) at 30 ^oC. The amount of adsorbent taken for this study was 0.020 g.

3.5.1 Pseudo First order kinetics

The mathematical equation of pseudo first-order kinetic is stated as follows [122,123],

$$q_t = q_e(1 - e^{-k_1 t}) \quad \textbf{(3.5)}$$

where q_t is the experimental adsorption amount at time *t* and k_1 (min^{-1}) is the pseudo-first order rate constant.

3.5.2 Pseudo Second order Kinetics

The mathematical equation of pseudo second order kinetic is defined as given [124],

$$q_t = \frac{(k_2 q_e^2 . t)}{1 + (k_2 q_e . t)} \quad \textbf{(3.6)}$$

where k_2 (g/mg-min) is the pseudo-first order rate constant.

3.6 Adsorption mechanism

The adsorbate follows either one or more than one mechanism to travel from bulk solution phase to pores of the adsorbents, e.g. surface diffusion, film diffusion, intraparticle diffusion or a combination of two mechanisms. In adsorption, the external diffusion controls if the mixing of adsorbate in the solution is poor, the low adsorbate concertation or adsorbate affinity to adsorbent is very high. In contrast, the surface diffusion controls if the mixing between adsorbate in the system is good, the adsorbent is large in size, adsorbate concentration is high in solution and the adsorbent affinity is poor for adsorbent [125,126].

Weber's intraparticle diffusion model and Boyd's surface diffusion model were employed to investigate the diffusion mechanisms and the rate controlling steps in the adsorption of DBT on adsorbent [127]. The mechanism controlled by intraparticle diffusion is given by

$$q_t = k_{id} t^{1/2} + C \quad \textbf{(3.7)}$$

where C and K_{id} represent boundary resistance and intraparticle diffusion coefficient (mg/g (min) $^{0.5}$) respectively. The diffusion mechanism controlled by surface diffusion is given by Boyd's kinetic expression [128]

$$B_t = -0.4977 - \ln (1 - F) \quad \textbf{(3.8)}$$

$$F = 1 - \frac{6}{\pi^2}\exp(-B_t) \quad \textbf{(3.9)}$$

where $F = \frac{q_t}{q_e}$ is the equilibrium fractional factor, B_t =f_n(F).

3.7 Thermodynamic Studies

The thermodynamic properties of DBT on carbon nanomaterial were determined by investigating the different adsorption isotherms at 30,35,40,45 and for 55 °C. In each case, 0.02 g of adsorbent was taken for every 10 ml of MDF and the batch adsorption was done at 250 rpm. The change in Gibbs free energy (ΔG^0) was evaluated by given equation,

$$\Delta G^0 = -RT \ln K_d \quad \textbf{(3.10)}$$

where R is Gas constant, K_d is distribution coefficient (Concentration of DBT adsorbed amount/concentration of DBT remained at the solution), and T is temperature in K. The (ΔH^0) and (ΔS^0) were calculated according to Van't Hoff equation:

$$\ln K_d = \left(\frac{\Delta S^0}{R}\right) - \left(\frac{\Delta H^0}{RT}\right) \quad \textbf{(3.11)}$$

3.8 Data analysis

The data obtained from isotherm fitting was evaluated by error function with optimization. $\mathbf{R^2}$, the residual root mean square error **(RMSE)**,$\boldsymbol{\chi^2}$ were employed to check the fitness of models.

$$R^2 = \frac{1 - \sum_{n=1}^{n}\left(q_{e,n} - q_{m,n}\right)^2}{\sum_{n=1}^{n}\left(q_{e,n} - \overline{q_{e,n}}\right)^2} \quad \textbf{(3.12)}$$

$$RMSE = \sqrt{\frac{1}{n-1}\sum_{n=1}^{n}\left(q_{e,n} - q_{m,n}\right)^2} \quad \textbf{(3.13)}$$

$$\chi^2 = \sum_{n=1}^{n} \frac{\left(q_{e,n} - q_{m,n}\right)^2}{q_{e,n}} \quad \textbf{(3.14)}$$

where q_e is sulfur adsorbed by an adsorbent at equilibrium calculated by experiments and 'q_m' is the predicted values from the isotherm models, n denotes the number of observations. The conclusion is based on the values of linear and nonlinear coefficients. Higher values of R^2 and lower values of RMSE and χ^2 usually indicate the best fitting with experimental data. The average relative error (ARE) and normalized standard deviation (NSD) were considered to probe the best fit to kinetic models. In general, the better model fitting exhibit lower values of NSD and ARE.

where $q_{t,e,}$ and $q_{t,m}$ are experimental and model predicted the amount of DBT adsorbed on M-CNT and M-CNF. 'N' = the number of observations and 't' = time at which experiments are performed.

$$\mathrm{NSD} = 100 \times \sqrt{\frac{1}{N-1}\sum_{i=1}^{N}\left[\frac{q_{t,e} - q_{t,m}}{q_{t,e}}\right]_i^2} \quad \textbf{(3.15)}$$

$$\mathrm{ARE} = \frac{100}{N}\sum_{i=1}^{N}\left[\frac{q_{t,e} - q_{t,m}}{q_{t,e}}\right]_i \quad \textbf{(3.16)}$$

3.9 Results and Discussion

3.9.1 Physical properties of adsorbents

The isotherms for adsorption/desorption of nitrogen on M-CNT and M-CNF at 77 K are **Figure 3.1**. The BJH results of M-CNF and M-CNT are shown in **Figure 3.2 (a)** M-CNF **(b)** M-CNT and one can expect from these figures that M-CNT and M-CNF have relatively more

mesopores. The surface area, average pore size and mesopore volume values of M-CNT are 171.450 m^2/g, 20.380 nm and 1.892 cm^3/g respectively and for M-CNF the values are 55.620 m^2/g, 6.610 nm and 0.059 cm^3/g respectively as given in **Table 3.1**. It can be observed that the sample M-CNT has the relatively larger surface area, possess large pore size and large pore volume as compared to that of M-CNF. The surface and morphology of the MWCNTs & MWCNFs was examined by the field emission Transmission electron microscopy (FETEM) and the same results have been given in elsewhere [12, 13].

Table 3.1 Physical properties of adsorbents.

Adsorbents	**Surface Area (m^2/g)**	**Pore Size (nm)**	**Total pore volume (cm^3/g)**
M-CNT	171	20.3	1.89
M-CNF	55	6.6	0.05

3.9.2 Adsorption of DBT on M-CNT and M-CNF

The DBT removal was increased with increasing time from 10 to 60 min. There were no significant changes observed after 60 min as shown in **Figure 3.3.** Therefore one can observe that equilibrium was attained between adsorbate and adsorbent at around 60 min (the optimized time). As usual, the adsorption capacity increases with increasing amount of

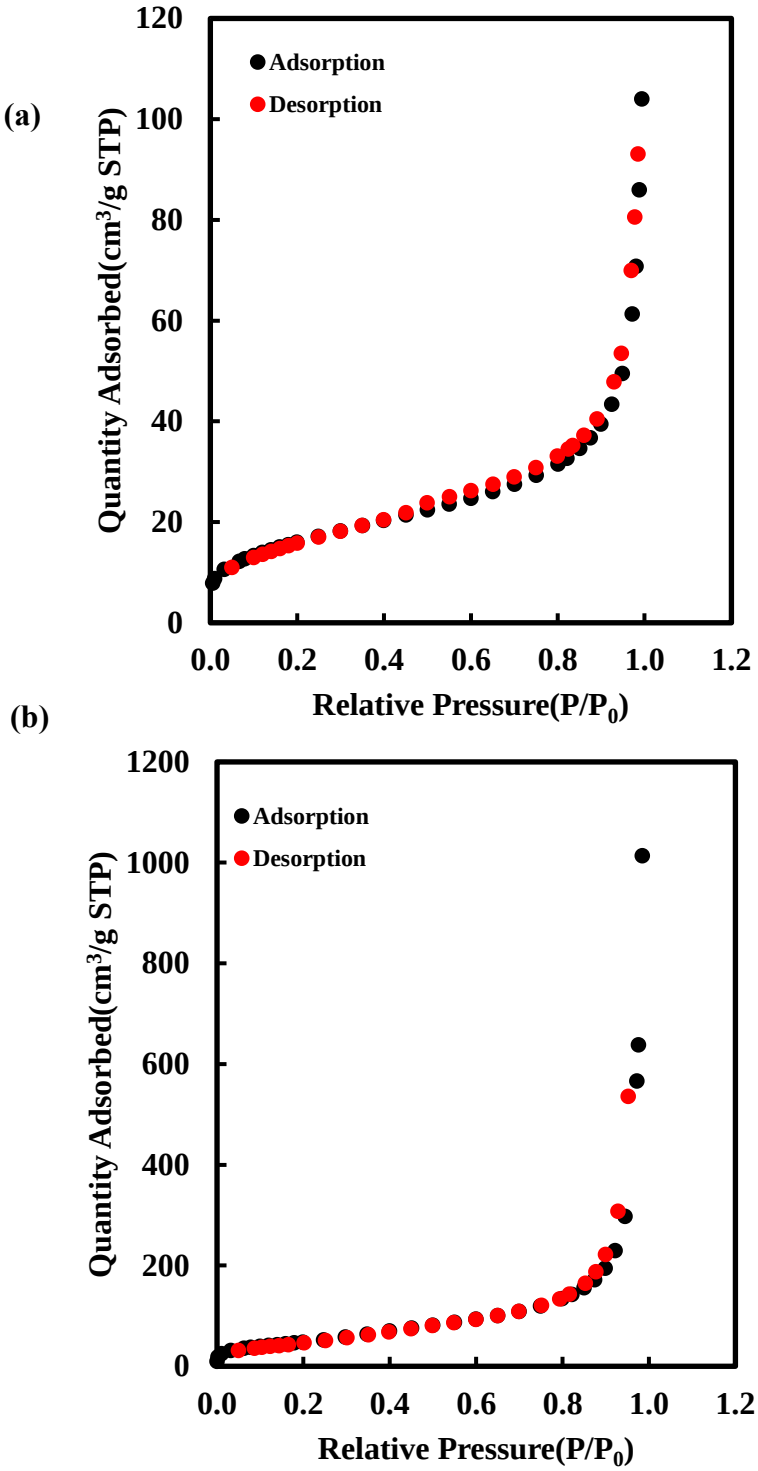

Figure 3.1 Nitrogen adsorption-desorption isotherm for **(a)** M-CNF and **(b)** M-CNT at 77 K

adsorbent from 0.025 to 0.25 g [129]. The maximum DBT adsorption by M-CNT and M-CNF were 43% and 35 % and adsorptive capacity were approximately 25 mg/g and 20 mg/g

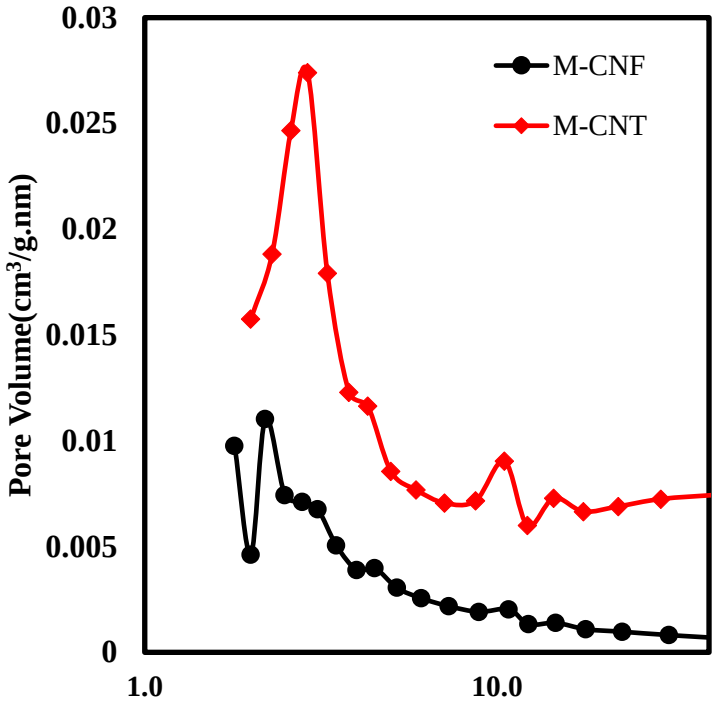

Figure 3.2 BJH Adsorption dv/dD pore volume curve

respectively, for an adsorption condition of 0.25 g of adsorbent, 250 mg/l of DBT in MDF, 30 ^{o}C, 60 min and 250 rpm. The sample M-CNT showed relatively higher adsorptive capacity due to its high surface area as compared to that of M-CNF. The DBT removal capacity of M-CNT/M-CNF was also compared with recently published results. Fallah et al. examined Activated Charcoal Cloths (ACCs) for desulfurization of sulfur compounds and observed adsorptive capacities for ACC and ACC-HNO_3 were approximately 20 mg/g and 50 mg/g for DBT removal [130].Similarly, Ag/AC-(Ultrasonic-assisted Impregnation) UI, Cu/AC-UI, and Fe/ACUI were involved for DBT removal and the adsorptive capacity were found approximately 25 mg/g, 23 mg/g and 10 mg/g respectively [131]. Activated Carbons Derived from Hydrothermally Carbonized Sucrose, activated carbon manganese oxide

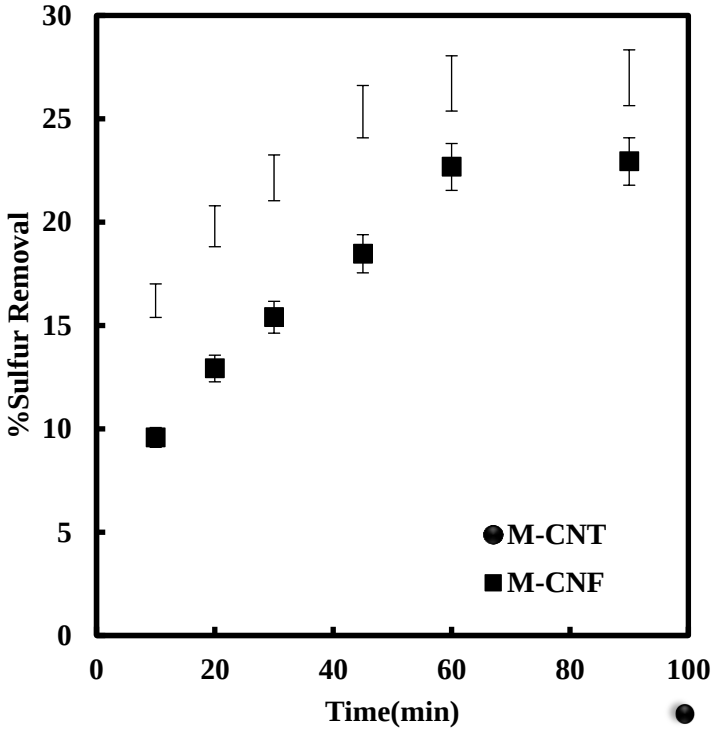

Figure 3.3 Effect of time on sulfur removal

nanocomposite, Activated carbon fiber thermally treated, Activated carbon fiber thermally treated and modified with copper cation, NaY /CNT and activated carbon fiber were incorporated for DBT removal and the adsorptive capacity was found 41.5,11.4, 14.0, 19.0, 6.7,100 mg/g respectively [132–135].

The adsorption equilibrium experimental data of DBT on M-CNT and DBT on M-CNF at 30 ^{o}C are shown in **Figure 3.4.** The experimental results of DBT adsorption on M-CNT at 30 ^{o}C were correlated well by the Sips isotherm model as shown in **Figure 3.4**. The values of R^2, χ^2 and RMSE were calculated and analyzed to check the best fit of experimental data to the isotherm[136]given in **Table 3.2**. In case of adsorption equilibrium data of DBT on M-CNF, the Sips equation correlates the results.

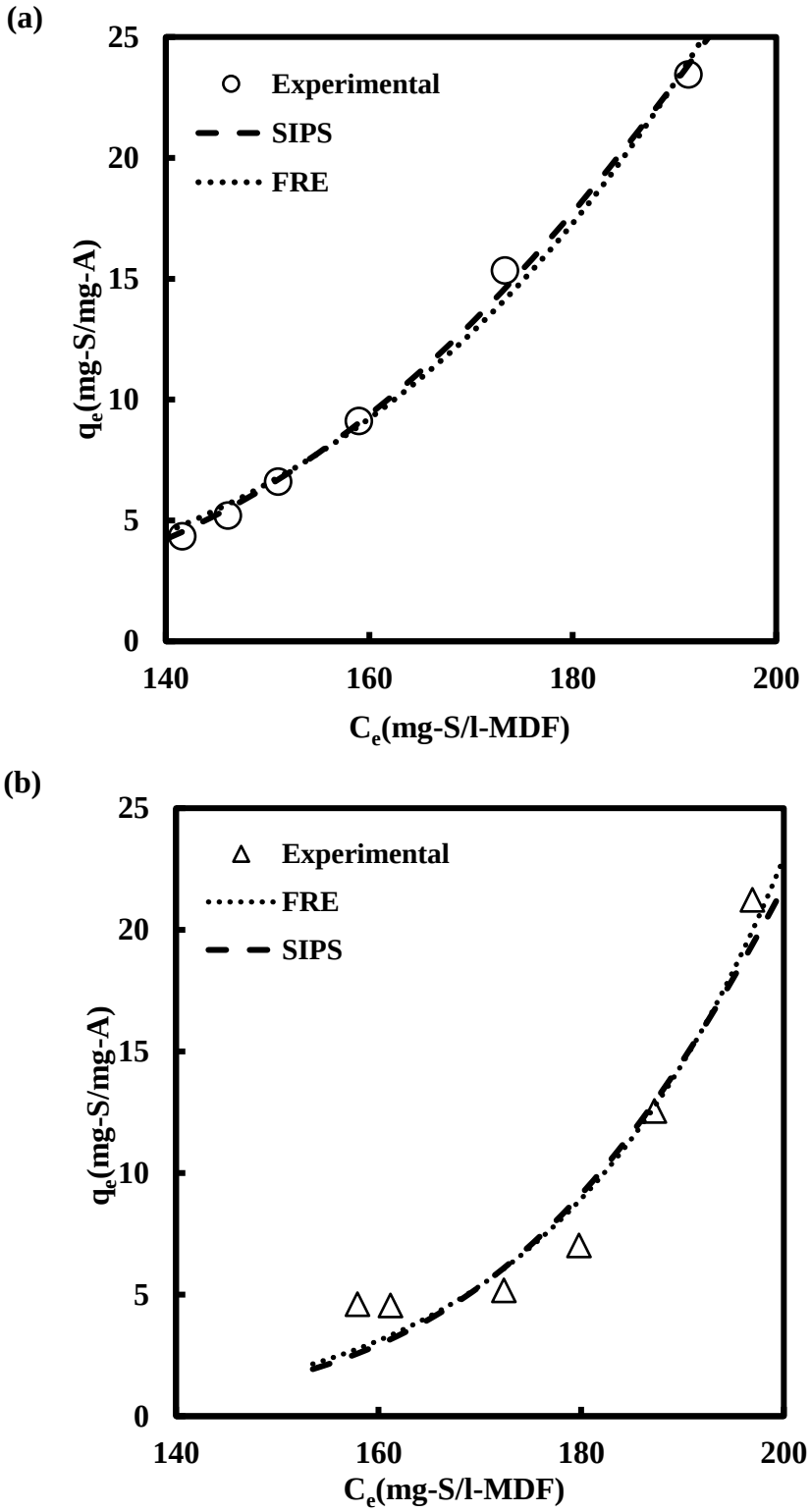

Figure 3.4 Adsorption isotherms of DBT on **(a)** M-CNT and **(b)** M-CNF at 30 ^{o}C.

Table 3.2 The adsorption isotherm parameters**.**

Isotherms	**Parameters**	
	M-CNF	**M-CNT**
Freundlich	K_f= 5.650E-20(mg/g)	K_f=1.520E-11(mg/g)
	n_f= 0.112	n_f= 0.187
	R^2= 0.918	R^2=0.980
	χ^2=2.287	χ^2=0.123
	RMSE=0.667	RMSE=0.144
Sips	q_m= 70.380 (mg/g)	q_m= 80.390 (mg/g)
	b_s=4.230E-25(L/mg)	b_s= 6.570E-16(L/mg)
	n_s=0.096	n_s= 0.154
	R^2=0.942	R^2=0.996
	χ^2=3.004	χ^2=0.072
	RMSE=0.903	RMSE=0.055

3.9.3 Kinetics and thermodynamic Studies

The kinetics involved in DBT removal by M-CNF and M-CNT was calculated and presented, as shown in **Figure 3.5.**The calculated kinetic parameters are listed in **Table 3.3(a) and (b)**. The higher regression coefficient (R^2), smaller the values of nonlinear error functions: average relative error (ARE) and normalized standard deviation(NSD) and lesser deviation in q_e values are the deciding factors to conclude the controlling kinetic behavior of the system. It was observed that the kinetic study of DBT removal by M-CNF follows pseudo first-order kinetics whereas DBT removal by M-CNT follows pseudo-second order kinetic model. Hence, DBT removal by M-CNT was relatively faster as compared to that of M-CNF.

The intraparticle diffusion coefficient K_{id} was calculated from the slope and the value of boundary resistance *C* was calculated from the intercept of the linear plot q_t versus $t^{0.5}$, **Figure 3.6 (a).** If the intercept is large then the benefaction of the surface adsorption will be the rate limiting step. Also, the intraparticle diffusion contribute more as a rate controlling step if the

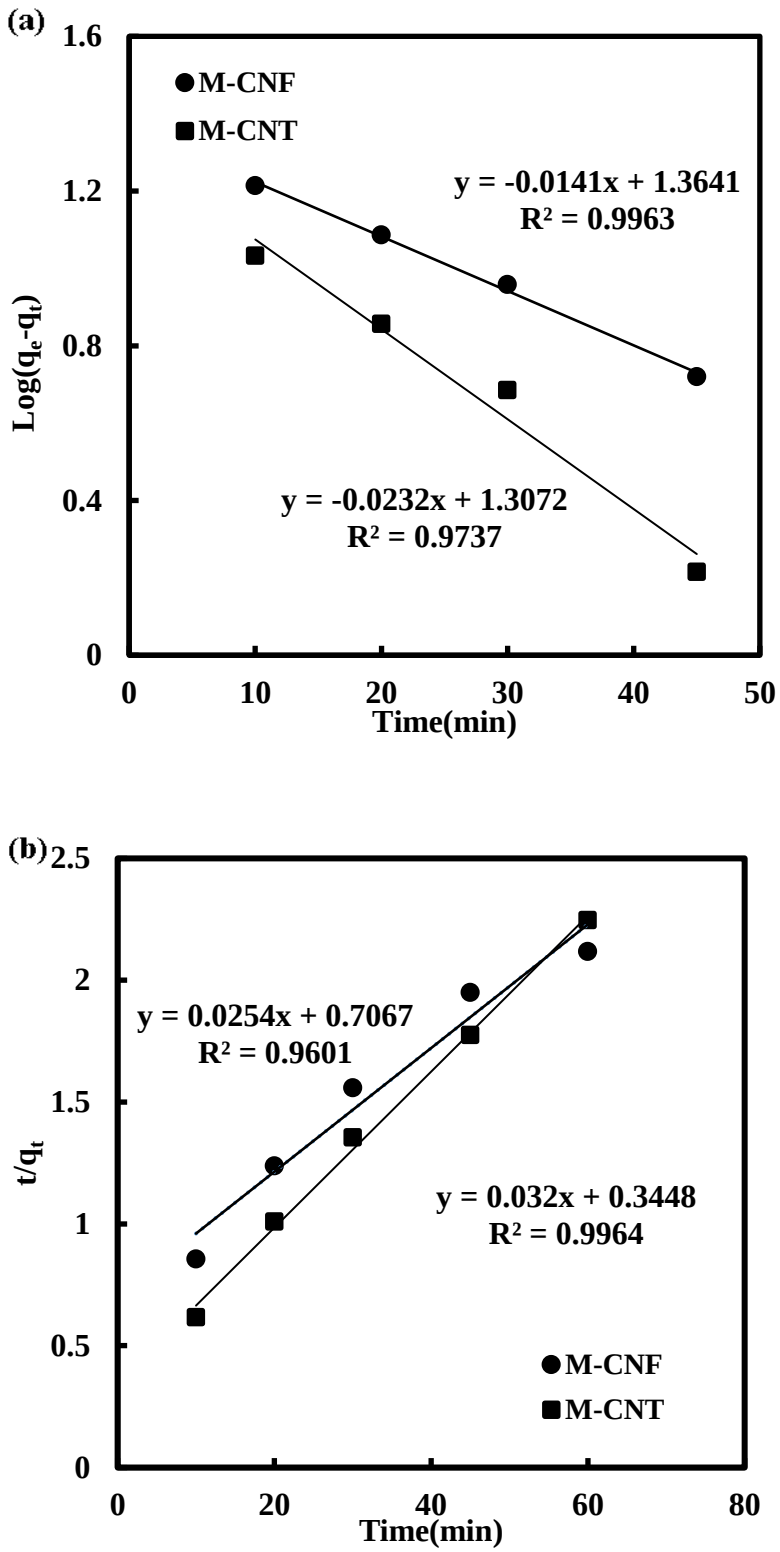

Figure 3.5 Kinetics for M-CNF and M-CNT **(a)** pseudo first order **(b)** pseudo second order kinetics

liner plot exhibit no intercept in general. Besides if the data exhibit multilinear plots and show more than one stages, then two or more steps controls the overall adsorption process.

Table 3.3 (a) Parameters for the kinetics of pseudo 1st order models for the adsorption of **DBT** on **M-CNT and M-CNF**

Adsorbent	k_1 (1/min)	Qe (mg/g)		R^2	NSD	ARE
		Calculated	Experimental			
M-CNF	0.025	23.125	28.337	0.994	0.175	1.678
M-CNT	0.053	0.267	26.711	0.974	0.080	1.022

Table 3.3 (b) Parameters for the kinetics of pseudo 2nd order models for the adsorption of **DBT** on **M-CNT** and **M-CNF.**

Adsorbent	k_2 (g/mg min)	Qe (mg/g)		R^2	NSD	ARE
		Calculated	Experimental			
M-CNF	0.001	39.370	28.337	0.960	45.788	60.939
M-CNT	0.093	31.250	26.711	0.996	0.072	0.416

It is evident from the **Figure 3.6 (a)** that M-CNT and M-CNF plots are non-linear for the entire range deducing that multiple steps influences the adsorption process. Furthermore, the linear plots possess an intercept and therefore intraparticle diffusion is not the sole limiting mechanism. The roles of both intraparticle diffusion and surface diffusion were clearly identified from the first and second stages of plot, respectively. Therefore the adsorption follows complex dual mechanism that is surface diffusion and intraparticle transport simultaneously within the pores of M-CNT and M-CNF [137].

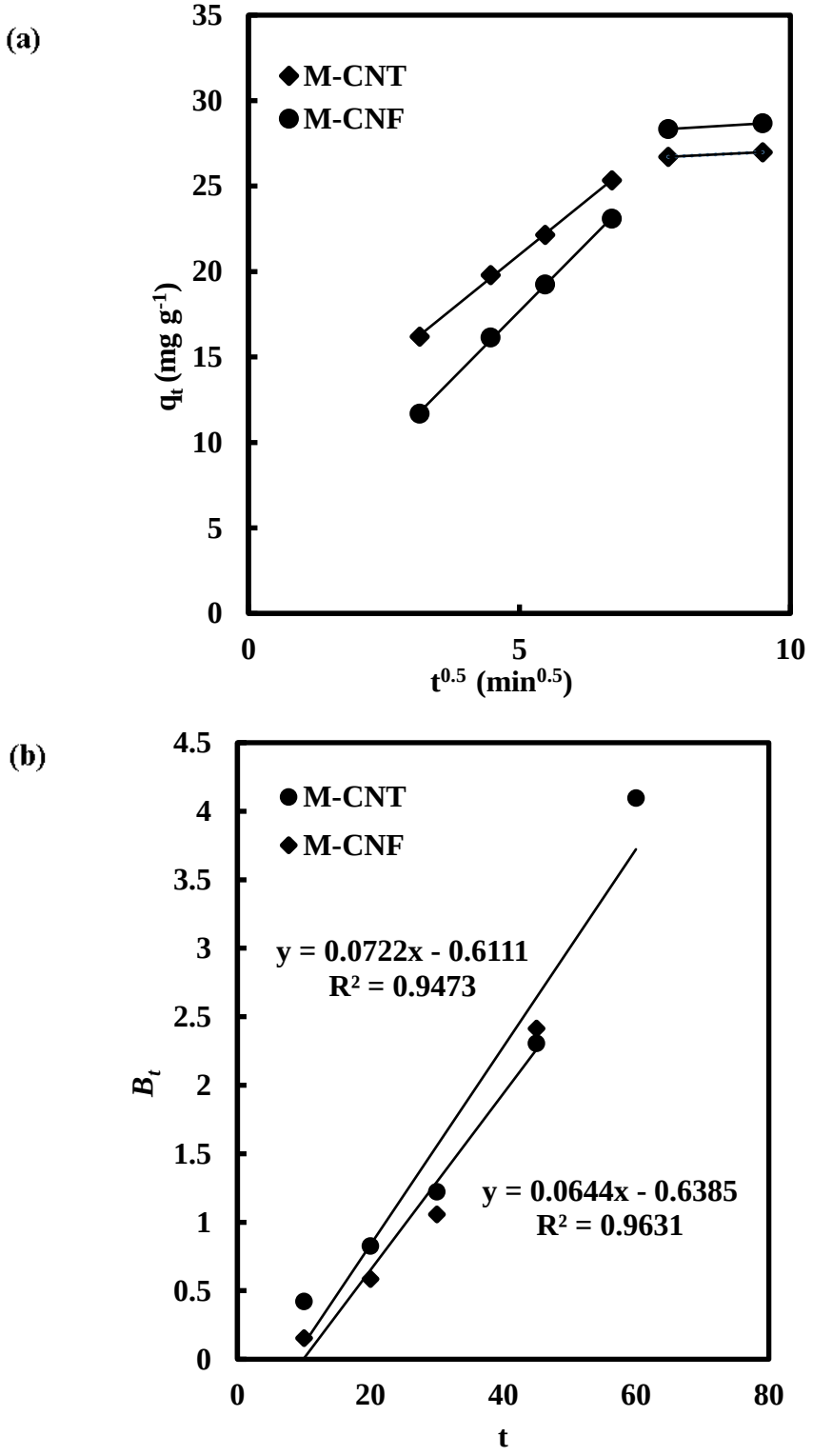

Figure 3.6 Intraparticle diffusion of DBT by **(a)** Weber and Morris Model **(b)** Boyd kinetic model for DBT adsorption.

To predict the slowest step between the surface and intraparticle diffusion, the kinetic data was further examined by employing Boyd kinetic expression as given by **equation 3.8.** The R^2 values of B_t versus time (t) given in **Figure 3.6 (b),** for both M-CNT and M-CNF confirms the linearity of the plot. Thus DBT adsorption for both M-CNT and M-CNF surface diffusion is the rate limiting step [138]. The values of intercept are given in **Table 3.4** depicts that the boundary layer thickness of M-CNT is greater than M-CNF, thus M-CNT possesses more surface diffusion controlling as compared to that of M-CNF.

Table 3.4 Intraparticle diffusion parameters for adsorption of DBT on M-CNT and M-CNF by Weber and Morris model

Adsorbent	**k_{id} (mg/g $min^{0.5}$)**	**C (mg/g)**	**R^2**
M-CNF	2.561	8.181	0.999
M-CNT	3.208	1.643	0.999

The thermodynamic behavior studies were done only for DBT and M-CNT, as the adsorption capacity and kinetic of M-CNT is much better than M-CNF. It was noticed that the sulfur removal decreases with increasing temperature as shown **Figure 3.7(a).** The reduction in adsorption with increasing temperature shows the physisorption phenomena of DBT of M-CNT. Using **equation 3.10, t**he value of ΔG° was calculated for which the temperature was varied from 30 to 50°C. ΔH° and ΔS° were obtained from the intercept and slope of linear Van't Hoff plot as shown in **Figure 3.7(b).**The calculated values for the thermodynamic behavior of the system are listed in **Table 3.5.** ΔG° confirmed the extemporaneous nature of system [139]. The value of (ΔH°) specifies that the adsorption is exothermic in nature. A negative value of ΔS° signifies that the adsorbed DBT molecule possess less degree of

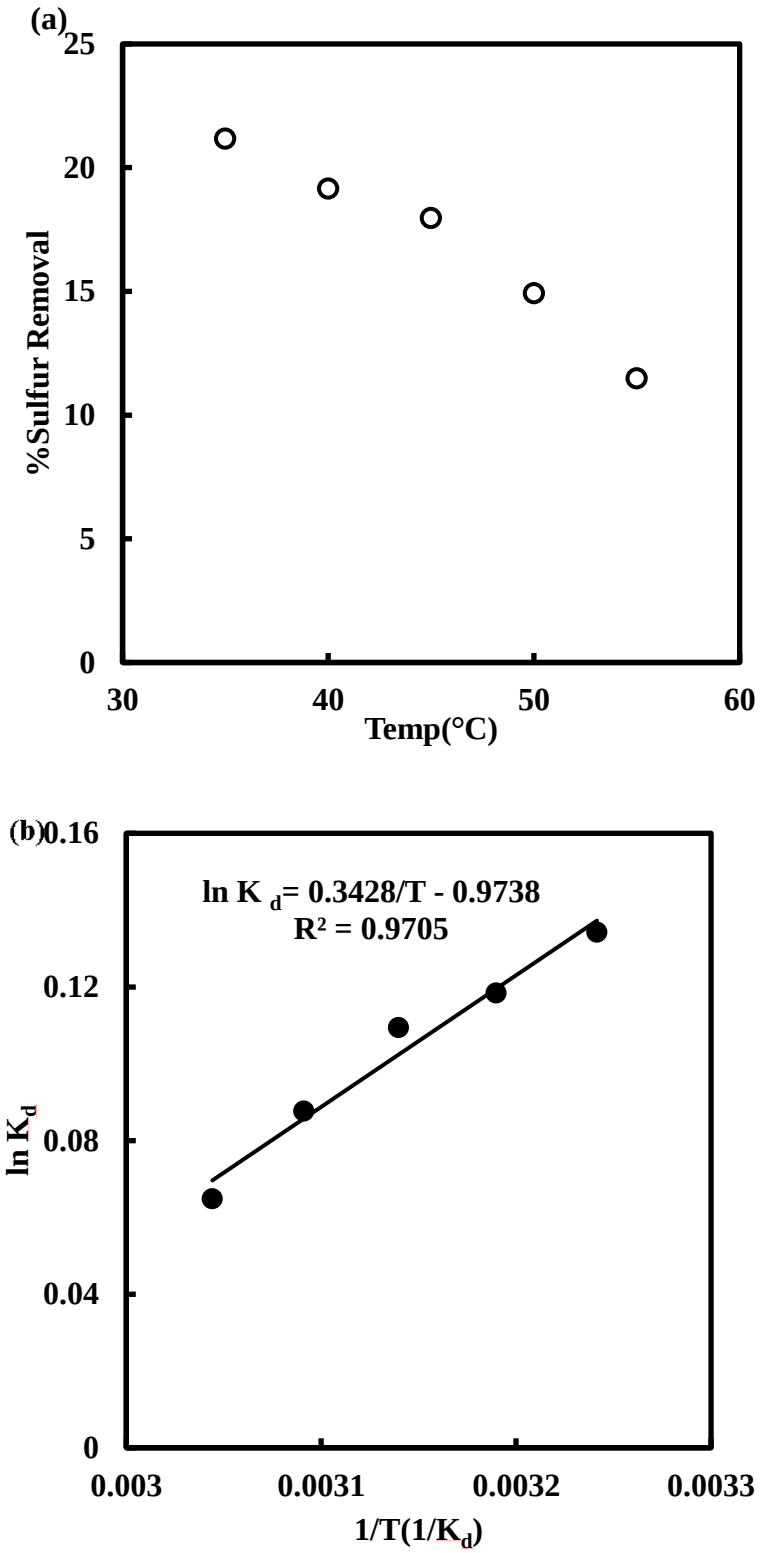

Figure 3.7 (a) Effect of temperature on DBT adsorption on M-CNT **(b)** Modelling for thermodynamic behavior of DBT on M-CNT using Van't Hoff equation

freedom on M-CNT. Hence the system of DBT on M-CNT shows non-random adsorption behavior [140].

Table 3.5 Thermodynamic parameters for the adsorption of **DBT** on **M-CNT**

T(˚C)	K_d	ΔG^0(Kcal/mol)	ΔH^0(Kcal/mol)	ΔS^0 (Kcal/(mol.K))
35	1.144	-82.289		
40	1.126	-73.745		
45	1.116	-69.267	-0.681	-1.935
50	1.092	-56.331		
55	1.067	-42.319		

3.10 Design of batch sorption from isotherm data

The design of single stage batch adsorption system can be predicted by using adsorption isotherm [141–143]. A schematic diagram is shown in **Figure 3.8.** The design objective is to reduce the dye solution of volume V (L) from an initial concentration of C_0 to C_1 (mg/L). The amount of adsorbent is M and the solute loading changes from q_0 (mg/g) to q_1 (mg/g). At time t = 0, q_0 = 0 and as time proceeds the mass balance equates the DBT removed from the MDF to that picked up by the solid. The mass balance equation for the sorption system in **Figure 3.8 (a)** can be

$$V (C_0-C_1) = M (q_0-q_1) = Mq_1 \quad \textbf{(3.17)}$$

Under equilibrium Conditions $C_1 \longrightarrow C_e$ $q_1 \longrightarrow q_e$

Since the sorption isotherm studies confirm that the equilibrium data for DBT onto M-CNT well in a Sips isotherm, a Sips isotherm equation can be used for q_1 in equation batch adsorber design.

$$\frac{M}{V} = \frac{(C_0 - C_e)}{q_1} = \frac{(C_0 - C_e)}{q_e} = \frac{C_0 - C_e}{\frac{q_m\, b\, C_e^{1/n_s}}{1 + b\, C_e^{1/n_s}}} \quad \textbf{(3.18)}$$

Figure 3.8(b) shows the plot between the predicted amount of M-CNT required to remove from MDF of initial concentrations 250 mg/L for 90, 80, 70, and 60% DBT removal at

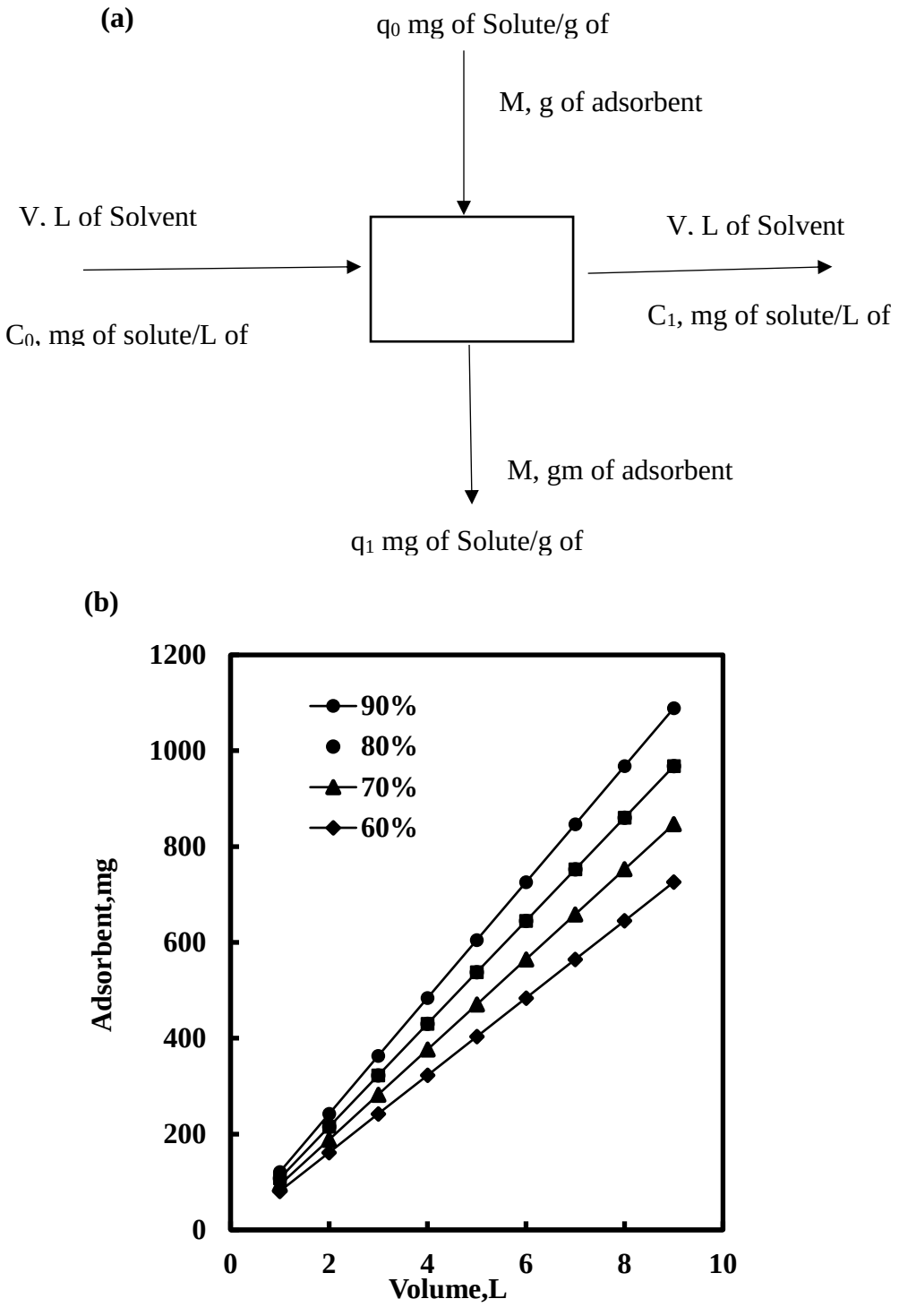

Figure 3.8(a) Single-stage batch-adsorber design **(b)** Adsorbent mass (M) against volume of solution treated (L).

different solution volumes (1, 2, 3, 4, 5, 6, 7 L). For a single-stage batch sorption system, the design procedure is outlined. For example, the amount of M-CNT required for the 90% removal of DBT from MDF of concentration 250 mg/L was 120.96, 241.93, 362.90, and 483.87 mg for MDF volumes of 1, 2, 3, and 4 L, respectively.

3.11 Conclusion

The study of DBT removal by M-CNT and M-CNF showed that M-CNT exhibits better performance as compared to M-CNF mainly because of the promising physical properties of M-CNT. The experimental results of DBT adsorption on M-CNT as well as on M-CNF were fitted well by the Sips isotherm. DBT on M-CNF as well as M-CNT followed the pseudo-first order of kinetic and pseudo second-order kinetics, respectively. In addition, the adsorption system proposed here fits well with the multi-stage diffusion model. The intra-particle diffusion and surface diffusion both control the DBT adsorption on M-CNT and M-CNF.The thermodynamic studies of DBT on M-CNT showed that the adsorption process possess exothermic behaviour and having less randomness at the interface.

Chapter 4

Adsorptive Desulfurization Using Mongolian Anthracite Based Activated Carbon

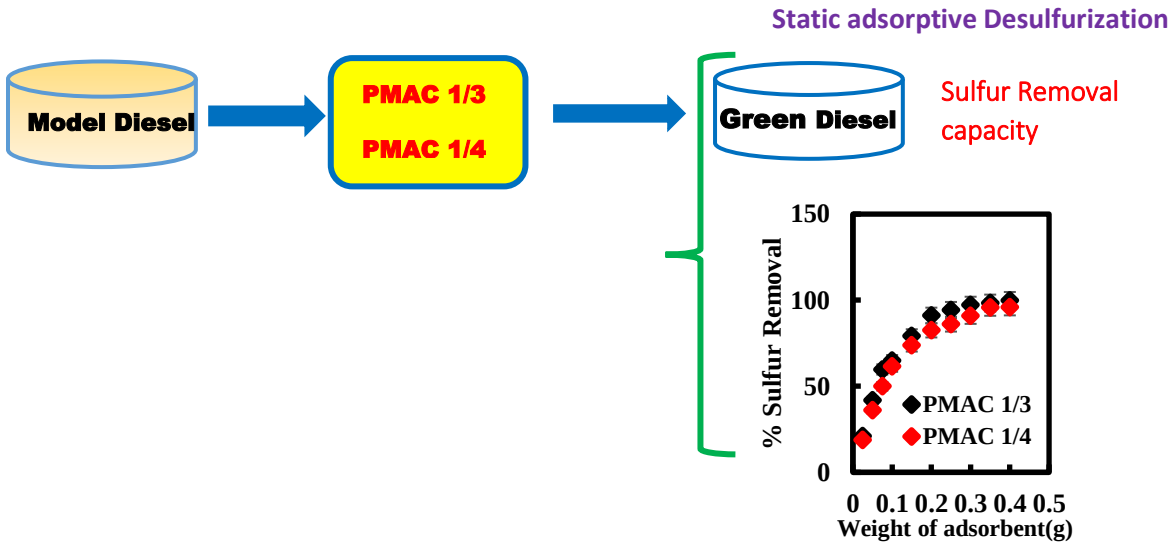

The content of this chapter has been published in

Divyam Jha, Mohd Belal Haider, Rakesh Kumar, Narandalai Byamba-Ochir, Wang Geun Shim, Balathanigaimani Marriyappan Sivagnanam, and Hee Moon, "Enhanced Adsorptive Desulfurization Using Mongolian Anthracite-Based Activated Carbon", ***ACS Omega, 2019,*** *4, 20844−20853. https://doi.org/10.1021/acsomega.9b03432.*

4.1 Introduction

Adsorptive desulfurization (ADS) has gained more attention, because adsorption process is simple to operate and can be done at ambient conditions. ADS has been utilized by various researchers for the removal of sulfur from liquid fuels using different types of adsorbents[1,110,144–148].The challenge for ADS process is to develop adsorbent with high adsorptive capacity. In addition, adsorbents employed must possess thio-selectivity for the adsorption of refractory sulfur compounds that are difficult to remove from the HDS process. In the past, several activated carbons produced from coal and biomass were used[39,110,121,149].

Activated carbons (ACs) are the most celebrated adsorbent for their application in separation and purification technologies and due to their large surface area and porous structure[150,151]. ACs have also become very popular for ADS due to their microstructure[39,152,153]. The adsorption performance of ACs depends upon the adsorbents surface properties. In general, surface area, pore volume and pore width plays important role in the desulfurization[23,150,154]. However, the surface properties do not always have linear relation with the desulfurization capabilities [155][156] and therefore to further enhance the adsorptive capabilities of adsorbents researchers have impregnated ACs with metal halide[150,152,157]. In addition, it has been stated that the ADS performance of AC greatly depends on the precursor materials used and preparation methods[158].

The Mongolian raw anthracite (MRA), which is highly rich in carbon content, has also been used to make adsorbents for gas and energy storage applications. The few qualities of MRA are: less ash content, exclusion of carbonization step, high bulk density, and strong physical strength[159,160]. In the present study, novel Mongolian anthracite based porous activated

carbons (PMACs) have been used to remove sulfur from model diesel fuel (DBT dissolved in n-heptane). It may be noted here that the ADS using PMACs has not been reported yet according to the best of our knowledge. The adsorption results of DBT on PMAC 1/3 as well as PMAC 1/4 are presented in this report. The Langmuir, Sips and Dual Site Langmuir isotherm models have been used to study the equilibrium sorption behavior of the adsorbents. The kinetic models, such as pseudo-first-order, pseudo-second-order, and diffusion models have been employed to study the adsorption kinetics of DBT on PMACs Further the thermodynamics of adsorption system has been investigated to determine the values of $\Delta G°$, $\Delta H°$ and $\Delta S°$. At last, a batch adsorption process design has also been proposed based on the results obtained from this study.

4.2 Experimental

4.2.1 Materials

Activated carbons (ACs) were prepared from Mongolian anthracite by keeping the mass ratio of activation agent to carbon precursor at 3:1 to 4:1. The activation agent, potassium hydroxide (KOH), was introduced by simple physical mixing and impregnation, prior to activation. This method involved mixing fine raw anthracite particles physically with powdered KOH that is denoted as PMAC. The mixture of anthracite and KOH was preheated up to 400°C at a heating rate of 5 °C min^{-1} and kept at this temperature for 2 h to remove volatile compounds. Then, the temperature was increased directly to 750 °C at a heating rate of 5 °C min^{-1} and kept at 750 °C for 2 h to activate the anthracite powder. After activation, the prepared activated carbons were rinsed with distilled and deionized water until the runoff pH became close to 7. They were then dried at 110 °C under vacuum for 24 h. The samples are named as PMAC 1/3, and PMAC 1/4 according to the mass ratio of the agent to anthracite used for activation [160]. The textural

properties of the prepared PMACs are as follows: Specific surface area (PMAC 1/3: 2038 m^2/g and PMAC 1/4: 2784 m^2/g), average pore volume (PMAC 1/3: 1.31 cm^3/g and PMAC 1/4: 2.27 cm^3/g) and average pore diameter (PMAC 1/3: 2.00 nm and PMAC 1/4: 2.20 nm) [160]. The adsorbents were dried in a hot air oven at 110°C for 12 h before every adsorption studies. Beside these activated carbons, the chemicals used in this study namely DBT of Purity >98 %, n-heptane of Purity >99 % and were purchased from Sigma Aldrich Pvt ltd., India.

4.2.2 Preparation of Model Diesel Fuel (MDF)

A model diesel fuel (MDF) was prepared by adding 0.1982 gram of DBT as purchased without any further purification into 500 mL of n-heptane. The concentration of DBT is selected such that the total sulfur concentration should be 500 ppm by weight. Since n-heptane has volatile nature therefore to avoid change in sulfur concentration the prepared MDF was stored in amber vials.

4.2.3 Adsorption Equilibrium

The studies for adsorption of DBT on PMACs were done at 30 °C and 250 rpm. The 20 mL of the solution was taken in an Erlenmeyer flask with 0.025-0.40 g of adsorbents for each adsorption run. The adsorption experiments were conducted in an incubator Shaker. The mixture of MDF and the adsorbent was agitated for 1hr. The adsorbent was later filtered out using a Whatman paper. The concentration of DBT in the desulfurized samples was analyzed by Gas Chromatograph equipped with flame ionization detector (Perkin Elmer Claurs 580, GC-FID). GC is equipped with Elite-1 (length 50 m and inner diameter 200 µm) as well.

The quantity adsorbed qe (mg-S/g-A) was calculated by the following equation (4.1),

$$q_e = (C_0 - C_e) \times \frac{V}{W} \quad \textbf{(4.1)}$$

where q_e is sulfur adsorbed by adsorbent (mg-S/g-A), C_0 is initial concentration of sulfur (mg-S/L-MDF), C_e is the equilibrium concentration of sulfur after the removal of sulfur by adsorption in (mg-S/ L -MDF), and V is volume of MDF (L) and W is mass (g) of adsorbent. The percentage of sulfur removal can be calculated using the equation given below,

$$\% \text{ Sulfur Removal} = \frac{(C_0 - C_e)}{C_0} \times 100 \quad \textbf{(4.2)}$$

Where C_0 is initial concentration of sulfur (mg-S/L-MDF), C_e is the equilibrium concentration of sulfur after the removal of sulfur by adsorption in (mg-S/ L -MDF).

4.2.4 Data analysis

The data analysis, which requires an error function to evaluate the fit of the coefficient of determination (R^2), nonlinear error functions, the residual root mean square error (RMSE) and chi-square test (χ^2) was demonstrated to check fitness of models. The empirical equations used for this study are as follows:

$$R^2 = \frac{1 - \sum_{n=1}^{n} \left(q_{e,n} - q_{m,n}\right)^2}{\sum_{n=1}^{n} \left(q_{e,n} - \overline{q_{e,n}}\right)^2} \quad \textbf{(4.3)}$$

$$\text{RMSE} = \sqrt{\frac{1}{n-1} \sum_{n=1}^{n} \left(q_{e,n} - q_{m,n}\right)^2} \quad \textbf{(4.4)}$$

$$\chi^2 = \sum_{n=1}^{n} \frac{\left(q_{e,n} - q_{m,n}\right)^2}{q_{e,n}} \quad \textbf{(4.5)}$$

Where q_e is quantity of sulfur adsorbed by adsorbent at equilibrium obtained by experiments and q_m is the predicted values obtained from the isotherm models, n is the number of observations. The values of linear and nonlinear coefficients decides the results for the data analysis. Lower values of RMSE and χ^2 and higher the values of R^2 generally show the good fitting with experimental data. The normalized standard deviation (NSD) and average relative error (ARE) were considered to probe the fitness of for kinetic models. In general, the lower the values of NSD and ARE indicate better model fitting. The equations for the calculation of NSD and ARE are given as follows:

Where $q_{t,\,e}$ and $q_{t,\,m}$ are experimental and model predicted amount of adsorbed DBT on PMACs. 'N' = the number of observations and't' = time at which experiments are performed.

$$\mathrm{NSD} = 100 \times \sqrt{\frac{1}{N-1}\sum_{i=1}^{N}\left[\frac{q_{t,e}-q_{t,m}}{q_{t,e}}\right]_i^2} \quad \textbf{(4.6)}$$

$$\mathrm{ARE} = \frac{100}{N}\sum_{i=1}^{N}\left[\frac{q_{t,e}-q_{t,m}}{q_{t,e}}\right]_i \quad \textbf{(4.7)}$$

4.3 Results & discussion

4.3.1 Effect of Adsorbent Dosage

The removal capacity of sulfur was studied for different doses of adsorbents using MDF containing 500 ppm of total sulfur content. The dosage was taken in the range of 0.025-0.4 g of adsorbent for 20 ml of MDF as shown in the **Figure 4.1.** The removal of DBT was rigorously increased with an increase in the adsorbent dose from 0.025-0.25 g. Thereafter the removal efficiency has become constant for adsorbent dose greater than 0.25 g for PMAC 1/3 & PMAC 1/4. The relative successive S-removal is small compared to removal with initial adsorbent dosage. This may be attributed to equilibrium attainment between adsorbate and adsorbent at

operating conditions[161]. This effect is termed as solid concentration effect or overcrowding of particles[162]. The increase in the adsorption dosage can be attributed to the availability of greater surface area and more adsorption sites.

4.3.2 Equilibrium Isothermal Adsorption

In this study the adsorption isothermal analysis was conducted using MDF with initial sulfur concentration 500 ppm and adsorbent dosage (2.5-40 g/l) with a contact time 1 h at 30 °C. **Figure 4.2** shows the relationship of equilibrium amount of DBT adsorb on the surface of

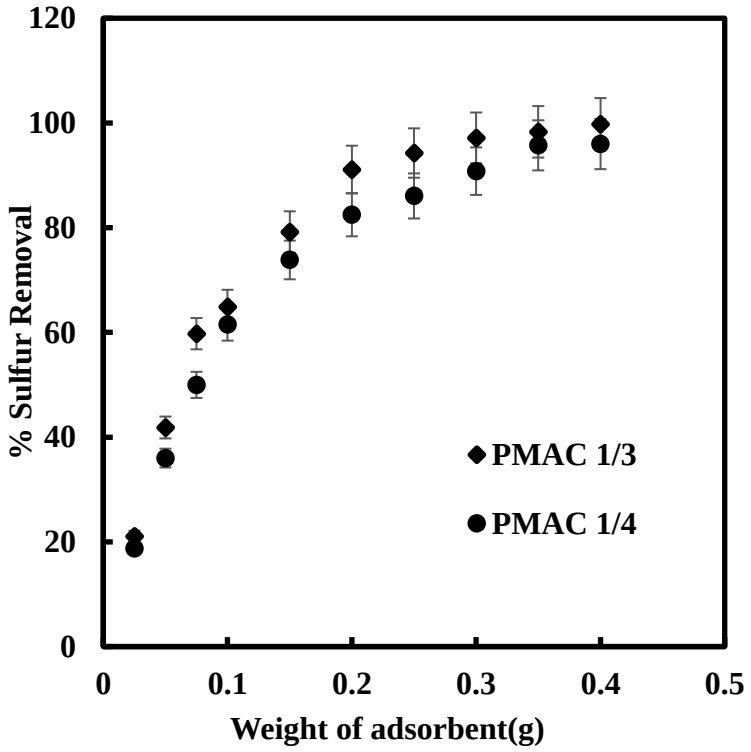

Figure 4.1 Effect of Adsorbent weight on sulfur removal at 303.15 K.

PMAC 1/3 & PMAC 1/4 against the equilibrium concentration of DBT. As shown in the **Figure 4.2**, q_e increases with C_e and reach to saturation which is the maximum adsorption capacity for PMAC 1/3 (~2.489 kmol/kg) & PMAC 1/4 to (~ 2.183 kmol/kg).

The observation of heterogeneity and homogeneity of the solid surface, calculation of adsorption energy, interaction between fluid compound and solid phase adsorbent and the type of coverage were observed by the plot between equilibrium concentration C_e (kmol/m^3) and equilibrium sulfur adsorbed q_e (kmol /kg). The available greater surface area and more adsorption sites can be the reason for increasing adsorption with increasing amount of adsorbent from 0.025-0.4 g[129] .The maximum DBT adsorption by PMAC 1/3 and PMAC 1/4 were 99.7% and 95.7 %, respectively, as shown in **Figure 4.1**, for 0.4 g of adsorbent, 500 mg/L of DBT in MDF at 30 °C , 1 hr and 250 rpm. The sample PMAC 1/3 showed relatively

(a)

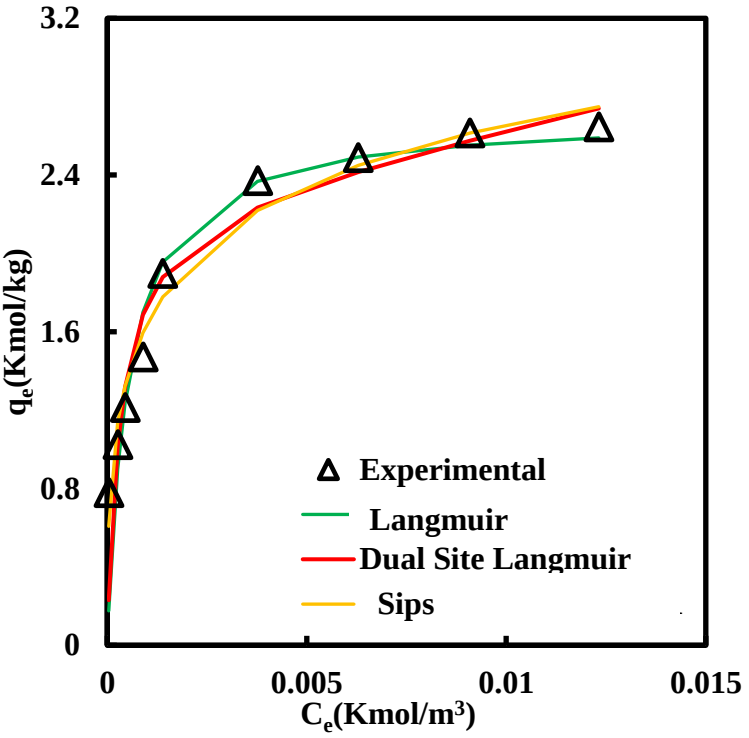

(b)

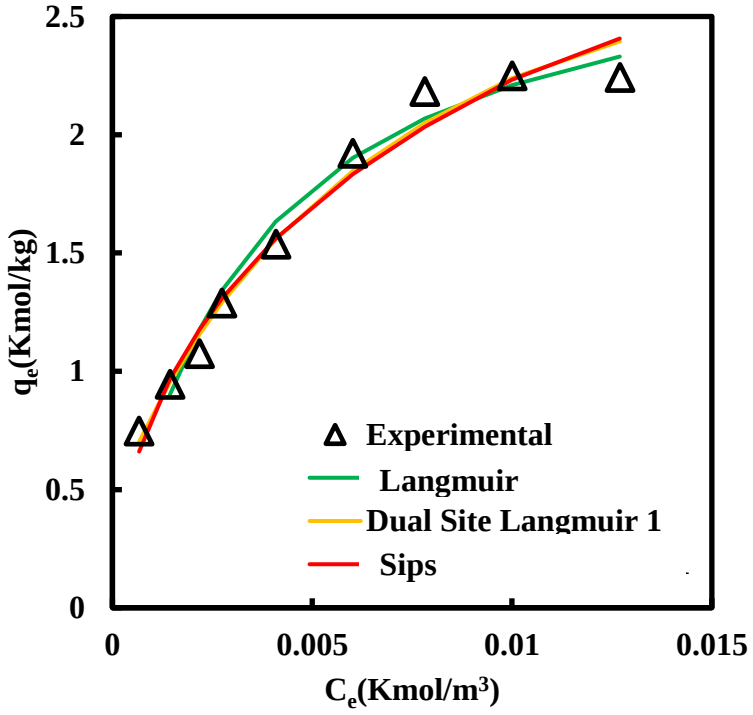

Figure 4.2. Adsorption isotherms of DBT on **(a)** PMAC 1/3 and **(b)** PMAC 1/4 at 303.15 K.

higher adsorptive capacity though PMAC 1/3 having lesser surface area as compare to PMAC 1/4.The probable reason of higher removal using PMAC 1/3 could be its higher micropore volume fraction (66.4 %) available as compare to PMAC 1/4 (42.2 %). The DBT molecule size (0.8 nm)[163] is more closer to the pore diameter of the PMAC 1/3 (2.0 nm)[160] than PMAC 1/4 (2.2 nm) which allows PMAC 1/3 to preferentially adsorb more DBT molecule.[162,164,165] **Table 4.1** shows the adsorptive desulfurization capabilities of different adsorbents synthesized. It can be observed that the adsorptive capacity of PMACs synthesized in this work have potential to adsorb DBT molecule significantly.

4.3.3 Aspen Adsorption Isotherm Modelling

The critical properties of n-heptane and DBT were evaluated by the Peng-Rob equation of state thermodynamic model. Peng-Robinson equation[166] of state (PR-EOS) is given by

$$P = \frac{RT}{v-b} - \frac{a}{v(v+b)+b(v-b)} \tag{4.8}$$

Where a and b are the binary interaction parameters and are the functions of critical properties

$$a = \frac{0.45724(RT_C)^2}{P_C}[1 + m(1 - T_r^{0.5})]^2 \tag{4.9}$$

$$b = 0.0778\frac{RT_C}{P_C} \tag{4.10}$$

$$m = 0.37464 + 1.5422\omega - 0.2699\omega^2 \tag{4.11}$$

4.3.3.1 Langmuir

In its formulation, Langmuir presumes monolayer adsorption that can only takes place at a finite number of definite localized, identical and equivalent sites, with no steric hindrance

Table 4.1. DBT adsorption capacities of different adsorbents at room temperature.

Adsorbent	Surface area(m^2/g)	Adsorption Time(min)	Adsorption capacity(mg/g)	Initial sulfur content(ppm)	Ref.
Microwave synthesized carbon nanotubes	171.0	60	21.50	250	[167]
AC_{TD}	493.0	90	8.60	150	[168]
AC_{WS}	1570.0	30	47.10	220	[169]
ACFH-Cu^{+2}	1090.0	480	19.00	330	[134]
Mesoporous carbon-silica nano-composite via copper modification	276.0	2880	13.95	960	[170]
Carbon aerogels	741.0	96	15.10	250	[171]
Activated carbon/γ-Fe_2O_3 nanocomposite	363.0	40	38.00	--	[172]
Magnetic mesoporous carbon	705.0	60	62.00	1000	[173]
PMAC 1/3	2038.0	60	84.67	500	This Chapter
PMAC 1/4	2784.0	60	74.97	500	This Chapter

between the adsorbed molecules and lateral interaction even on adjacent sites [119,174]. The Langmuir isotherm is represented by the following equation,

$$q_e = \frac{q_m K_a C_e}{1 + K_a C_e} \quad \textbf{(4.12)}$$

Where q_e is sulfur adsorbed by adsorbent at equilibrium (mol-S/kg-A), q_m signifies the maximum sulfur adsorbed (mol/kg) at saturation, C_e is the equilibrium concentration of sulfur after the removal of sulfur by adsorption in (mol-S/L-M) and K_a is energy of adsorption.

4.3.3.2 Dual Site Langmuir

Adsorption of component on a heterogeneous adsorbent composed of two homogeneous but energetically different patches can be describe by single-gas Dual Site Langmuir model. If free energy of adsorbate-adsorbent on each patch is constant, the amount adsorbed n for component is given [175]

$$n = \left(\frac{n_1^s b_1 C}{1 + b_1 C}\right)_{site\ 1} + \left(\frac{n_2^s b_2 C}{1 + b_2 C}\right)_{site\ 2} \quad \textbf{(4.13)}$$

Where n_1^S and n_2^S are the saturation capacities on site 1 and 2 respectively, b_1 and b_2 are the affinity parameter on site 1 and 2 respectively .*C* is the solute concentration. The assumptions for the Langmuir model can be applied to each patch, and the saturation capacity for each component on each site is allowed to be different but the two patches do not interact with each other.[176]

The free energy or affinity parameter for two different sites is given as

$$b_j = b_{i0}\, exp\, \frac{E_i}{RT} \quad \textbf{(4.14)}$$

Where the subscript i represents the free-energy level of site 1 or 2, b_{i0} is the pre-exponential factor of component on site i and E_i is the adsorption energy of component on site i. The higher

and lower adsorbate-adsorbent free energy is donated by, i = 1 and i = 2 respectively, the free energy of site 1 is always higher than that of site 2 for single-gas adsorption.

4.3.3.3 Sips

The limiting behavior of the Langmuir and Freundlich isotherms is best described by sips isotherm[153]. The Sips nonlinear equation model is expressed as

$$q_e = \frac{q_m \, b \, C_e^{1/n_s}}{1 + b \, C_e^{1/n_s}} \tag{4.15}$$

where q_m, b and n_s are the Sips characteristics parameters, b is in $(l/kmol)^{1/ns}$, and n_s is Sips constant. The constant n_s is the heterogeneity factor (heterogeneous >1 and homogenous < 1)[120].

The Langmuir, Sips and Dual Site Langmuir isotherms were used to analyse the adsorption equilibrium behavior of the adsorbate and adsorbent using Aspen Adsorption 8.4.

The adsorption equilibrium experimental data of DBT on PMAC 1/3 and PMAC 1/4 at 30 ^oC are shown in **Figure 4.2.** The fitness of isotherm models with the experimental data was analyzed using calculated values of χ^2 and RMSE[152], which are given in **Table 4.2.** The data obtained from error analysis confirm the best fit of Sips for PMAC1/3 and Dual site Langmuir for PMAC1/4 respectively.

4.3.4 Effect of Contact Time

The size of the adsorbent, the diffusion coefficient of the adsorbate and the degree of mixing decides the quantity and rate at which adsorbate adsorbs on the surface of adsorbent [177].MDF with DBT concentration 500 ppm were kept in contact with PMAC 1/3 and

Table 4.2. The adsorption isotherm parameters.

Isotherms	**Aspen Adsorption Parameters**	
	PMAC 1/3	**PMAC 1/4**
Langmuir	q_m=2.701	q_m=2.936
	K_a=1890.620	K_a=306.981
	R^2=0.976	R^2=0.960
	χ^2=2.124	χ^2=0.052
	RMSE=0.027	*RMSE*=0.003
Dual Site Langmuir	n_1 =0.683	n_1 =3.109
	b_1 =2.520E-04	b_1 =2.730E-03
	n_2 =2.215	n_2 =4.410E-01
	b_2 =1.470E-03	b_2 =8.950E-02
	R^2=0.968	R^2=0.990
	χ^2=1.360	χ^2=0.014
	RMSE=0.024	*RMSE*=0.001
Sips	q_m=4.629	q_m=6.300
	b=8.138	b=7.602
	n_s=0.390	n_s=0.570
	R^2=0.986	R^2=0.975
	χ^2=0.101	χ^2=0.028
	RMSE=0.007	*RMSE*=0.002

PMAC 1/4 for 2 g/l adsorbent amount at room temperature for 10-90 min. After 60 min a steady state approximation was achieved and a quasi-equilibrium situation was obtained for both the adsorbents as shown in the **Figure 4.3**.The adsorption rate was rapidly increased in the initial stage of experiments due to free sites available for adsorbates to adsorb on the surface. The initial fast adsorption depicts the large number of available active adsorption sites and it slows down at equilibrium due the few available sites and the mutual repulsive forces between the adsorbate present in the solution and at the surface of the adsorbent [178].

4.3.5 Adsorption Kinetic Studies

The study of adsorption kinetics is vital for designing an adsorption process. In the initial stage of adsorption meso and macro pores gets saturated with DBT molecules. Thereafter the

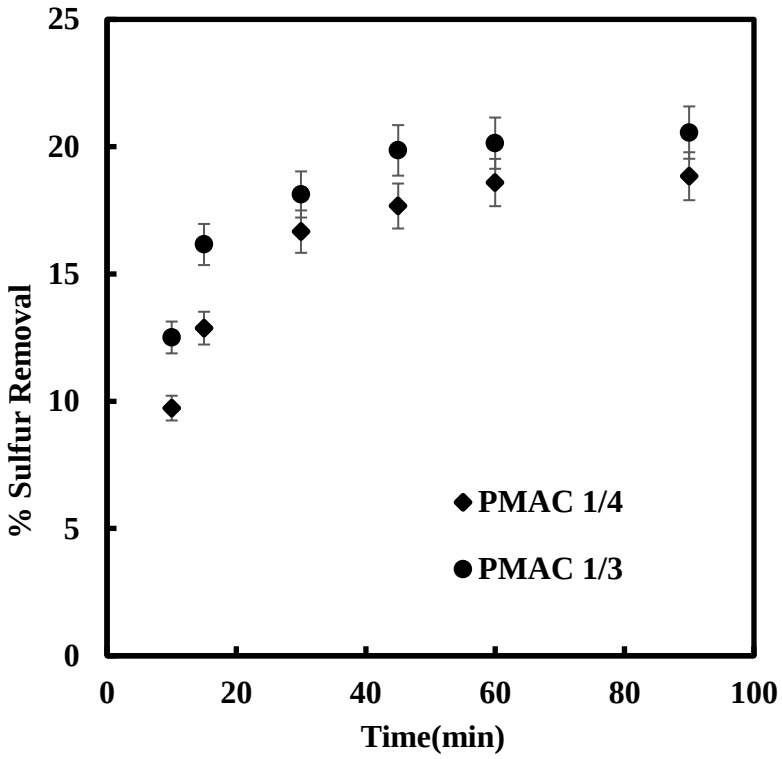

Figure 4.3 Effect of Time of Sulfur Removal at 303.15 K.

adsorption rate gets slow down when the DBT molecules traverse further deep into the microspores experiences larger resistance in the later stage [179]. Thus to get a better understanding of adsorption process, the experimental adsorption kinetic data were correlated with the pseudo-first order and the pseudo-second order models.

4.3.5.1 Pseudo First order kinetics

The assumptions are non-dissociating behavior of DBT molecules on the surface of adsorbents and no DBT molecule present initially on the surface of adsorbents PMAC 1/3 and PMAC 1/4. The pseudo first order kinetic is given by[122,123],

$$q_t = q_e(1 - e^{-k_1 t}) \qquad \textbf{(4.16)}$$

where q_e is sulfur adsorbed by adsorbent at equilibrium (mg-S/g-A),q_t is the experimental adsorption amount at time *t* and k_1 (1/min) is the rate constant of pseudo-first order adsorption.

4.3.5.2 Pseudo Second order Kinetics

.The pseudo second order kinetic is given by [124]**,**

$$q_t = \frac{(k_2 q_e^2 . t)}{1 + (k_2 q_e . t)} \quad \textbf{(4.17)}$$

The kinetics involved to remove DBT by PMAC 1/3 and PMAC 1/4 was investigated using linear plots of log (q_e -q_t) versus t and t/q_t versus t for the pseudo first order kinetic model and for pseudo second order kinetic model, respectively as shown in **Figure 4.4**. The calculated values of kinetic parameters are given in **Table 4.3.** Lower values of ARE and NSD , higher values of R^2 and less difference between calculated and experimental q_e values generally show the good fitting with experimental data . These were the deciding factors to conclude the controlling kinetic behavior of the system. It was investigated that the kinetic study of DBT removal by PMAC 1/3 and PMAC 1/4 follows pseudo second order kinetics.

Table 4.3. Kinetics parameters of pseudo 1st and 2nd order models for the adsorption of **DBT** on **PMAC 1/3** and **PMAC 1/4 at** 303.15 K.

Adsorbent	**k_1 (1/min)**	**k_2 (g/mg min)**	**Q_e (mg/g)**				**R^2**	**NSD**	**ARE**	**R^2**	**NSD**	**ARE**
			Calculated	**Exp**	**Calculated**	**Exp**						
			1st order		**2nd order**		**1st order**			**2nd order**		
PMAC1/4	0.026	0.156	2.76	23.55	27.70	23.55	0.89	28.15	31.11	0.99	0.42	0.07
PMAC1/3	0.017	0.103	3.07	25.69	26.45	25.69	0.84	19.77	18.03	0.99	0.08	1.12

4.3.6 Diffusion mechanism

The transportation of adsorbate from bulk solution to adsorbent surface may be controlled by one or more mechanism[126] i.e. film or external diffusion, pore diffusion, surface diffusion or a combination of two. The system controlled by film diffusion may have poor mixing, lower concentration of adsorbate, higher affinity of adsorbate for adsorbent and small adsorbent particle size similarly the intraparticle diffusion controls the system where the mixing is proper, high adsorbate concentration and lower affinity of adsorbate for adsorbent[125].

$$B_t = -0.4977 - \ln(1 - F) \quad \textbf{(4.18)}$$

$$F = 1 - \frac{6}{\pi^2}\exp(-B_t) \quad \textbf{(4.19)}$$

where$F = \frac{q_t}{q_e}$ is the fractional attainment of equilibrium, B_t is the mathematical function of F, q_e is quantity of sulfur adsorbed by adsorbent at equilibrium (mg-S/g-A) and q_t is the experimental adsorption amount at time *t*.

Weber's intraparticle diffusion model and the Boyd's surface diffusion model were used to predict the diffusion mechanisms affecting the kinetics of adsorption [127].The mechanism controlled by intraparticle diffusion is given by

$$q_t = k_{id}t^{1/2} + C \quad \textbf{(4.20)}$$

Where K_{id} is the intraparticle diffusion coefficient (mg/g (min) $^{0.5}$) and C depicts the thickness of the boundary layer (boundary resistance). The diffusion mechanism controlled by surface diffusion is given by Boyd's kinetic expression [128].

(a)

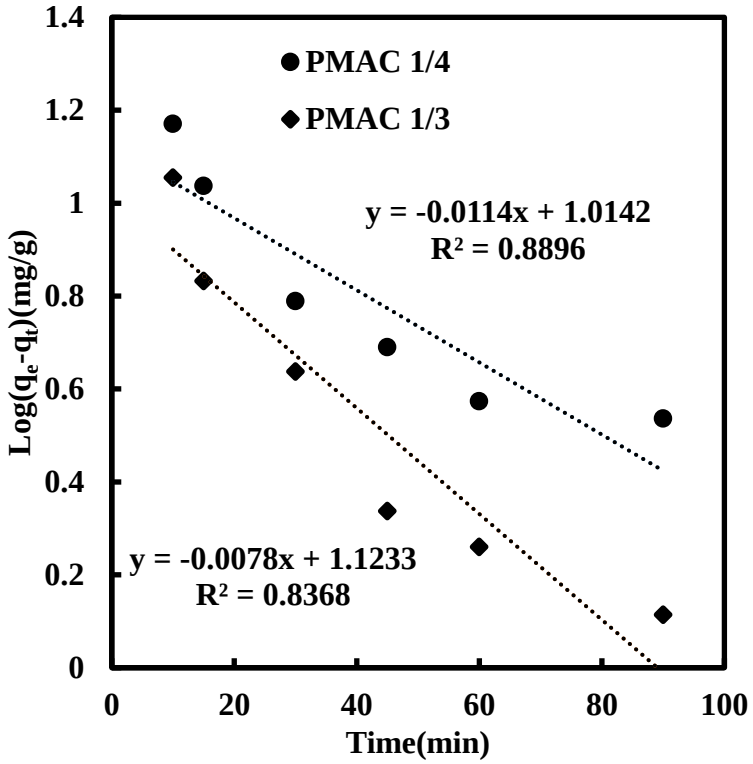

(b)

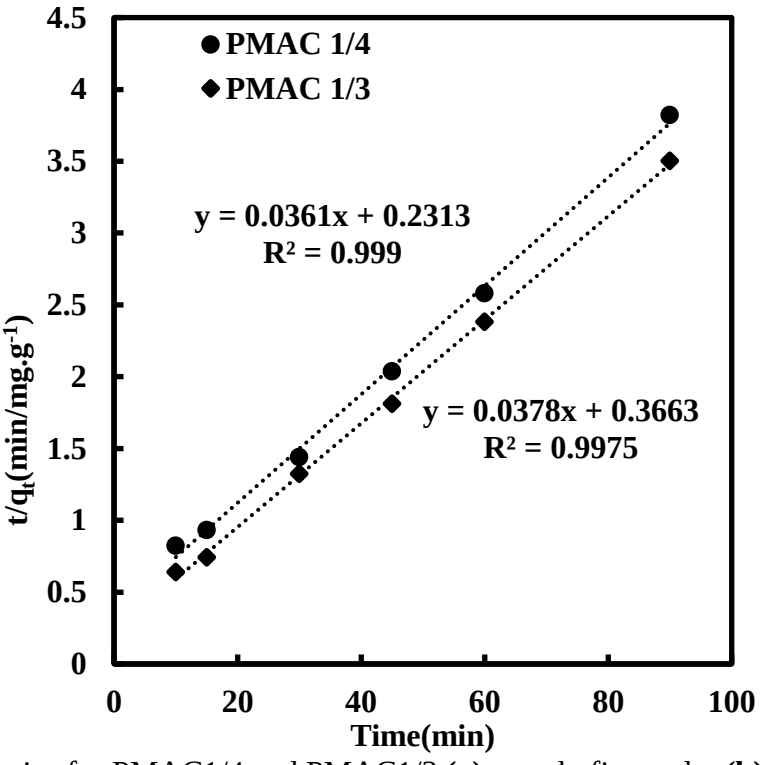

Figure 4.4. Kinetics for PMAC1/4 and PMAC1/3 **(a)** pseudo first order **(b)** pseudo second order kinetics at 303.15 K

The slope and intercept of the linear plot q_t versus $t^{0.5}$ given in **Figure 4.5(a)** were calculated to obtain the intraparticle diffusion coefficient K_{id} and boundary resistance C respectively. Two or more steps control the overall adsorption if the data exhibit multilinear plots and show more than one stages. It is shown in the **Figure 4.5 (a)** that PMAC 1/3 and PMAC 1/4 plots are not linear for the overall range concludes that one or more processes are influencing the adsorption. Hence, the adsorption process follows complex mechanism, consisting of both surface and intraparticle diffusion within the pores of PMAC 1/3 and PMAC 1/4 [137]**.**

The initial and final linear portion indicates the boundary layer diffusion effect (surface adsorption)[136]intraparticle diffusion effect[177] respectively. The nearly parallel final portion of the plots suggests the comparability of rates of adsorption for DBT into the pores of PMACs at all temperatures. Further, to find the slowest step between surface and intraparticle diffusion, the Boyd kinetic expression as given by **equation 4.20** was employed to further examine the kinetic data. The R^2 values of Boyd's plots given in **Figure 4.5 (b),** for both PMAC 1/3 and PMAC 1/4 confirms the linearity of the plot. Thus surface diffusion seems to be the rate controlling step in the adsorption for both PMAC 1/3 and PMAC 1/4. The values of intercept are given in **Table 4.4** depicts that the boundary layer thickness of PMAC 1/4 is greater than PMAC 1/3, thus PMAC 1/4 possess more surface diffusion controlling as compared to that of PMAC 1/3. This conclusion is also well supported by the SEM images of PMAC 1/3 and PMAC 1/4, as shown in **Figure 4.6,** that PMAC 1/3 is more porous in nature and therefore it has lower surface diffusion resistance for DBT molecule to adsorb on the surface than PMAC 1/4. This result also explains the less pore diffusion controlling mechanism for PMAC 1/3.

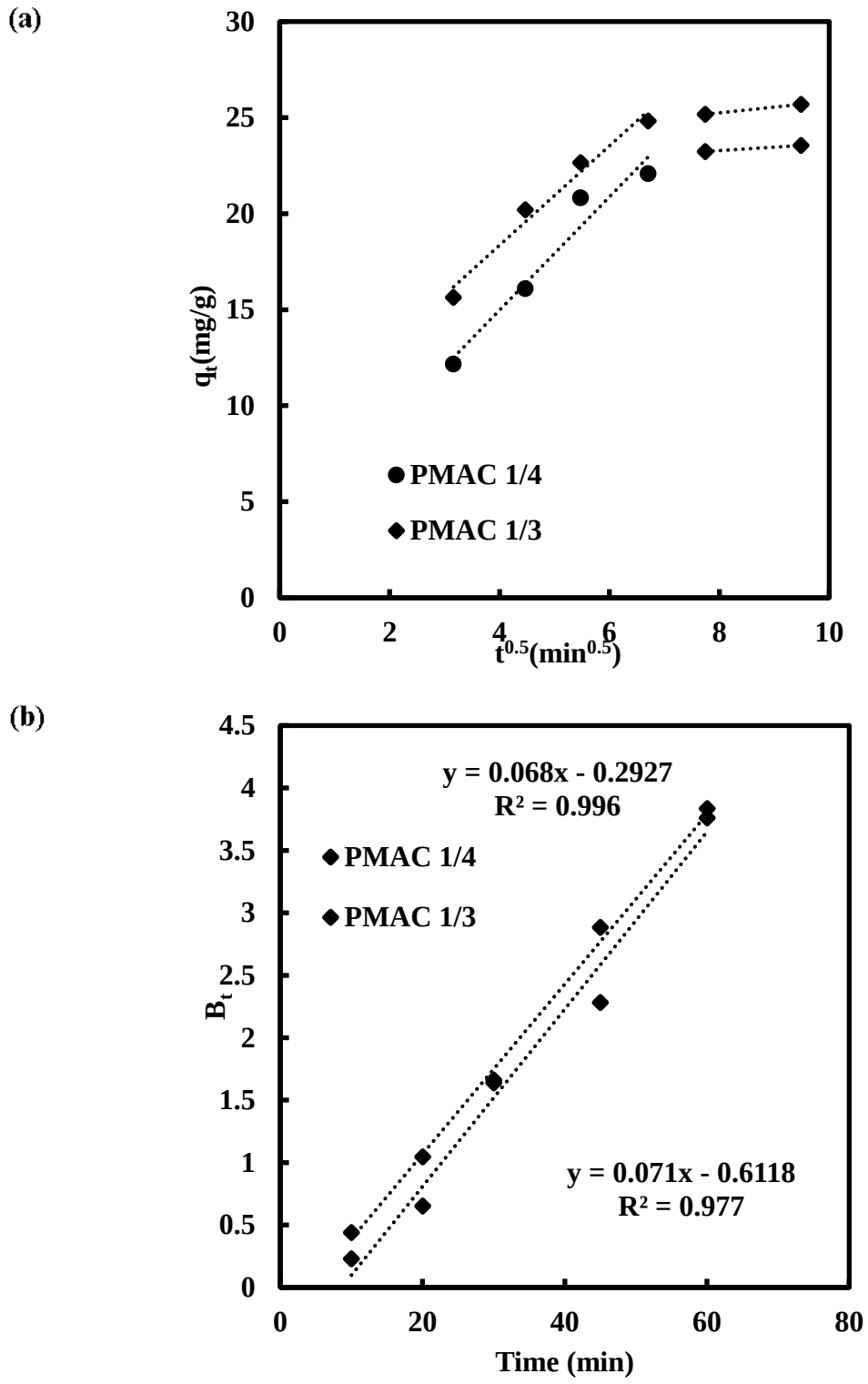

Figure 4.5 Intraparticle diffusion of DBT by **(a)** Weber and Morris Model **(b)** Boyd kinetic model for DBT adsorption.

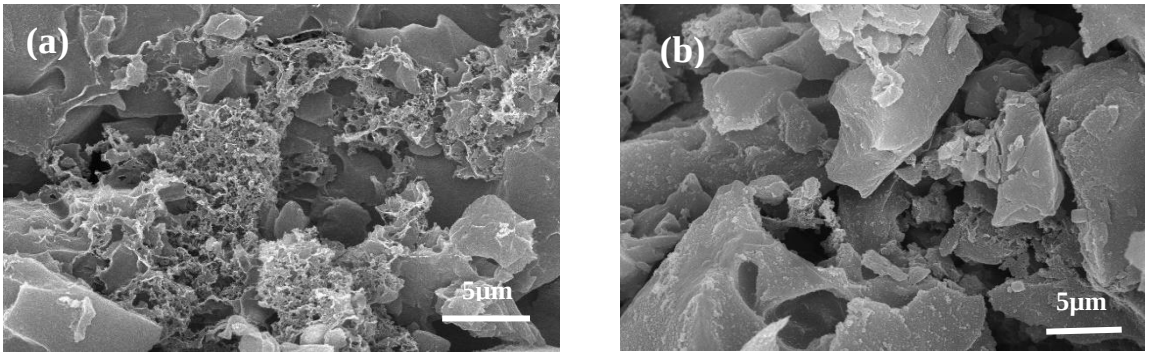

Figure 4.6 (a) DFT pore size distributions of PMACs, SEM images of **(b)** PMAC 1/3 and **(c)** PMAC 1/4

Table 4.4. Intraparticle diffusion parameters for adsorption of DBT on **PMAC 1/3** and **PMAC 1/4** by Weber and Morris model at 303.15 K.

Adsorbent	$\mathbf{k_{id}(mg/g\ min^{0.5})}$	**C(mg/g)**	$\mathbf{R^2}$
PMAC1/4	2.948	3.183	0.949
PMAC1/3	2.586	1.643	0.999

4.3.7 Thermodynamic Studies

The effect of temperature was studied and the results are shown in **Figure 4.7.** It was found that with increasing temperature sulfur removal decreases as shown **Figure 4.7 (a).** The reduction in adsorption of DBT on PMACs with increasing temperature shows the physisorption phenomena. The ΔG° was calculated by using **equation 4.21** whereas ΔH° and ΔS° were determined from the intercept and slope of linear Van't Hoff plot between ln K_d and 1/T shown in **Figure 4.7(b),** which depicts the thermodynamic behavior of adsorption process. The ΔG^0 was evaluated by given equation,

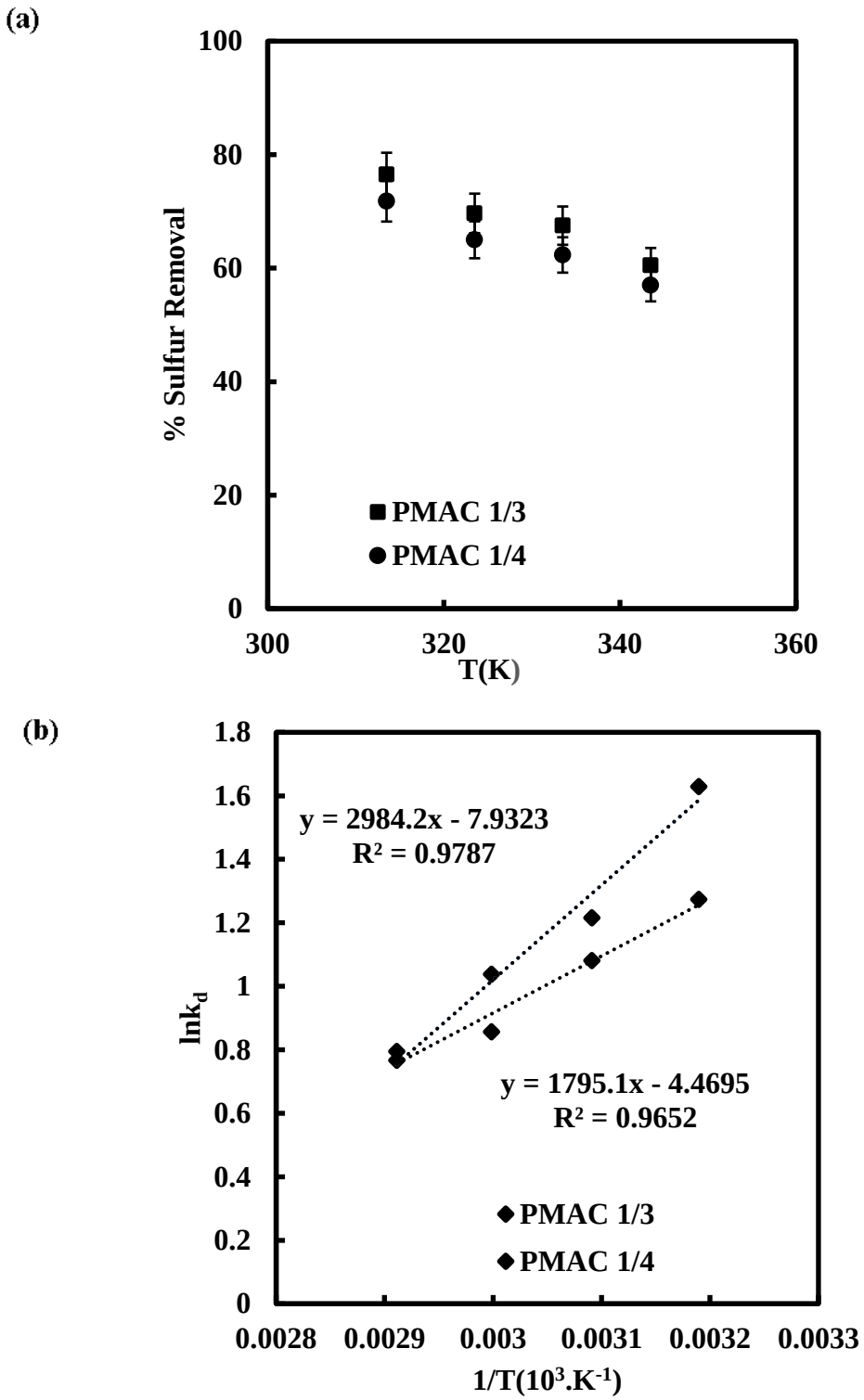

Figure 4.7. (a) Effect of temperature on DBT adsorption on PMAC1/3 and PMAC1/4 **(b)** Modelling for thermodynamic behavior of DBT on PMAC1/3 and PMAC1/4 using Van't Hoff equation.

$$\Delta G^0 = -RT \ln K_d \quad \textbf{(4.21)}$$

$$K_d = \frac{\text{Concentration of DBT adsorbed}}{\text{concentration of DBT remained in the solution}}$$

Where $\Delta G^0$is Change is Gibb's free energy, K_d is distribution coefficient, R is Gas constant and T is temperature in K. The $\Delta H^0$and change in entropyΔS^0 was calculated according to Van't Hoff equation:

$$\ln K_d = \left(\frac{\Delta S^0}{R}\right) - \left(\frac{\Delta H^0}{RT}\right) \quad \textbf{(4.22)}$$

Thermodynamic parameters of the system are shown in **Table 4.5.** The negative value of ΔG° confirms spontaneity and feasibility of the system[175] .The calculated negative values of ΔHº confirm the exothermic nature of the overall-adsorption process. Negative value of ΔS° indicates that decrease in degree of freedom of the adsorbed DBT molecule on PMACs[122,178,179]**.**

Table 4.5. Thermodynamic parameters for the adsorption of DBT on PMAC1/3 and PMAC1/4.

T	**K_d**		**ΔG°(Kcal/mol)**		**ΔH°(Kcal/mol)**		**ΔS° (Kcal/(mol. K))**	
(K)	**PMAC1/3**	**PMAC1/4**	**PMAC1/3**	**PMAC1/4**	**PMAC 1/3**	**PMAC1/4**	**PMAC1/3**	**PMAC1/4**
40	5.099	3.572	-4.244	-3.317				
50	3.372	2.948	-3.267	-2.907	-14.890	-0.037	-24.760	-0.065
60	2.825	2.354	-2.877	-2.372				
70	2.153	2.214	-2.189	-2.269				

4.3.8 Design of batch sorption from isotherm data

The design of single stage batch adsorption system can be predicted by using adsorption isotherm.[125], [141,174,180] A schematic diagram is shown in **Figure 4.8** considering volume of MDF, V (L), the DBT concentration reduces from C_0 to C_1 (mg/L), the DBT loading changes from q_0 to q_1 (mg/g) and the amount of adsorbent is M (mg) was taken . At time t = 0, $q_0 = 0$ and as time passes the mass balance equates the DBT removed from the MDF to that picked up by the solid. The mass balance equation for the system shown in **Figure 4.8(a)** is

$$V (C_0-C_1) = M (q_0-q_1) = Mq_1 \quad \textbf{(4.23)}$$

Under equilibrium Conditions $C_1 \longrightarrow C_e$ $q_1 \longrightarrow q_e$

Since the isotherm studies confirms that the equilibrium data for DBT onto PMAC 1/3 fits well to the Sips isotherm, the Sips isotherm equation can be used to modify the batch adsorber design equation as presented below,

$$\frac{M}{V} = \frac{(C_0 - C_e)}{q_1} = \frac{(C_0 - C_e)}{q_e} = \frac{C_0 - C_e}{\frac{q_m\, b\, C_e^{1/n_s}}{1 + b\, C_e^{1/n_s}}} \quad \textbf{(4.24)}$$

Figure 4.8(b) shows the plot between the predicted amount of PMAC 1/3 required to remove 90, 80, 70, and 60% DBT from MDF of initial concentrations 500 mg/L at different solution volumes (1, 2, 3, 4, 5, 6, and 7 L). The design procedure is defined for a single-stage batch sorption system .For example, the amount of PMAC 1/3 required for the 90% removal of DBT from MDF of concentration 500 mg/L was 97.21, 194.43, 291.64, and 388.84 mg for MDF volumes of 1, 2, 3, and 4 L, respectively.

(a)

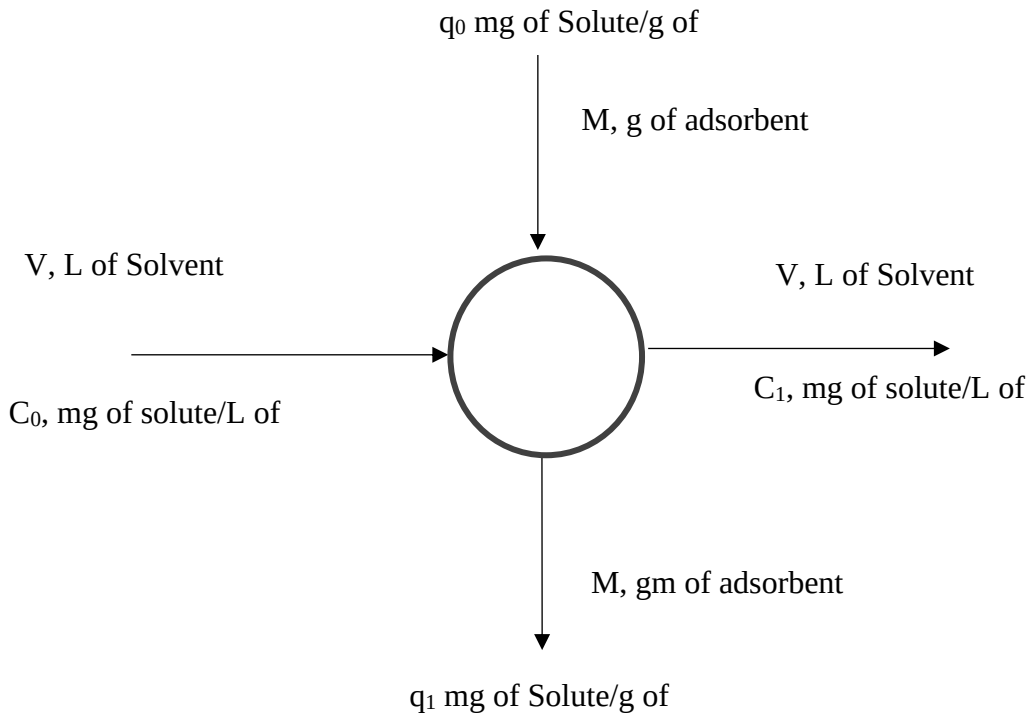

(b)

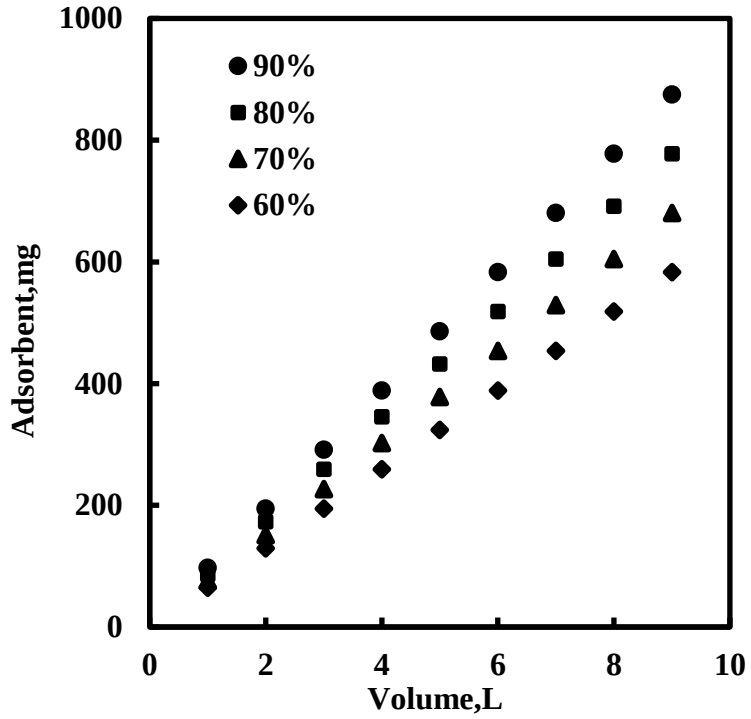

Figure 4.8(a) Single-stage batch-adsorber design for **PMAC 1/3 (b)** Adsorbent mass (M) against volume of solution treated (L) at 303.15 K.

4.4 Conclusion

In this chapter, DBT adsorption capacity of Mongolian anthracite based porous activated carbons (PMACs) have been studied. The study shows that the desulfurization ability of PMAC 1/3 (84.56 mg/g) exhibits better performance compared to PMAC 1/4 (74.25 mg/g). The higher desulfurization capabilities of PMAC 1/3 has direct correspondence with the better micro-porosity. PMAC 1/3 follow Sips and PMAC 1/4 follow Dual Site Langmuir adsorption isotherms model. The diffusion of DBT in PMACs follow complex diffusion model which means both intra-particle and surface diffusions. In addition, DBT adsorption on PMACs follow pseudo second order kinetics. The thermodynamic studies showed that DBT adsorption on PMACs was spontaneous and exothermic process having less randomness at the interface. These results suggests that the Mongolian based activated carbon have potential to use industrially for the adsorptive desulfurization process due to its high adsorptive capacities.

Chapter 5

Batch and Continuous Adsorptive Desulfurization Using Graphene Nanoplatelets

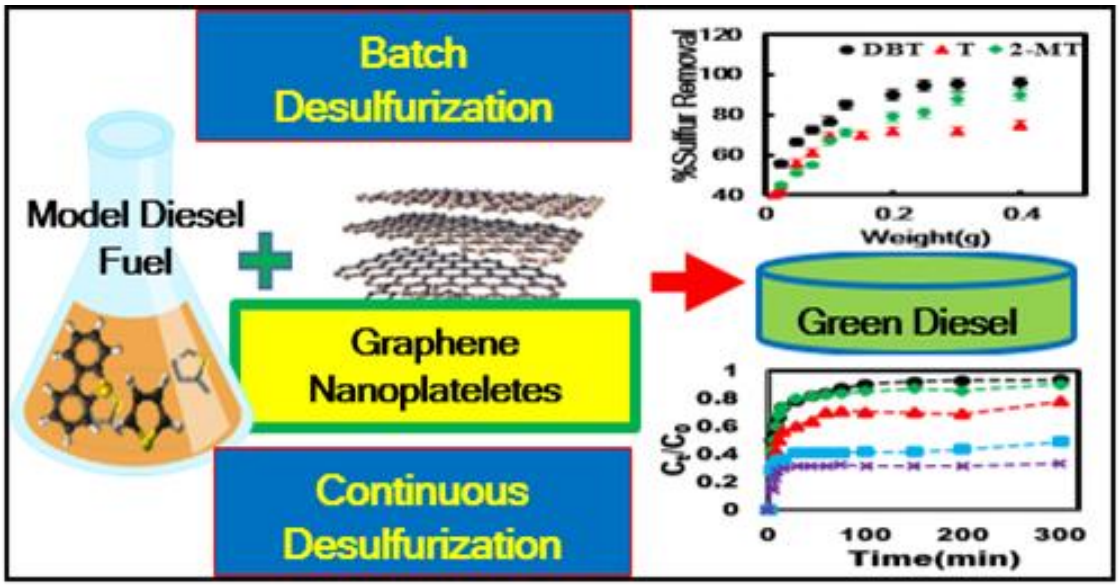

The content of this chapter has been published in

Divyam Jha, Mohd Belal Haider, Rakesh Kumar, Wang Geun Shim, Balathanigaimani Marriyappan Sivagnanam, "Batch and Continuous Adsorptive Desulfurization of Model Diesel Fuels Using Graphene Nanoplatelets*".* ***Journal of Chemical & Engineering Data, 2020,*** *65, 4, 2120–2132* ***.****https://dx.doi.org/10.1021/acs.jced.9b01204.*

5.1 Introduction

The main challenge in adsorptive desulfurization is the choice of the adsorbents which should have high desulfurization capacities and should be thio-selective over olefinic and aromatic compounds at the same time. Several studies on adsorption desulfurization for liquid fuels have been performed with different materials such as zeolites [146,181–183],they have high mechanical and thermal stabilities, and are size-selective for the adsorptive desulfurization, activated carbon, activated aluminas, meso-silicas, silica–zirconia cogel, zeolites, ion exchange resins, Ti-HMSs, Ni-based adsorbents and NiMos, Mesoporous materials(MSU-S) and cobalt,Iron & chromium(Fe_2O_3-MSU-S and CrO_2-MSU-S), cerium, phosphotungstic acid (HPW) and nickel oxide-HPW (NiO-HPW)modified (MSU-S),Acid treated activated carbon. These aluminate silicate mesostructured adsorbent showed significant sulfur removal [184–191].

Graphene is a new captivating adsorbent that has gained the researchers attention in the recent years. The carbon in graphene is sp^2-bonded and a one atom- thick and have two-dimensional layer. Graphene also has remarkable properties, such as excellent electrical, thermal, mechanical, optical properties and have very high specific surface area. In addition, due to delocalized p-electron system which can form strong interaction with S-compounds graphene have shown potential to use as adsorbent for the desulfurization[192–195]. Graphene nanopleteles (GNP) has been used for water pollutant removal and hydrodesulfurization processes [196,197]. Adsorptive desulfurization over GNP has not been investigated as of now.

In this chapter, we have investigated the adsorptive desulfurization using GNP as the adsorbent for the removal of Thiophene (T), 2-Methylthiophene (2-MT) and Dibenzothiophene (DBT) from model diesel fuels (MDFs). To understand the fundamental adsorption process adsorptive

desulfurization was conducted in batch as well as continuous mode. The adsorption capacity of GNP for single component MDFs and multicomponent MDF were studied in detail. The isotherm modelling was done for equilibrium studies. The kinetic and thermodynamic studies were conducted for single component MDFs and later it was compared with the multicomponent system. The process design for the single batch adsorber process has also been studied. Further, the study of adsorption of DBT, 2-MT & T was continued in a fixed bed column for continuous process to obtain breakthrough capacity of the adsorbent bed for different variables .In addition, The Adam –Bohart's model was used for continuous studies.

5.2 Experimental

Materials

N-heptane (Purity>99 %), Thiophene (T), 2-Methylthiophene (2-MT) and Dibenzothiophene (DBT) were purchased as given in **Table 5.1.** Graphene nanoplatelets (GNP) were purchased from Sigma Aldrich. Adsorbents were kept in an oven and dried overnight before using them for the adsorption studies. The physical textural characteristics GNP was obtained using nitrogen adsorption/desorption (Micromeritics ASAP 2010) isotherm data measured at 77 K. The BET equation was considered for the calculation of specific surface area of the adsorbent. Furthermore, the pore size distribution of the adsorbent was obtained based on the DFT method.

Table 5.1 List of Chemicals.

Chemical name	Source	Purity (%)	CAS-number
N-heptane	Spectrochem	>99	142-82-5
Dibenzothiophene	Spectrochem	≥98	132-65-0
2-Methylthiophene	Alfa Aesar	≥98	554-14-3
Thiophene	Alfa Aesar	>98	110-02-1

Methods

5.2.1 Preparation of Model Diesel Fuels (MDF)

Three single component (T, 2-MT and DBT) and a multicomponent model diesel fuels named as MDF_s and MDF_m were prepared. MDF_{sD}, MDF_{sT}, MDF_{sM} contains n-heptane and DBT, T and 2-MT as a sulfur component respectively whereas MDF_m consists n-heptane and T, 2-MT and DBT as sulfur compounds. The single component model diesel fuels (MDF_s) with an initial concentration of 500 ppmw were prepared by separately mixing 0.1982 g of DBT, 0.1370 g of 2 –MT and 0.1046 g of T with 100 mL of n-heptane in three different containers. The multicomponent model diesel fuels (MDF_m) was prepared with a total concentration of 1500 ppm by mixing each 500 ppmw of T, 2- MT & DBT in 100 ml of n-heptane to study the effects of flowrate and bed height on continuous adsorption. MDF_m were also prepared by varying the initial concentrations of T, 2- MT & DBT from 200 to 600 ppmw to investigate the effect of initial concentrations of S compounds on continuous adsorption. Further due to volatile nature of n-heptane, MDF_s and MDF_m were stored in amber vials to avoid change in sulfur concentration as prepared.

5.2.2 Batch adsorption experiments

The adsorption studies of DBT, 2-MT and T on GNPs were conducted at 30 °C and 400 rpm to investigate the effect of dosage by varying the adsorbent amounts from 0.025-0.4 g. A fixed volume of 20 mL MDFs was used for all these batch adsorption studies. All adsorption experiments were performed in an Incubator Shaker (*BR Biochem*) for 60 min, except for the kinetic studies. In case of kinetic studies, the experiments were carried out to the specified time and then the specific sample container itself was taken out for samples collection. This phenomena was chosen for not to disturb the fuel to adsorbent ratio in the middle of experiments.After each adsorption studies, the adsorbent was filtered out using a Whatman paper.

The concentrations of T, 2-MT & DBT in the desulfurized samples were analyzed by Gas Chromatograph equipped with flame ionization detector (Perkin Elmer Claurs 580 GC-FID detector). GC is equipped with Elite-1 column having length of 50m and inner diameter of 200 µm. Helium gas was used as carrier with constant 1 cm^3/min of flow rate. Injector temperature was kept at 340 °C with sample injection volume of 1 µL. The oven temperature was varied from 50 °C to 350 °C increasing the heating rate of 3 °C / min.

The amount of sulfur adsorbed q_e (mg-S/g-A), is given by the equation (5.1),

$$q_e = \frac{V}{W} \times (C_0 - C_e) \quad \textbf{(5.1)}$$

where C_e and C_0 are the equilibrium and initial concentration of sulfur for W gram of adsorbent and V(l) volume of the MDF. The % sulfur removal is given by the equation,

$$\% \text{ Sulfur Removal} = \frac{(C_0 - C_e)}{C_0} \times 100 \quad \textbf{(5.2)}$$

5.2.3 Continuous adsorption experiments

In order to discover the adsorption capacity of GNP, dynamic adsorption experiments were carried out by flowing MDF_m through a fixed bed adsorber of 1 cm diameter at 30 °C. To conduct the dynamic adsorption experiments a vertical custom made glass adsorber was used. A glass adsorption column loaded with 3 -10 g of GNP was used for this continuous study. The adsorbent sample was loaded with the support of glass wool. The bottom section of the column was connected with peristaltic pump and a feed tank. MDF_m was fed from of the column in upward direction continuously at different flow rates (0.5-3.0 ml/min) as given in **Figure 5.1.** The MDF_m passed through the adsorbent bed and the samples were collected at regular interval of 5 min till the bed was saturated. The sulfur present in MDF was analyzed using GC-FID after desulfurization. Further, the adsorption breakthrough curves were obtained by normalizing the plot of amount of sulfur adsorbed vs. cumulative time. **Table 5.2** summarizes the experimental conditions used for these experiments.

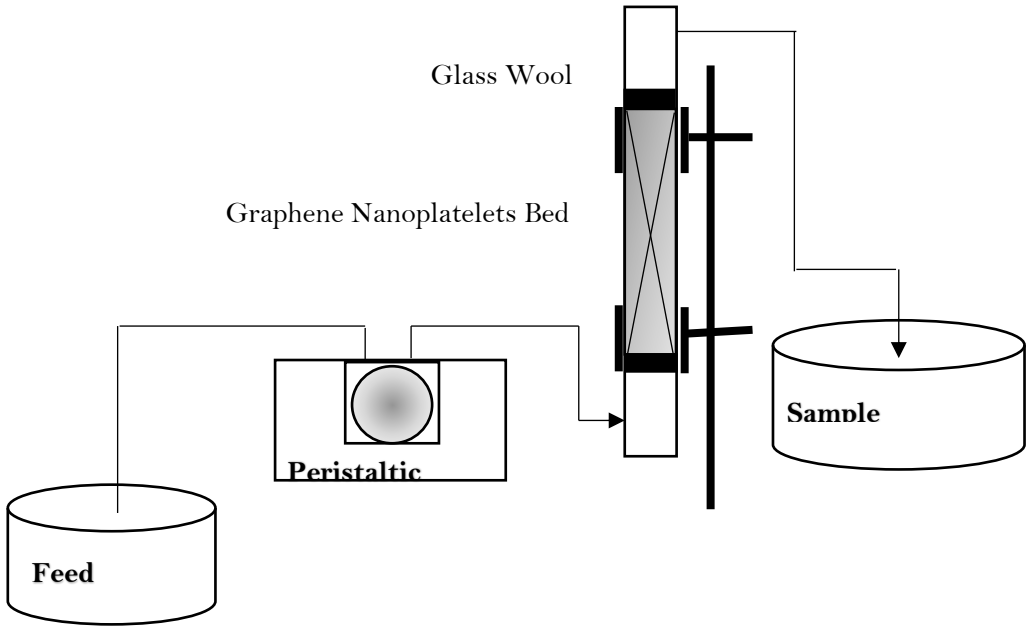

Figure 5.1 Schematic Experimental setup for the fixed-bed adsorption process

Table 5.2 Experimental conditions for fixed bed column experiments.

Adsorbent	GNP
Temperature Ambient	25 °C
Pressure	1 atm
Adsorbent dose	3–10 g
MDFm flow rate	0.5–3.0 mL/min
Inlet sulfur content	1500 ppmw
Diameter of column	1 cm
Height of bed	3–10 cm

5.3 Results and discussions

5.3.1 Physical Properties of adsorbent

The isotherms for adsorption/desorption of nitrogen on GNP at 77 K are given in **Figure 5.2(a).**The DFT result of GNP is shown in **Figure 5.2(b).** The surface area, average pore size and total pore volume values of GNP are 635 m^2/g, 3.34 nm and 0.24 cm^3/g respectively.

5.3.2 Equilibrium studies and adsorption isotherm

The adsorption of T, 2-MT and DBT on GNP was studied in batch mode. Adsorbent dosage effect on the desulfurization capacity was studied by mixing 500 mg/l sulfur solution at 30°C. The adsorbent dosage was varied from 0.025-0.4 g for 20 ml of MDF shown in **Figure 5.3** and **Table 5.3** to obtain the optimum condition **e**quilibrium studies were conducted for removal of T, 2- MT and DBT over GNP. It can be observed that at equilibrium adsorption capacity reaches maximum after which there was no further change in the sulfur

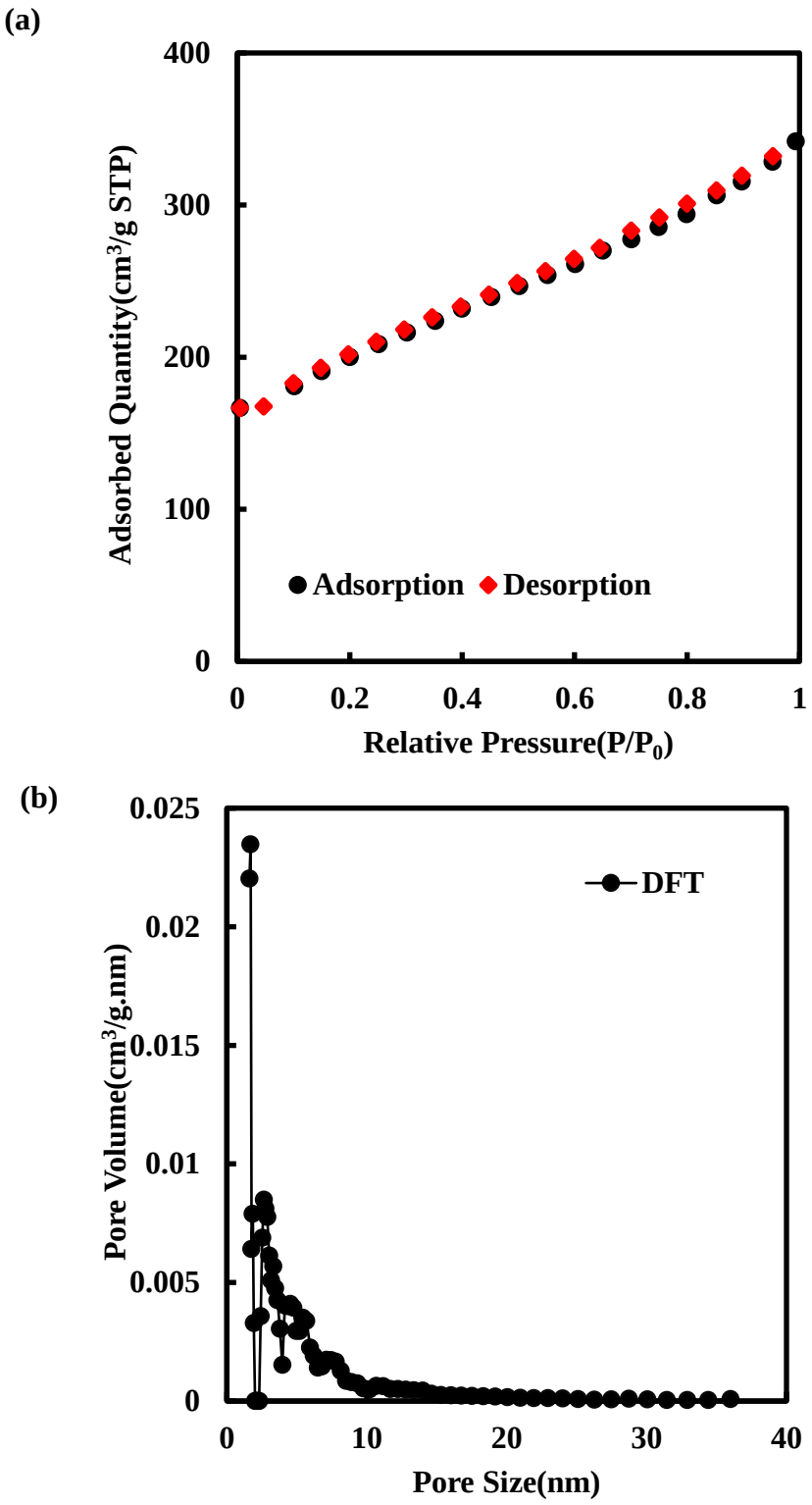

Figure 5.2(a) Nitrogen adsorption-desorption isotherm for GNP at 77 K **(b)** DFT Pore size distribution curve.

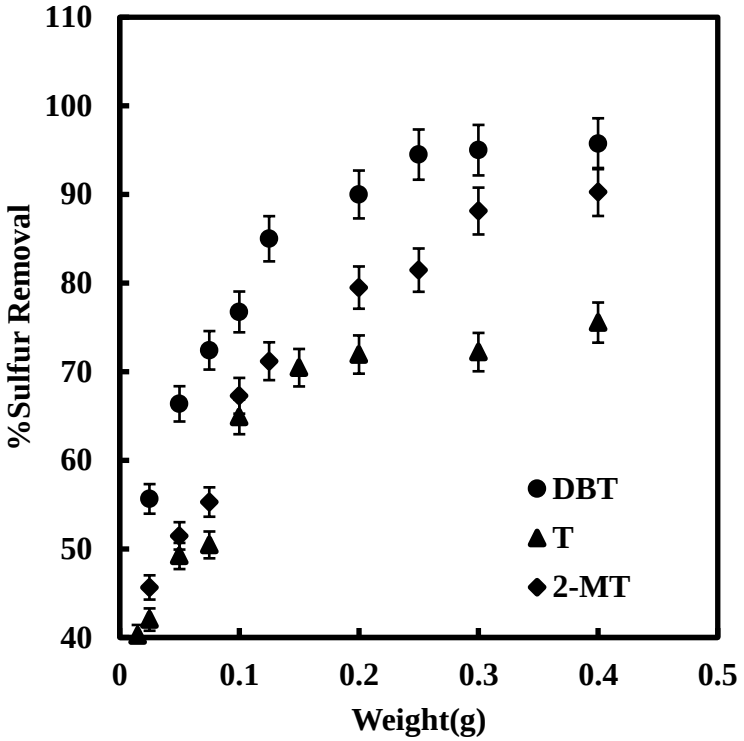

Figure 5.3 Effect of adsorbent weight on sulfur removal

(Temperature = 30°C, Initial Sulfur Concentration = 500 ppm, Time= 60 min)

concentration. Langmuir equation was used to correlate the data obtained by experimental adsorption. The Langmuir isotherm equation is given below[119]

$$q_e = \frac{q_m \mathbf{b} C_e}{1 + q_m \mathbf{b} C_e} \qquad \textbf{(5.3)}$$

Where q_m and b signifies the maximum sulfur adsorbed (mg/g) at saturation and affinity of adsorption, respectively.

Freundlich isotherm is applied for multilayer adsorption and for adsorbents with heterogeneous surfaces. It is given by the equation [120]

$$q_e = K_F C_e^{1/n_f} \quad \textbf{(5.4)}$$

Table 5.3 Sulfur removal efficiency for different Adsorbent/MDF ratio

Adsorbent/ 20 ml of MDF (wt-g)	**% Sulfur Removal**		
	DBT	**2-MT**	**T**
0.025	55.64	45.65	35.01
0.050	66.37	51.47	37.22
0.075	72.41	55.29	40.21
0.100	76.74	67.28	42.02
0.125	85.00	71.18	49.20
0.200	90.00	79.49	50.45
0.250	94.50	81.46	64.89
0.300	95.00	88.13	70.45
0.400	95.72	90.28	71.93

n_f and K_F are the Freundlich constant and adsorption coefficient (mg/g) (L/mg) respectively. The higher the adsorbent heterogeneity larger will be the value of n_f.

With increasing time DBT, 2-MT & T removal was also increased till 60 minutes and then becomes constant. Therefore, the optimum time for desulfurization is 60 minutes. In addition, with increasing adsorbent dosage from 0.025-0.4 g the adsorption capacity also increases[181]. The adsorption by GNP was observed to be 95.7%, 90.1 and 75 % for DBT, 2-MT& T and adsorptive capacity was 98 mg/g, 80 mg/g, and 58 mg/g, respectively. These results are comparable with the desulfurization efficiency previously reported [198–200]. **Figure 5.4** shows that **t**he adsorption equilibrium data for DBT, 2-MT & T on GNP. As shown in the figure, the experimental results of DBT were correlated well with Langmuir isotherm. The

goodness of fit of predicted and experimental data was analyzed using R^2, χ^2, and RMSE. The value so obtained is given in **Table 5.4**[136].

Table 5.4 The adsorption isotherm parameters.

Isotherms	**Adsorption Parameters**		
	DBT	**2-MT**	**T**
Langmuir	q_m=181.650 (mg/g)	q_m=268.500(mg/g)	q_m=360.10E-02(mg/g)
	b=0.004(g/mg)	b =0.002(g/mg)	b =4.79E-07
	R^2=0.986	R^2=0.943	R^2=0.955
	χ^2= 6.770	χ^2= 4.680	χ^2=3.760
	RMSE= 5.790	*RMSE*= 5.278	*RMSE*=2.690
Freundlich	K_F=3.010	K_F =0.151	K_F =0.088
	n_F = *1.61*	n_F =0.835	n_F =0.893
	R^2=0.948	R^2=0.989	R^2=0.995
	χ^2= 8.270	χ^2=1.090	χ^2=1.670
	RMSE=7.520	*RMSE*=2.760	*RMSE*=0.965

5.3.3 Kinetic Studies

The effect of contact time on the removal of T, 2-MT, and DBT adsorbed was investigated at a constant temperature of 30°C. It can be observed that adsorption increases with increasing contact time and also the maximum adsorption was obtained at 60 min as shown in **Figure 5.5.** On the further increasing time, there was no significant increase in the adsorption. This can be explained due to a large number of active sites are available for the adsorption of sulfur compounds initially, which decreases with time due to the adsorption of adsorbate on the active sites which leads to a reduction in the sulfur removal rate. Further, the initial stage of the adsorption of the molecules happens at the macropores and mesopores and followed by the

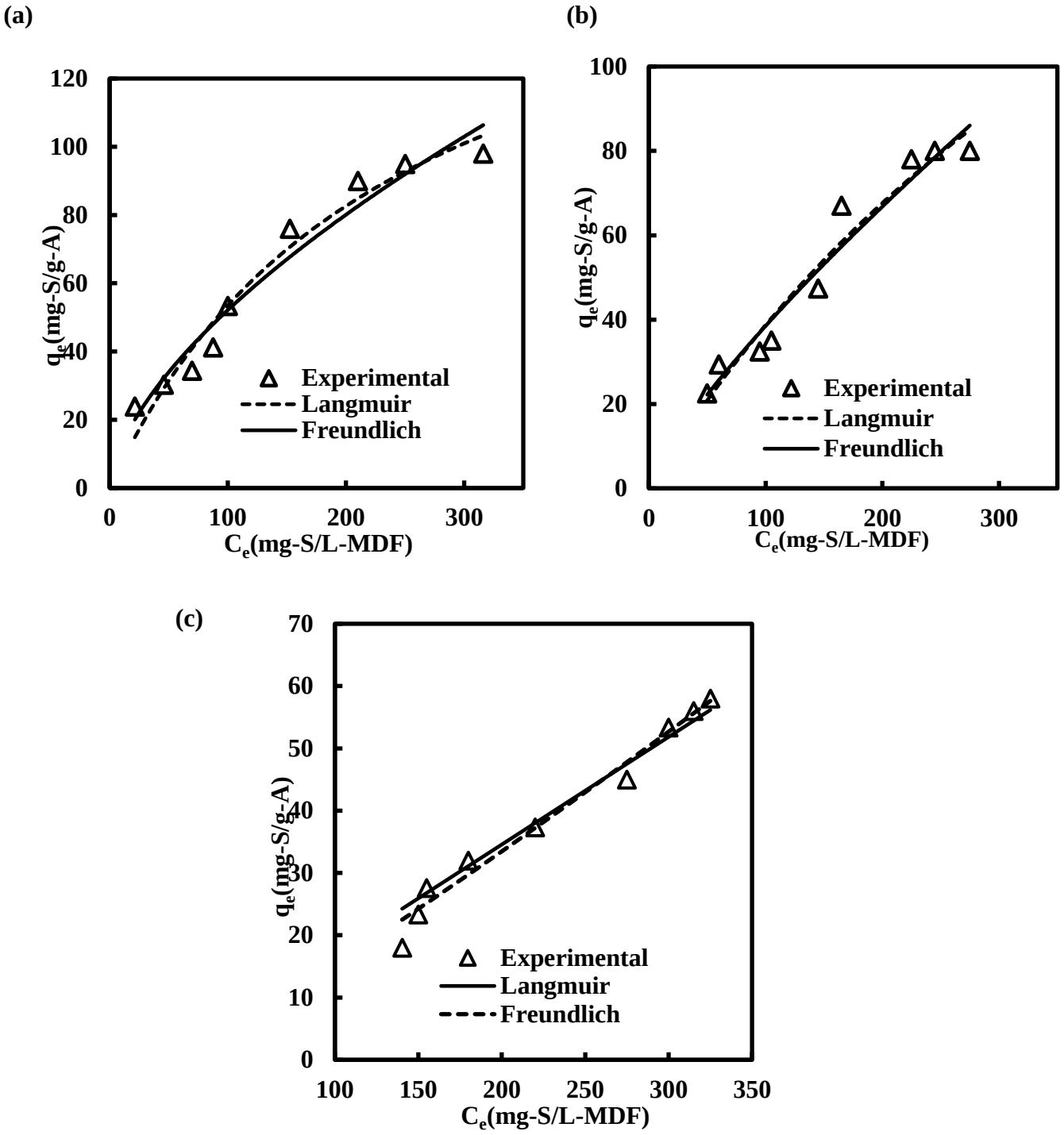

Figure 5.4 Adsorption isotherms on GNP of **(a)** DBT **(b)** 2-MT and **(c)** T

deeper penetration of molecules into the micro-pores of the adsorbent. Therefore, it is observed in this study that the sulfur removal rate was reduced mainly due to the increase in the

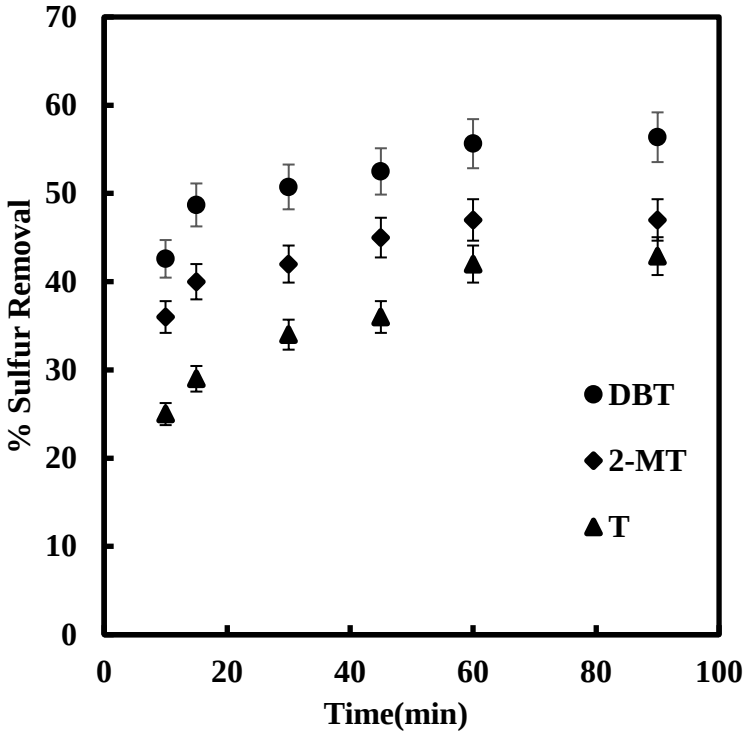

Figure 5.5 Effect of Time on Sulfur Removal.

(Temperature = 30°C, Initial Sulfur Concentration = 500 ppm, Adsorbent weight= 0.01 g)

resistance to the molecule diffusion[201–203]. Therefore 60 minutes has been chosen as equilibrium contact time.

The adsorption rate slows down after the S-compounds saturates the meso and micro-pores, which may be due to the microspores experience larger resistance in the later stage when the S molecules move further[179].

For interpreting the experimental data, the first-order equation, the pseudo second-order equation, and an intraparticle diffusion equation was studied. The pseudo first-order kinetics is given by[122,123],

$$q_t = q_e(1 - e^{-k_1 t}) \quad \textbf{(5.5)}$$

Similarly, pseudo second order kinetic is given by,[124]

$$q_t = \frac{(k_2 q_e^2 . t)}{1 + (k_2 q_e . t)} \quad \textbf{(5.6)}$$

Where k_1, k_2 is t pseudo-first order and second order rate constant and q_t is the adsorption at time *t*.

Boyd's surface diffusion model and Weber's intraparticle diffusion were used to predicting the diffusion mechanism [126]. The intraparticle controlled diffusion mechanism is given by

$$q_t = k_{id} t^{1/2} + C \quad \textbf{(5.7)}$$

Where C and K_{id} and is the boundary layer thickness and intraparticle diffusion coefficient (mg/g (min) $^{0.5}$), respectively. Boyd's kinetic expression is given by

$$B_t = -0.4977 - \ln(1 - F) \quad \textbf{(5.8)}$$

$$F = 1 - \frac{6}{\pi^2} \exp(-B_t) \quad \textbf{(5.9)}$$

$F = \frac{q_t}{q_e}$

Where F is the equilibrium attained in the fraction.

MDF containing DBT, 2-MT & T concentration 500 ppm were kept in contact GNP for a range of time 10-90 min. The adsorption rates attain equilibrium at 60 min. The adsorption rate increases rapidly initially due to available free sites for adsorbates to adsorb on the surface. Adsorption slows down at equilibrium due to the few available sites and the mutual repulsive forces between the adsorbate present in the solution and adsorbent surface[204]. The kinetics involved to remove DBT,2-MT & T by GNP was investigated using linear plots of log (q_e-q_t) versus t for the pseudo first-order and t/qt versus t for the pseudo second-order kinetic model

as shown in **Figure 5.6**. The kinetic parameters obtained are given in **Table 5.5(a) and (b).** The kinetic controlling behavior of the system was analyzed using regression coefficient (R^2), average relative error (ARE) and normalized standard deviation (NSD). This error analysis shows DBT, 2-MT & T removal by GNP follows pseudo second order kinetics.

The K_{id} and C values are the slope and intercept respectively of the plot between q_t and $t^{0.5}$ as shown in **Figure 5.7(a).** The figure shows that the plot is multilinear which means that the overall adsorption process is controlled by two or more steps. It can be observed from **Figure 5.7(a)** that DBT, 2-MT & T plots are multilinear concluding that both intraparticle transport and surface diffusion control the adsorption process [137].

The slowest step between the surface and intraparticle diffusion was predicted by Boyd's kinectic expression. The linearity of the plot in **Figure 5.7(b)** is confirmed by high R^2. This means that for DBT, 2-MT & T adsorption surface diffusion is the controlling factor. Further, **Table 5.5(c)** shows that the boundary layer thickness of DBT is greater than 2-MT & T, thus adsorption of DBT on GNP possess more surface controlling compared to 2-MT & T.

(a)

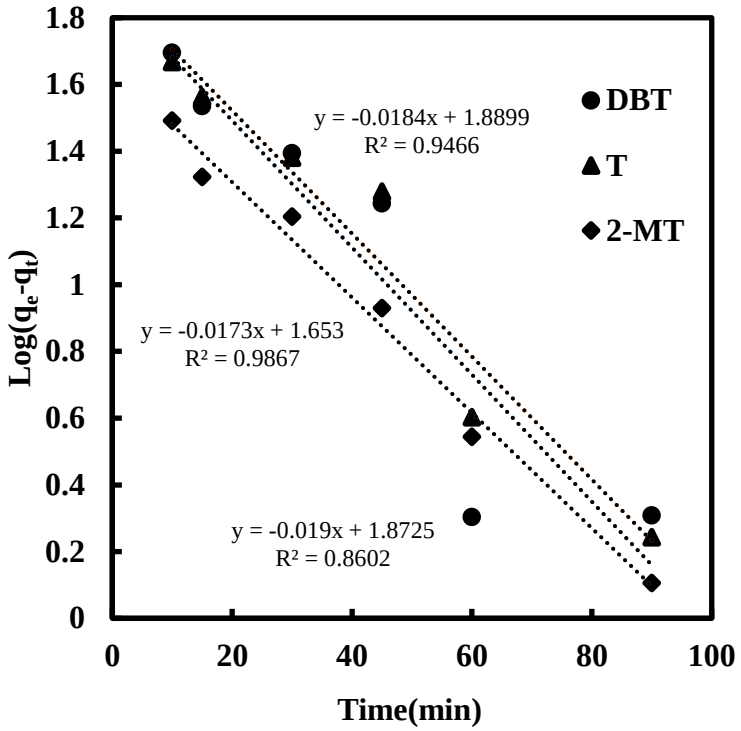

(b)

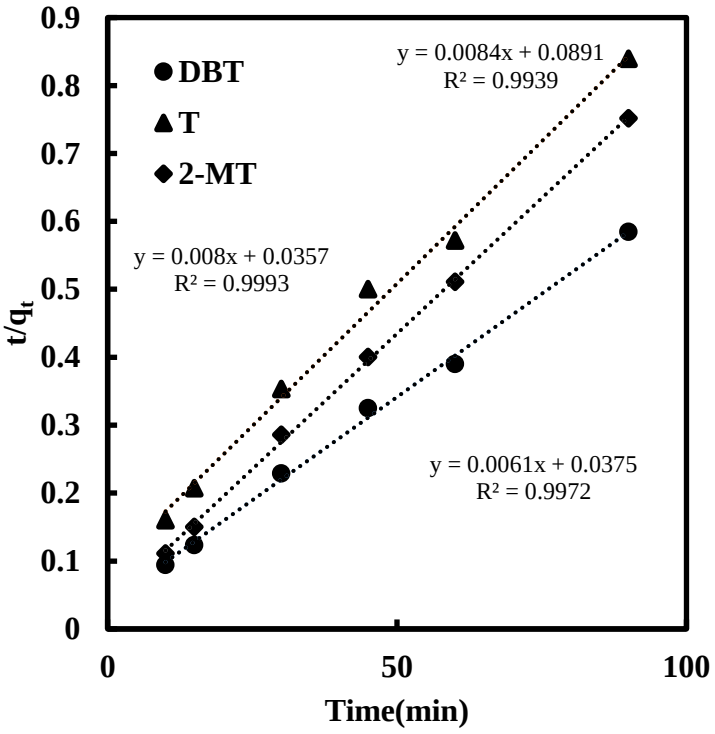

Figure 5.6 Kinetics for DBT, 2-MT & T **(a)** pseudo first order **(b)** pseudo second order model.

(a)

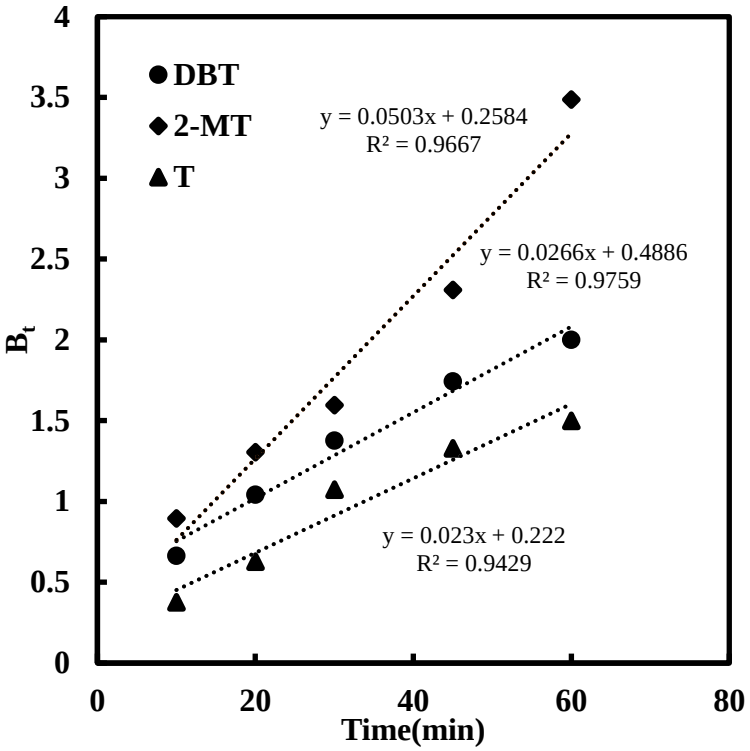

(b)

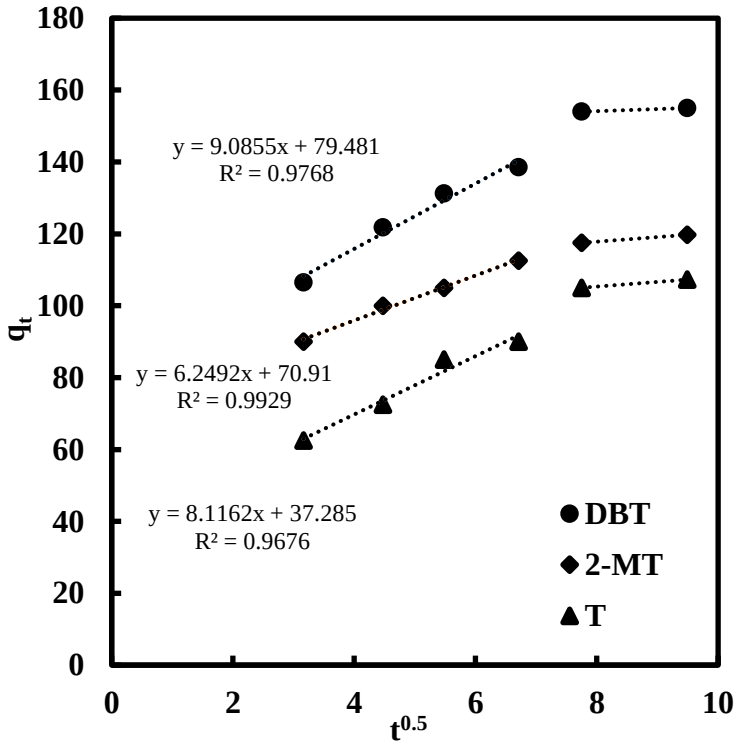

Figure 5.7 (a) Intraparticle diffusion of DBT, 2-MT, & T by the (a) Weber and Morris model and the **(b)** Boyd kinetic model.

Table 5.5 (a) Parameters for kinetics of pseudo 1st order model for the adsorption of **DBT, 2-MT & T** on GNP**.**

	k_1	Qe (mg/g)		R^2	NSD	ARE
	(1/min)	Calculated	Experimental			
DBT	0.044	6.504	153.970	0.860	68.540	1.654
2-MT	0.039	5.220	107.250	0.986	45.430	8.384
T	0.042	6.615	119.250	0.946	11.650	2.712

Table 5.5 (b) Parameters for kinetics of pseudo 2nd order model for the adsorption of **DBT, 2-MT & T** on GNP**.**

	k_2	Qe (mg/g)		R^2	NSD	ARE
	(g/mg min)	Calculated	Experimental			
DBT	9.920E-04	163.930	153.970	0.997	21.720	0.005
2-MT	8.792E-04	125.010	107.250	0.998	29.690	1.923
T	5.495E-04	114.940	119.250	0.993	5.920	0.884

Table 5.5(c) Intraparticle diffusion parameters for adsorption of **DBT, 2-MT & T** on GNP by Weber and Morris model.

	k_{id}(mg/g $min^{0.5}$)	C(mg/g)	R^2
DBT	9.085	79.480	0.976
2-MT	6.249	70.910	0.992
T	8.116	37.285	0.967

5.3.4 Error Data Analysis

The error functions were evaluated using residual root mean square error **(RMSE)**, coefficient of regression **(R^2)**, and chi-square test **(χ^2)** were employed to check fitness of models. The empirical equations are as follows:

$$R^2 = \frac{1 - \sum_{n=1}^{n}\left(q_{e,n} - q_{m,n}\right)^2}{\sum_{n=1}^{n}\left(q_{e,n} - \overline{q_{e,n}}\right)^2} \quad \textbf{(5.10)}$$

$$RMSE = \sqrt{\frac{1}{n-1}\sum_{n=1}^{n}\left(q_{e,n} - q_{m,n}\right)^2} \quad \textbf{(5.11)}$$

$$\chi^2 = \sum_{n=1}^{n}\frac{\left(q_{e,n} - q_{m,n}\right)^2}{q_{e,n}} \quad \textbf{(5.12)}$$

$$NSD = 100 \times \sqrt{\frac{1}{N-1}\sum_{i=1}^{N}\left[\frac{q_{t,e} - q_{t,m}}{q_{t,e}}\right]_i}^2 \quad \textbf{(5.13)}$$

$$ARE = \frac{100}{N}\sum_{i=1}^{N}\left[\frac{q_{t,e} - q_{t,m}}{q_{t,e}}\right]_i \quad \textbf{(5.14)}$$

Where $q_{t,m}$ and $q_{t,e}$ are model predicted and experimental amount of sulfur adsorbed on GNP.

5.3.5 Thermodynamic Parameters

To spontaneity of the process was determined by taking into consideration of energy and entropy. These parameters give the practical viability of the process. To determine the thermodynamic parameters, adsorption at different temperatures (20, 30, 35, and 40 ◦C) were conducted for the adsorption system, DBT, 2-MT & T.

The effect of temperature on the adsorption is shown in **Figure 5.8 (a).** It can be observed that with increasing temperature the sulfur removal decreases**.** This shows the physisorption behavior of DBT, 2-MT & T adsorption on GNP. Using **equation 5.15.** The change in Gibb's free energy was calculated. Van't Hoff plot was generated to determine the change in enthalpy and entropy were as shown in **Figure 5.8 (b).** The Gibbs free energy (ΔG^0) change was calculated by

$$\Delta G^0 = -RT \ln K_d \qquad \textbf{(5.15)}$$

$$K_d = \frac{\text{Concentration of S} - \text{compound adsorbed}}{\text{concentration of S} - \text{compound remained in solution}}$$

Where ΔG^0 is in (KJ/mol), R is in KJ/Kmol.K. K_d is distribution coefficient and T is the temperature in K. The Van't Hoff equation is given by:

$$\ln K_d = \left(\frac{\Delta S^0}{R}\right) - \left(\frac{\Delta H^0}{RT}\right) \qquad \textbf{(5.16)}$$

The thermodynamic parameters of the system are shown in **Table 5.6.** The value of ΔG^0 lies in between −20 and 0 kJ mol^{-1} for physisorption and −80 to −400 kJ mol^{-1} for chemisorption[205]. The feasibility of the system is checked by the negative value of ΔG°. The exothermic behavior of the adsorption process is confirmed by the negative values of ΔH^o.

(a)

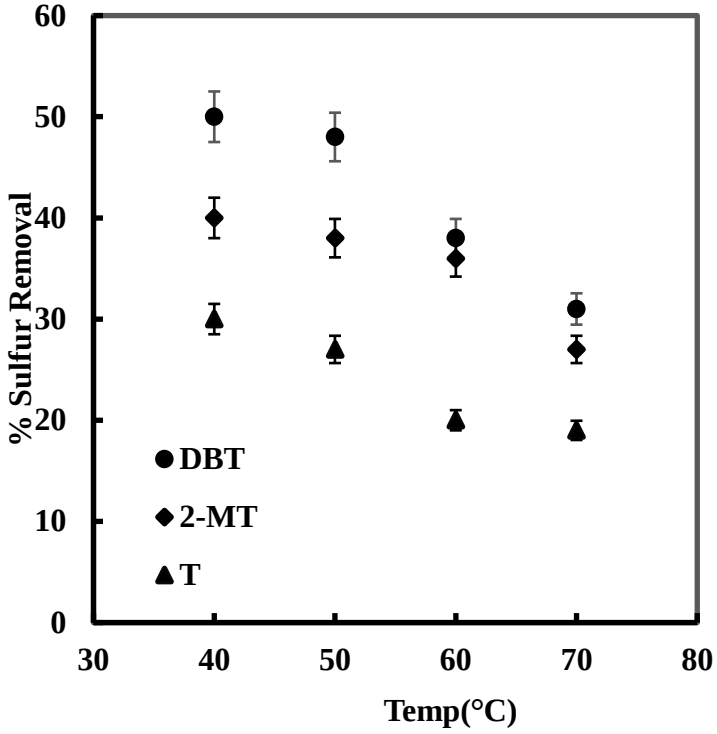

(b)

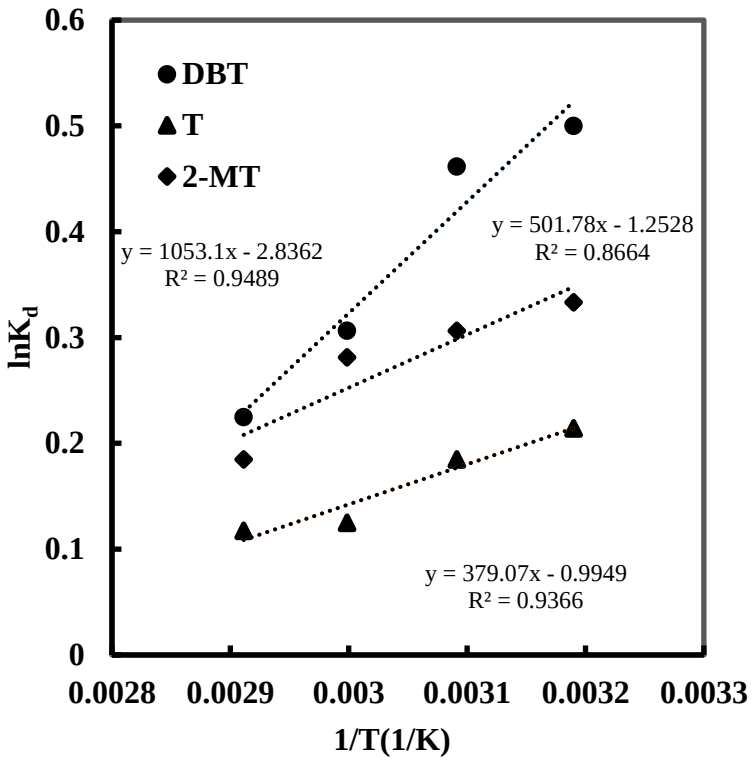

Figure 5.8 (a) Effect of temperature on DBT, 2-MT and T adsorption on GNP **(b)** Modelling for thermodynamic behavior of DBT, 2-MT and T on GNP using Van't Hoff equation.

(Temperature = 30°C, Initial Sulfur Concentration = 500 ppm, Adsorbent weight = 0.01g)

Table 5.6 Thermodynamic parameters for the adsorption of DBT, 2-MT & T on GNP.

T (°C)	K_d			ΔG°(kJ/mol)			ΔH°(kJ/mol)			ΔS° (kJ/(mol.	
	DBT	2-MT	T	DBT	2-MT	T	DBT	2-MT	T	DBT	2-M
40	1.648	1.395	1.238	-1.302	-0.868	-0.558					
50	1.586	1.358	1.203	-1.241	-0.824	-0.497	-8.751	-4.169	-3.150	-0.024	-0.01
60	1.358	1.324	1.133	-0.849	-0.779	-0.346					
70	1.252	1.203	1.124	-0.641	-0.527	-0.334					

The negative value of ΔS° indicates a decrease in the degree of freedom of the adsorbed DBT, 2-MT & T molecule on GNP. Hence the systems show non-random adsorption behavior. The change in enthalpy for DBT (-8.751 kJ/mol), 2-MT (-4.169 kJ /mol) & T (-3.15 kJ /mol) indicate that the adsorption is following physisorption behavior. The lower ΔH^0 value implies that the adsorbate molecules and the adsorbent surface is weak.[140,206,207]

5.3.6 Design of batch sorption from isotherm data

For designing a single batch system adsorption isotherm was used[141,142,180]. The single stage batch adsorption system schematic is shown in **Figure 5.9(a).** Consider MDF of volume V (L) and the DBT concentration reduces from C_0 to C_1 (mg/L). The adsorbent dosage is M (mg) and the s-loading changes from q_0 to q_1. Initially, $q_0 = 0$ and as time pass mass balance equates the s-compound removed from MDF by adsorption. The mass balance for **Figure 5.9(a)** is given by

$$V (C_0-C_1) = M (q_0-q_1) = Mq_1 \quad \textbf{(5.17)}$$

At equillibrium C_1 approaches C_e and q_1 approaches q_e.

(a)

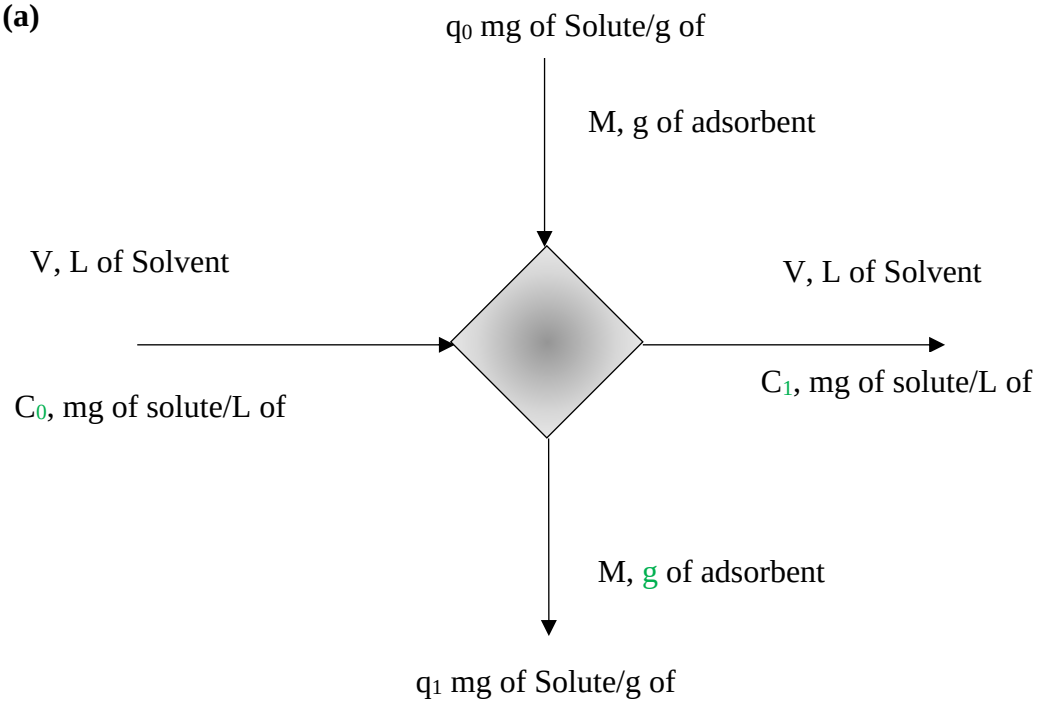
q_0 mg of Solute/g of
M, g of adsorbent
V, L of Solvent
V, L of Solvent
C_1, mg of solute/L of
C_0, mg of solute/L of
M, g of adsorbent
q_1 mg of Solute/g of

(b)

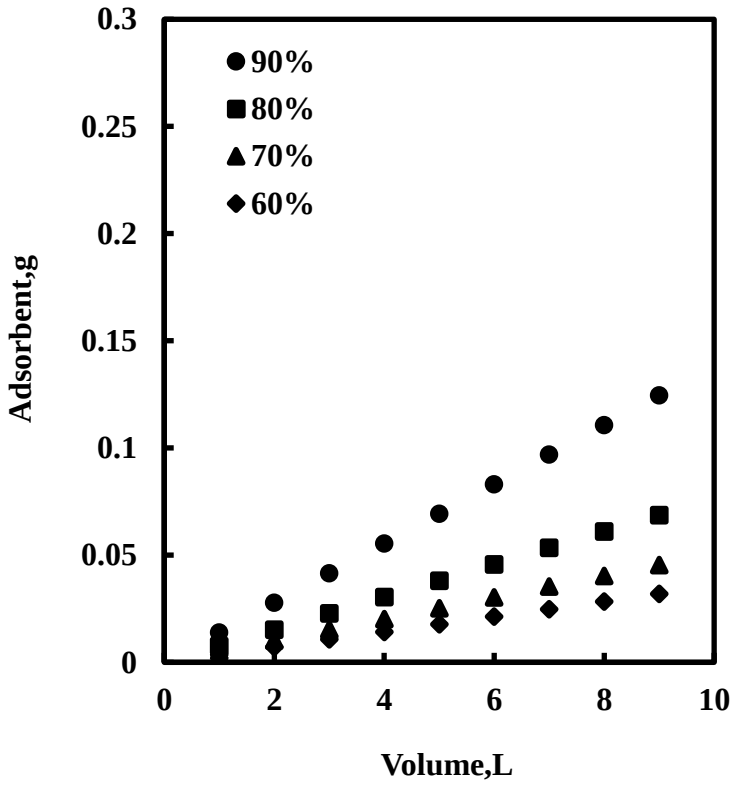
90%
80%
70%
60%
Adsorbent,g
Volume,L
0.3
0.25
0.2
0.15
0.1
0.05
0
0
2
4
6
8
10

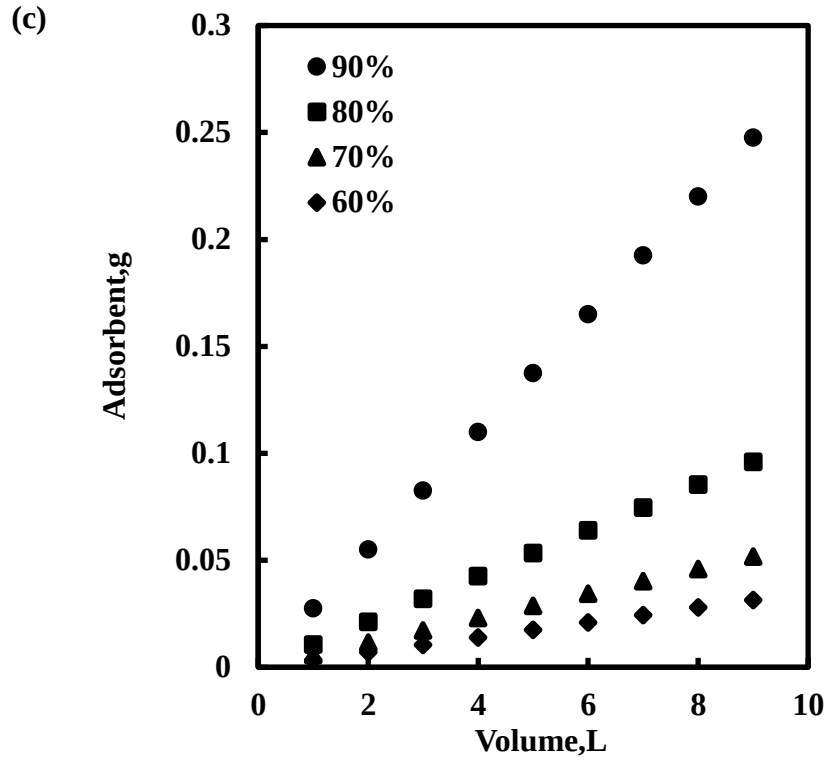

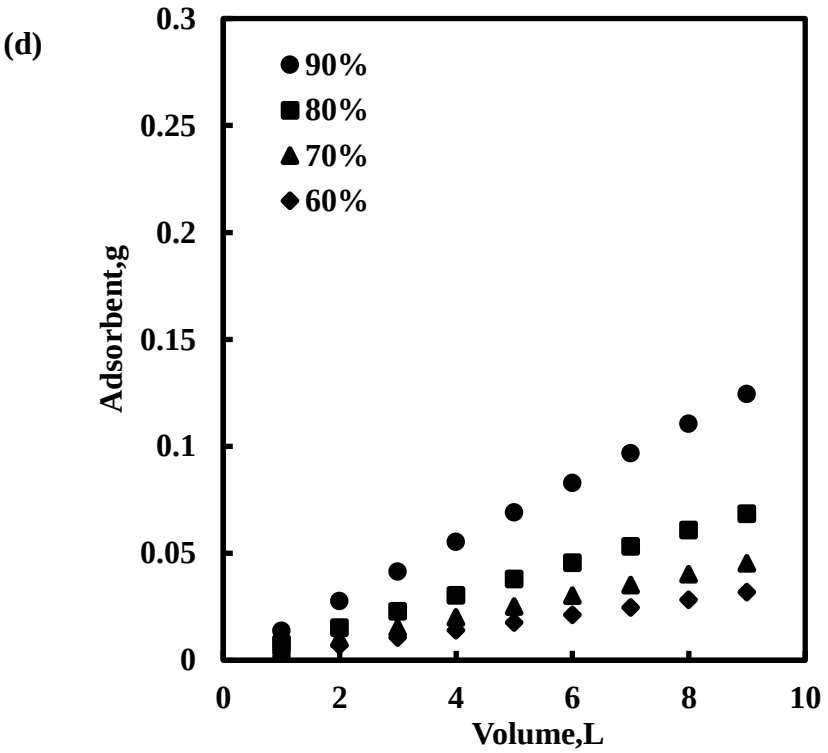

Figure 5.9(a) Single-stage batch-adsorber design **(b),(c) and (d)** Adsorbent mass (M) against volume of solution treated (L) for **DBT,2-MT and T**.

(Temperature = 30°C, Initial Sulfur Concentration = 500 ppm)

Since adsorption of DBT onto GNP follow Langmuir isotherm, and 2-MT &T follow Freundlich isotherm therefore adsorber design equation can be written as

$$\frac{M}{V} = \frac{(C_0 - C_e)}{q_1} = \frac{(C_0 - C_e)}{q_e} = \frac{C_0 - C_e}{\frac{q_m\, b\, C_e}{1 + bC_e}} \quad \textbf{(5.19)}$$

$$\frac{M}{V} = \frac{(C_0 - C_{e)}}{q_1} = \frac{(C_0 - C_e)}{q_e} = \frac{C_0 - C_e}{q_m K_f^{\,1/n_f}} \quad \textbf{(5.20)}$$

Figure 5.9(b), (c) and(d) shows the predicted GNP dosage required to remove DBT, 2-MT & T from MDF having initial concentrations of 500 mg/L for 90, 80, 70, and 60% with different solution volumes of 1, 2, 3, 4, 5, 6, and 7 L. The amount of GNP required to of DBT from MDF of concentration 500 mg/L was 0.013, 0.027, 0.041, and 0.055 g, for 2-MT was 0.027, 0.055, 0.085, and 0.011 g and for T was 0.011, 0.022, 0.033, and 0.445 g respectively for MDF volumes of 1, 2, 3, and 4 L, respectively.

5.3.7 Comparison with the multicomponent system

The multicomponent system was investigated to observe its adsorptive capacity on GNP. MDF_m with a total sulfur concentration of 1500 ppmw was mixed with GNP in different dosages and observed that the % sulfur removal for each sulfur component was decreased as compared to single component system. It was seen that the removal of DBT, 2-MT and T was decreased from 95.72, 90.21 & 75.42% to 93.24, 82.32 and 64.88 % respectively shown in **Figure 5.10.** The reason for the reduction in sulfur removal is the competitive behavior of each sulfur compound when all present together in a single model diesel fuel. Further, there were no significant changes in the equilibrium time observed in both cases shown in **Figure 5.11(a).** In addition, the multicomponent system was also following pseudo second order

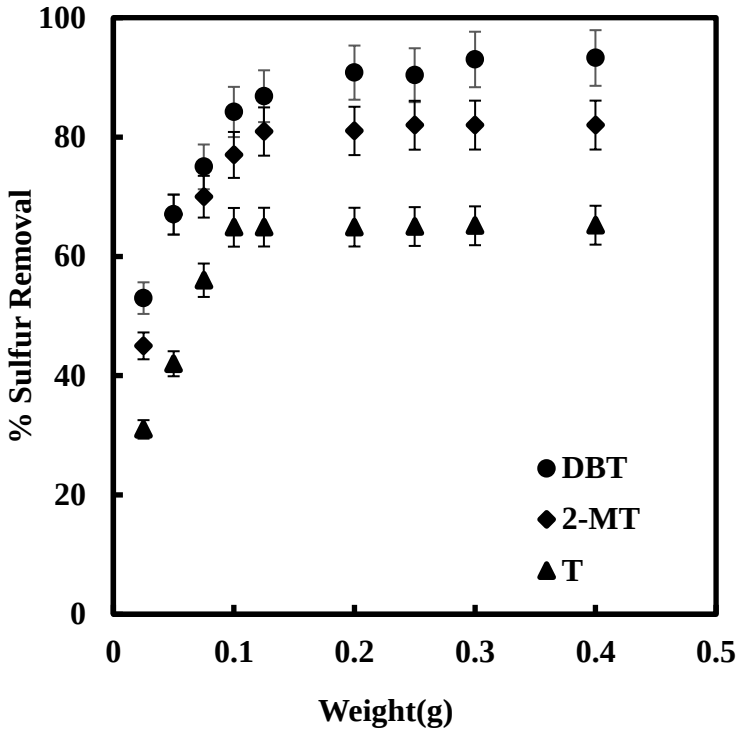

Figure 5.10 Effect of adsorbent weight on sulfur removal for multicomponent system. (Temperature = 30°C, Initial Sulfur Concentration = 500 ppm, Time = 60 min)

kinetics as shown in **Figure 5.11(b)** as similar as for single component MDFs. Although the values for second order rate constants given in **Table 5.7** deduced that the adsorption process kinetic gets slower for multicomponent system as compare to single component MDFs. Presence of other S- compounds are the primary reason for slowing down the reaction kinetics slightly. Also, there was a similar trend was observed for all DBT, 2-MT & T for temperature variation. The process possesses exothermic behavior as similar to single component system as shown in **Figure 5.12.**

(a)

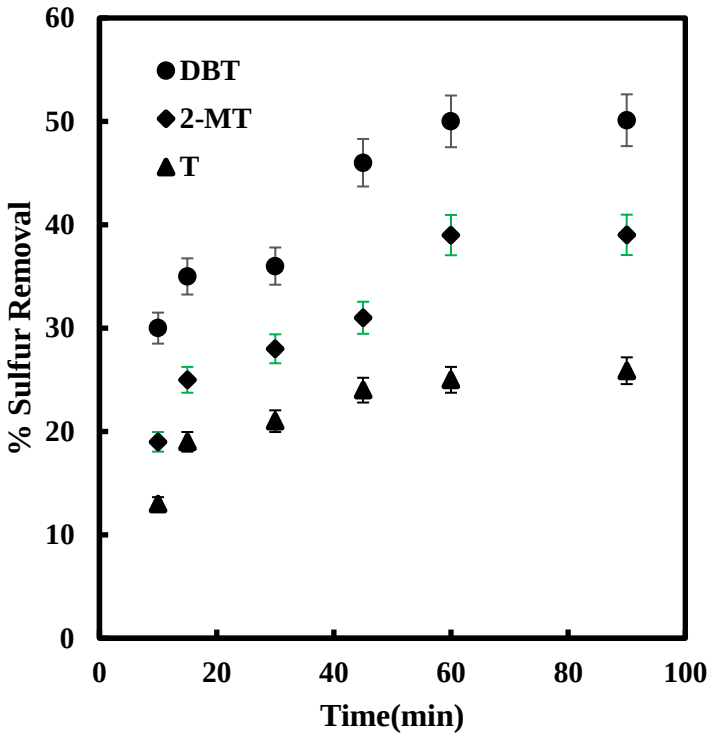
DBT
2-MT
T
% Sulfur Removal
Time(min)
0
10
20
30
40
50
60
0
20
40
60
80
100

(b)

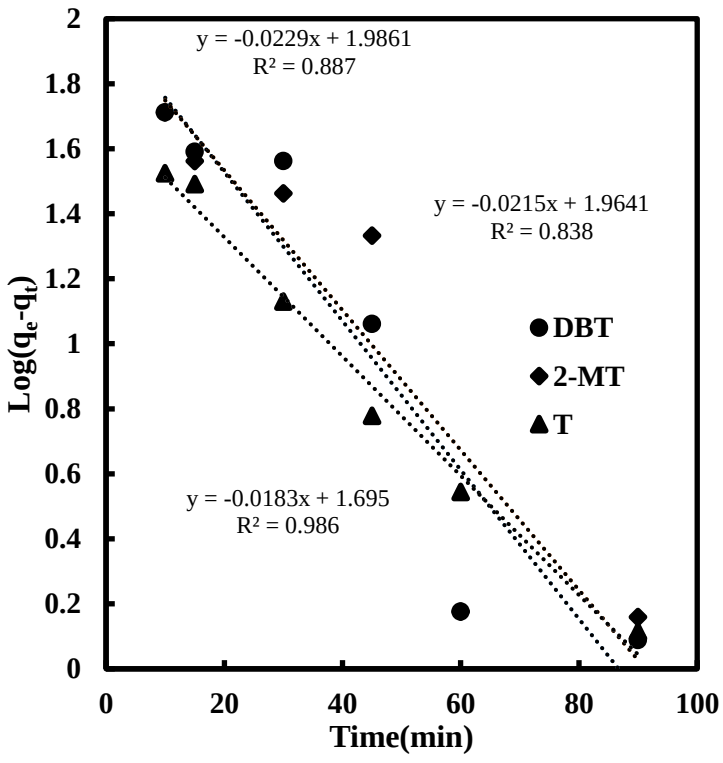
y = -0.0229x + 1.9861
R² = 0.887
y = -0.0215x + 1.9641
R² = 0.838
y = -0.0183x + 1.695
R² = 0.986
DBT
2-MT
T
Log(qe-qt)
Time(min)
0
0.2
0.4
0.6
0.8
1
1.2
1.4
1.6
1.8
2
0
20
40
60
80
100

(c)

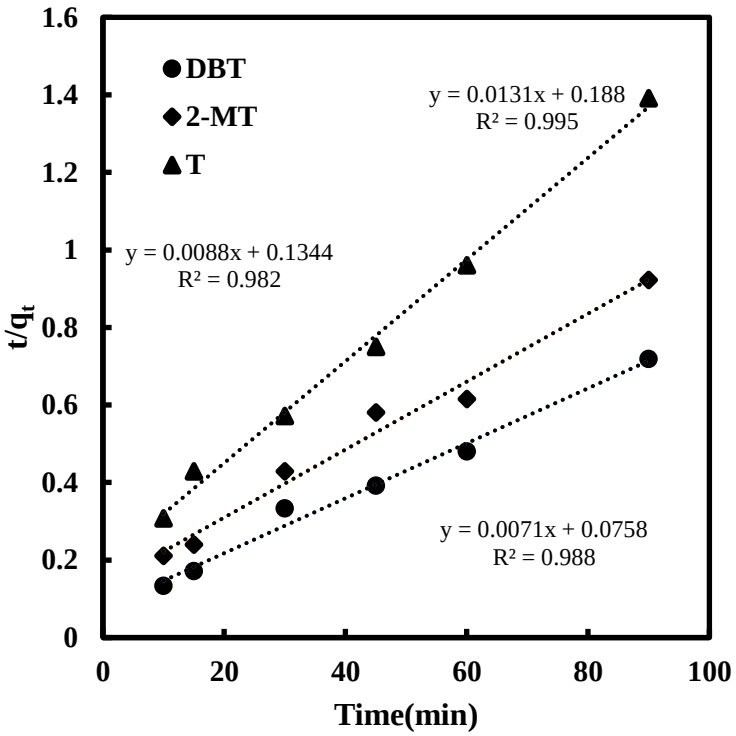

Figure 5.11 (a) Effect of time **(b)** pseudo first order and **(c)** pseudo second order kinetics for DBT, 2-MT & T adsorption on GNP in multicomponent system.
(Temperature = 30°C, Initial Sulfur Concentration = 500 ppm, Adsorbent weight = 0.01 g)

Table 5.7 Parameters for kinetics of pseudo 1st & 2nd order models for the adsorption of **DBT, 2-MT and T** on **GNP for** multicomponent system.

	k_1	k_2	Qe (mg/g)									
	(1/min)	(g/mg min)	Calculated	Experimental	Calculated	Experimental	R^2	NSD	ARE	R^2	NSD	ARE
			1st order		2nd order		1st order			2nd order		
DBT	0.052	6.651E-04	7.287	125.270	140.840	125.270	0.887	5.670	5.876	0.987	1.960	0.856
2-MT	0.049	5.761E-04	7.128	97.550	113.630	97.550	0.838	18.560	8.654	0.981	6.450	3.765
T	0.042	4.128E-04	5.446	64.730	76.330	64.730	0.986	9.760	4.923	0.995	2.980	1.456

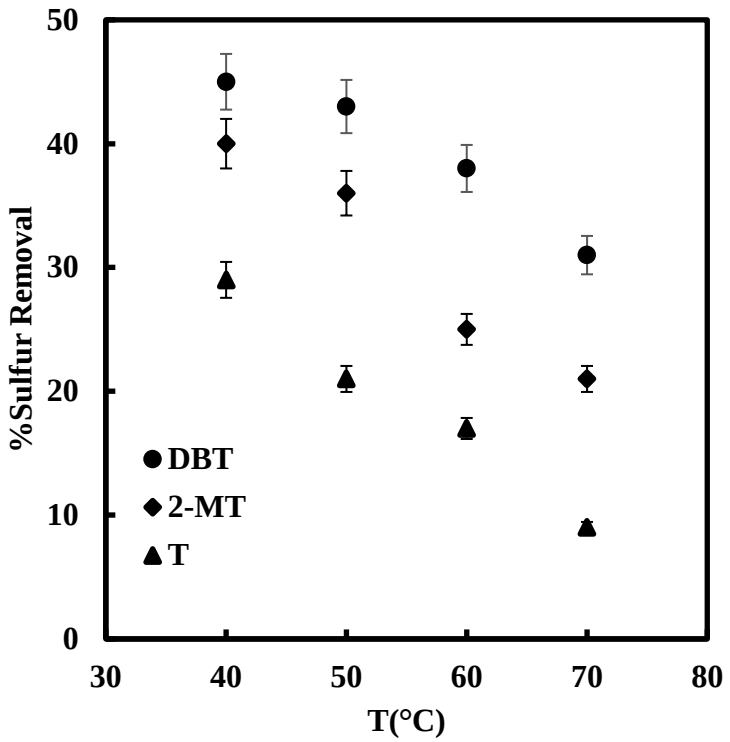

Figure 5.12. Effect of temperature on DBT, 2-MT & T adsorption on GNP in multicomponent system.
(Temperature = 30°C, Initial Sulfur Concentration = 500 ppm, Adsorbent weight = 0.01 g)

5.4 Continuous adsorptive experiments

The continuous adsorptive desulfurization experiments were conducted in a fixed bed with the adsorbent. The effect of bed height, flow rate and initial sulfur concentration were analyzed. All the experiments were repeated for 3 runs and the in each time error was found less than 5 %.

5.4.1 Effect of bed height and flow rate

The empty bed contact time (EBCT) plays important role in determining the adsorbent performance in continuous operation. Different adsorbent dosage and different inlet flow rates

were used to investigate EBCT effect on the breakthrough curves performance. The flow rate of MDF was varied from 0.2 mL/min to 2.0 mL/min in the column. As observed from **Figure 5.13** that with increasing flow rate, sulfur removal decreases. This is due to decreased contact time between adsorbent and MDF_m. The product yield also decreases in higher flow rates with the residence times in the time range from 0.1 to 2.4 s.[133,208] Also, It can be observed from **Figure 5.13** that with increasing flow rate, bed saturation also increases. For example, in the case of DBT with increasing feed flow rate from 0.5 ml/min to 3ml/min the value of C_t/C_0 increases from 0.29 to 0.89. This behavior is also observed in MT and T. This can be explained based on the number of active sites present got saturated since the low amount of feed is present. In addition, with increasing flow rate saturation time also increases. Further, **Figure 5.14** shows the bed height effect on sulfur removal**.** As the bed height increases the sulfur removal also increases and finally gets saturated. This is due to increasing adsorbent height, adsorbent mass also increased and therefore the corresponding adsorption sites also increases. It can also be observed from **Figure 5.14** that with increasing adsorbent dosage the breakthrough curve shifted towards higher saturation. For instance, in the case of DBT on increasing adsorbent dosage from 1g to 5 g the value of C_t/C_0 increases from 0.254 to 0.68. This can be ascribed to more adsorbent dosage will have a more active site to accommodate the thio-compounds.

5.4.2 Effect of initial sulfur concentration

The initial concentration effect of sulfur dosage on column performance was studied using different amounts of DBT, 2-MT and T. The concentration was varied from 200-600 ppmw of DBT,2-MT and T each keeping the concentration of other two S- compounds constantly at 500 ppmw each and observed for all the S-compounds that when the highest sulfur

(a)

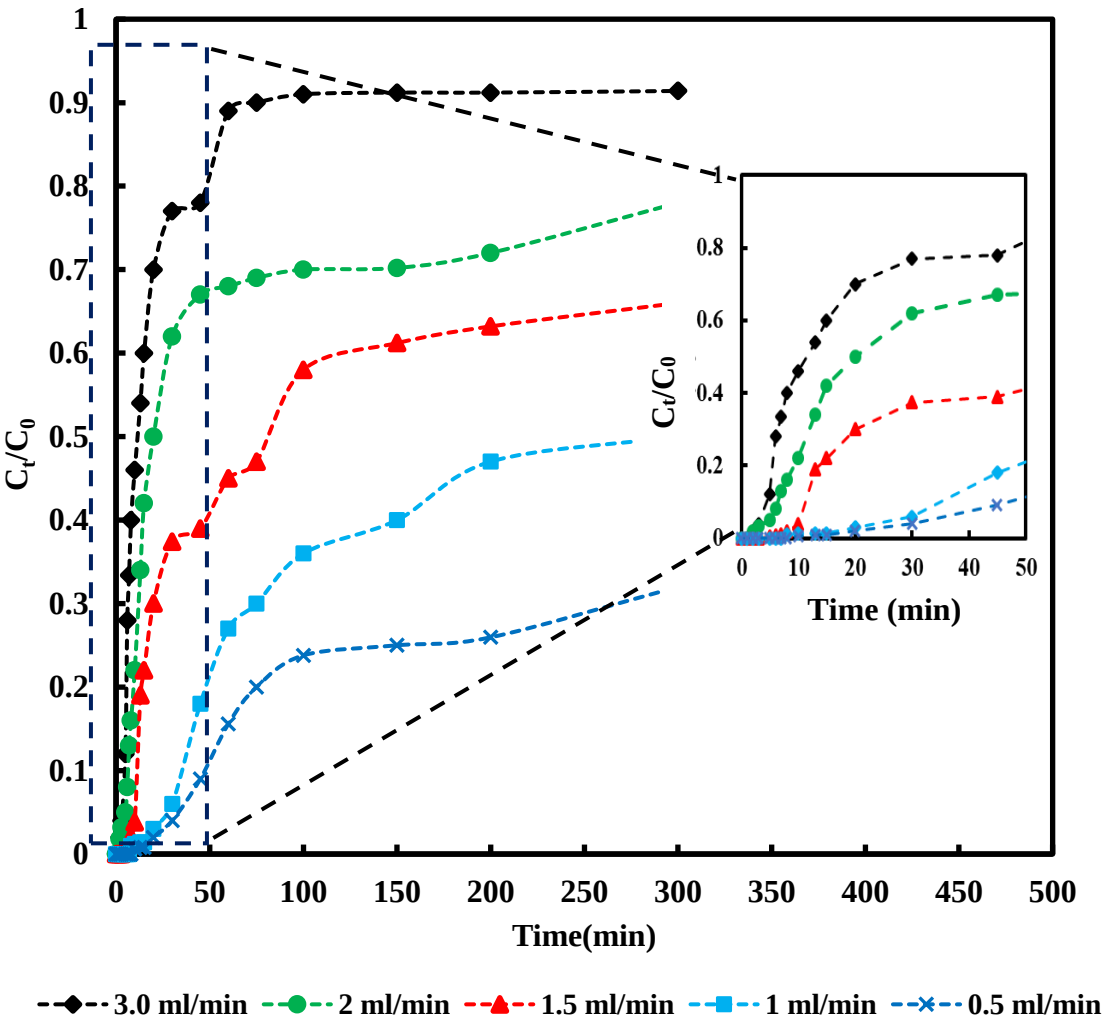
1
0.9
0.8
0.7
0.6
0.5
0.4
0.3
0.2
0.1
0
C_t/C_0
0
50
100
150
200
250
300
350
400
450
500
Time(min)
0.8
0.6
0.4
0.2
0
10
20
30
40
50
Time (min)
3.0 ml/min
2 ml/min
1.5 ml/min
1 ml/min
0.5 ml/min

(b)

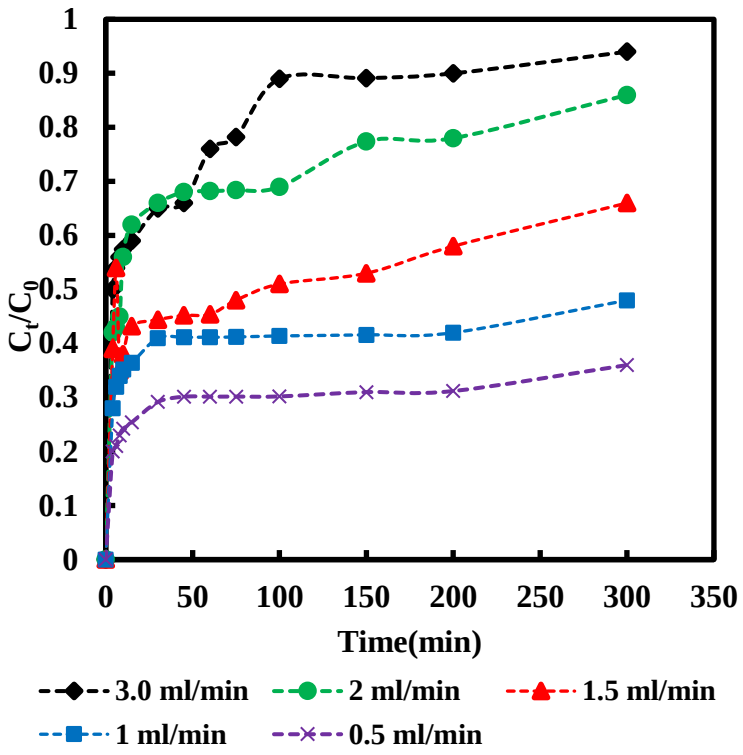

(c)

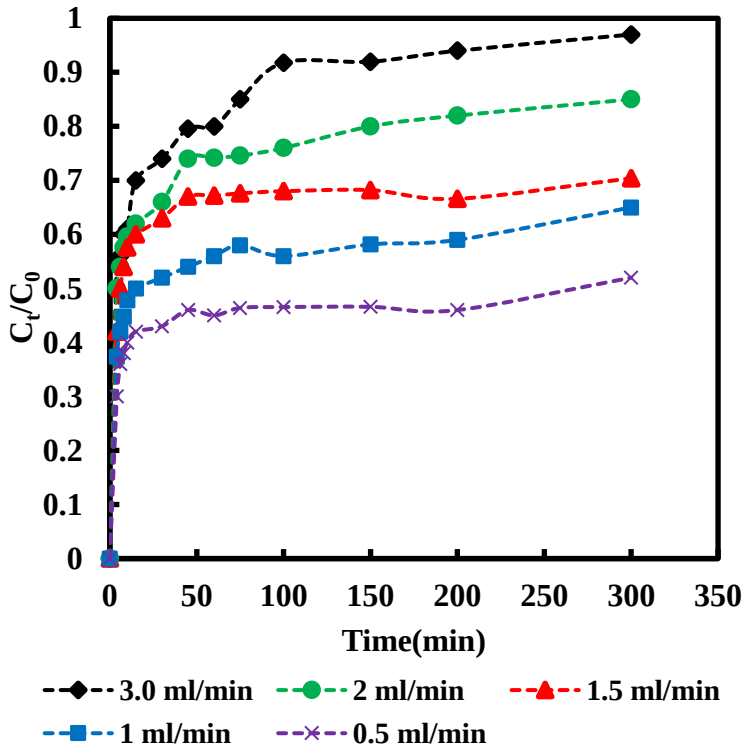

Figure 5.13 Effect of flow rate for multicomponent MDF **(a)** DBT **(b)**2-MT and **(c)** T. (Adsorbent weight= 3 g, Temperature = 30°C, Initial Sulfur Concentration = 1500 ppm)

(a)

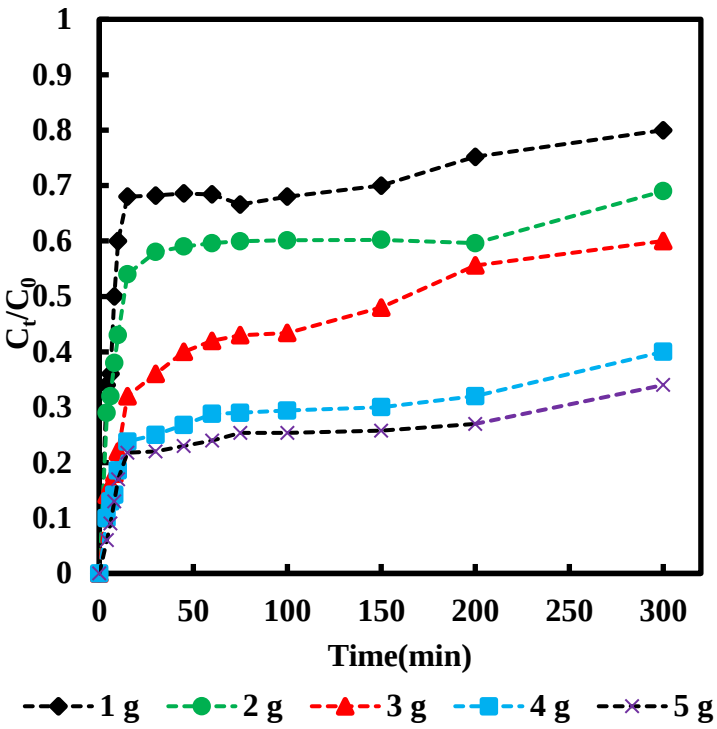
1
0.9
0.8
0.7
0.6
0.5
0.4
0.3
0.2
0.1
0
C_t/C_0
0
50
100
150
200
250
300
Time(min)
1 g
2 g
3 g
4 g
5 g

(b)

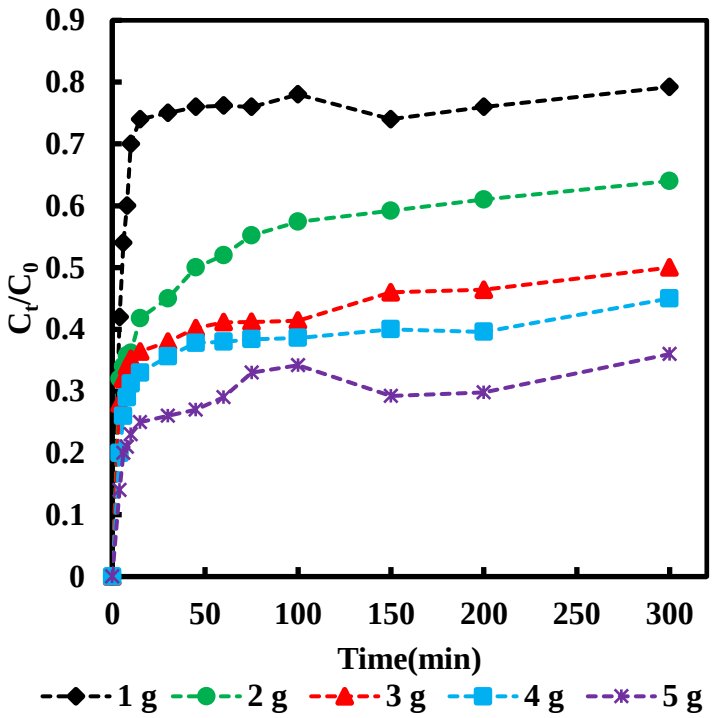
0.9
0.8
0.7
0.6
0.5
0.4
0.3
0.2
0.1
0
C_t/C_0
0
50
100
150
200
250
300
Time(min)
1 g
2 g
3 g
4 g
5 g

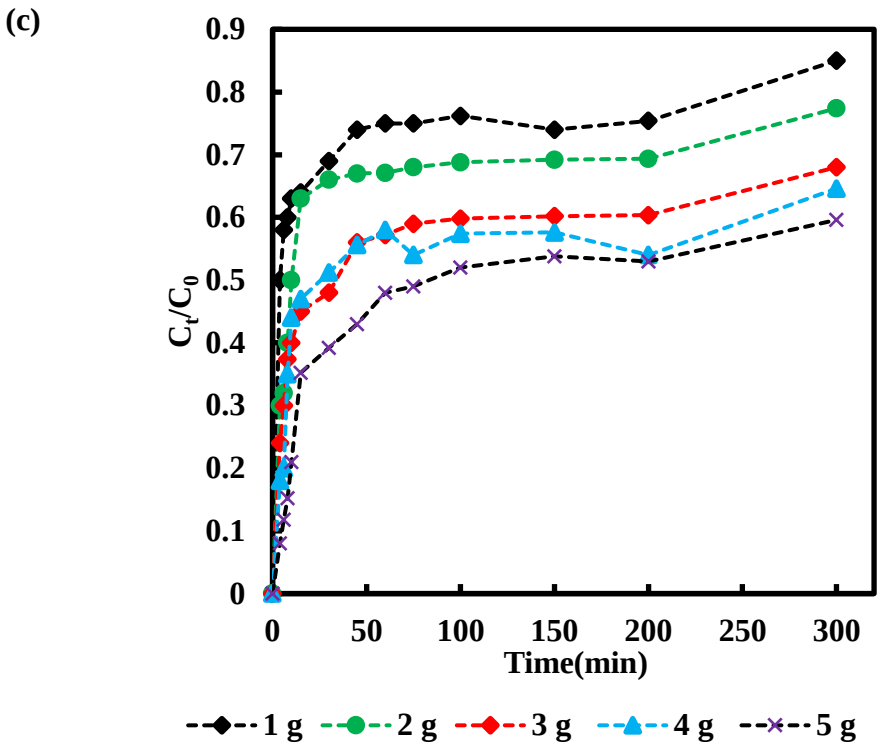

Figure 5.14 Effect of bed Height for multicomponent MDF (**a)** DBT **(b)** 2-MT and **(c)** T. (Flow rate of MDF = 1 ml/min, Temperature = 30°C, Initial Sulfur Concentration = 1500 ppm)

concentration was found to be the maximum. This is due to concentration gradient developed in the system. With increasing initial feed concentration of breakthrough curve slope become steeper and breakthrough time will also reduce. Therefore initial concentration has significant effect on the saturation rate and breakthrough time[209], With increasing feed concentration, the driving force for mass transfer also increases. The overall effect will increase the adsorption capacity as shown in the **Figure 5.15**[210]. It can be observed from **Figure 5.15** that with increasing concentration of sulfur compounds the saturation curve gets diminished. For example, the value of C_t/C_0 decreases from 0.76 to 0.32 on increasing the concentration from 200 ppmw to 600 ppmw.

(a)

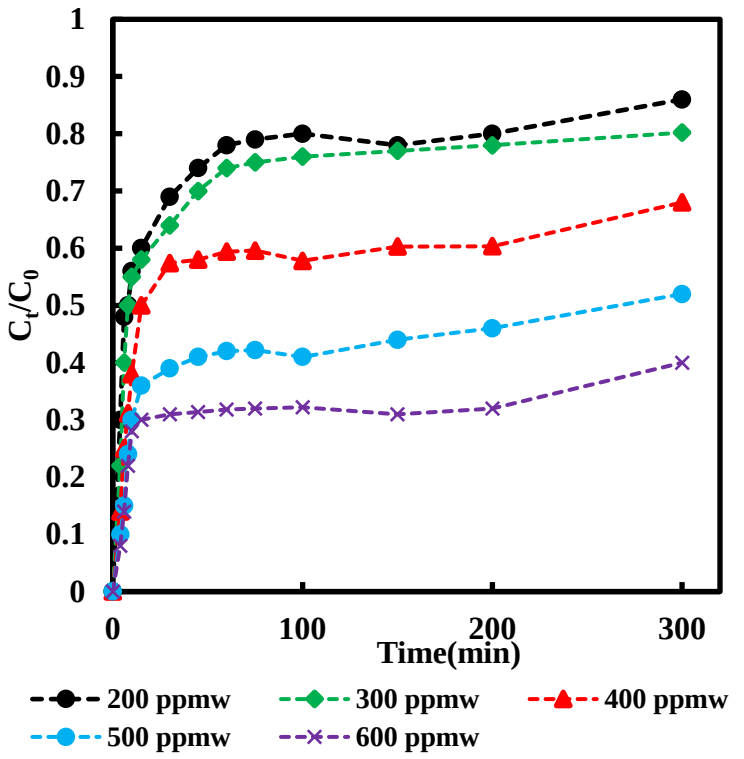
1
0.9
0.8
0.7
0.6
0.5
0.4
0.3
0.2
0.1
0
C_t/C_0
0
100
200
300
Time(min)
200 ppmw
300 ppmw
400 ppmw
500 ppmw
600 ppmw

(b)

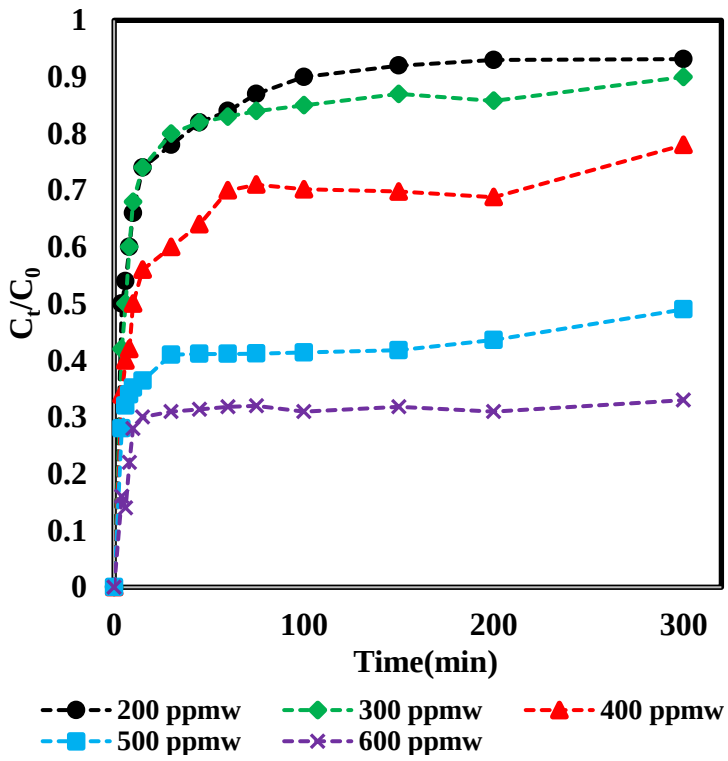
1
0.9
0.8
0.7
0.6
0.5
0.4
0.3
0.2
0.1
0
C_t/C_0
0
100
200
300
Time(min)
200 ppmw
300 ppmw
400 ppmw
500 ppmw
600 ppmw

(c)

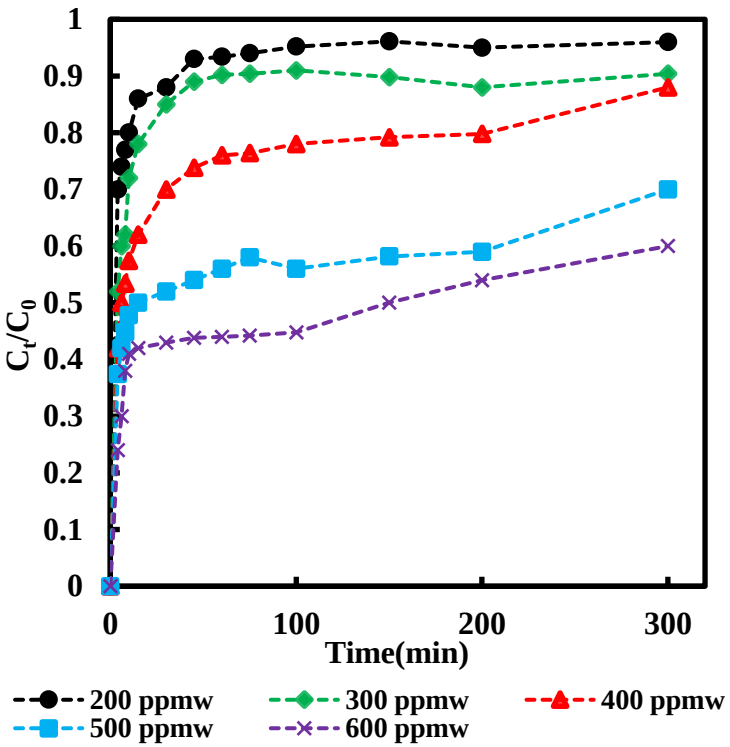

Figure 5.15 Effect of initial concentration of S-compounds for multicomponent MDF (**a)** DBT **(b)** 2-MT and **(c)** T.

(Temperature = 30°C, Flow rate of MDF = 1ml/min, Adsorbent weight = 3 g)

5.4.3 Modeling of column study results: Bohart–Adams model

To facilitate the design and analysis of a full scale system various mathematical models have been developed. In addition, various adsorption models must be investigated by the designer along with their applications to investigate the adsorber performance for desulfurization. The breakthrough curve is affected by the flow rates, bed height and feed concentration. There is a critical minimum bed height below which the solute concentration in effluent increases rapidly from the first appearance of effluent. At equilibrium, the area between curve and a line at C_t/C_0 = 1.0, is proportional to the sulfur adsorbed. Adam–Bohart model was used to predict the dynamic behavior of the column. It is based on the assumption that the adsorption rate is

directly proportional to adsorbent residual capacity and the initial concentration of feed. The present analysis is based on the estimation of maximum adsorption capacity and kinetic constants from Adam–Bohart model.

The Bed-depth Service Time (BDST) model was based on the fact that the service time (t) and bed height (Z) are correlated with the process parameters by the equation. Bed depth depends directly on the time service as given by below equation

$$t = \frac{N_0 Z}{C_0 V} - \frac{\ln\left(\frac{C_0 - C_t}{C_t}\right)}{K_a C_0} \quad \textbf{(5.21)}$$

Where C and C_0 is effluent and initial concentration (mg/l), v is velocity (cm/min), N_0 is adsorption capacity (mg adsorbed /liter of solution), k_a is the adsorption rate constant (l/ (mg h)), t is the time (min) and Z is the bed height (cm). The above equation can be written in the form of a straight line.

$$t = m'Z - B \quad \textbf{(5.22)}$$

Where m' is the slope and represents the time required by the adsorption zone to travel a unit length through the adsorbent. **Figure 5.16** shows the plot between the bed depth and service time**.** The adsorption capacity was found to be 496 mg S/kg of adsorbent and the rate constant is 0.006 $(mg/kg)^{-1}$ h^{-1}, respectively as shown in **Table 5.8.**

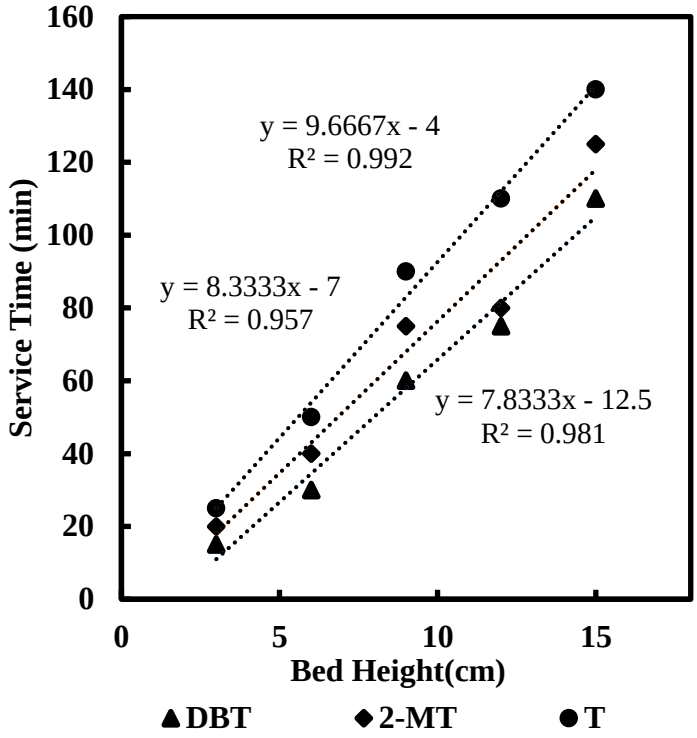

Figure 5.16 Plot of bed depth service time versus bed height (Adam-Bohart Model).

Table 5.8 Constants of the BDST equation

	Flow rate (ml/min)	**Initial concentration (mg/l)**	**Breakthrough (%)**	**N_0 (mg/g)**	**K_a $(mg/g)^{-1}min^{-1}$**	**R^2**
DBT	1.0	500	30	144.9	0.00042	0.981
2-MT	1.0	500	30	124.9	0.00021	0.957
T	1.0	500	30	117.4	0.00013	0.992

5.5 Conclusion

In this work, adsorptions of model diesel fuels containing sulfur compounds over GNP were conducted in both batch and continuous adsorption modes. The individual study of DBT, 2-MT & T removal by GNP from the batch studies showed that the removal capacity of GNP follows the order DBT>2-MT> T. The Langmuir adsorption isotherms model was fitted best to represent the adsorption equilibrium experimental data of DBT on GNP whereas Freundlich isotherm fit well with the experimental adsorption data of both 2-MT and T on GNP. The batch adsorption of DBT, 2-MT and T on GNP followed pseudo second order of kinetic. Each batch adsorption processes were well interpreted by a multi-stage diffusion model. The diffusion of DBT, 2-MT and T on GNP follows the complex diffusion model which means both intra-particle and surface diffusions was involved in the batch adsorption mechanism. The negative values of ΔG, ΔH and ΔS from the thermodynamic studies of DBT, 2-MT and T removal by GNP that indicated that the adsorption was spontaneous in nature with an exothermic behavior and with less randomness on the GNP's surface. Investigation of continuous desulfurization study shows that the adsorption breakthrough curve strongly depends on the bed height, flow rate & initial S-compounds concentration. The determined adsorption capacities and the rate constants from the continuous adsorption studies showed that the adsorptive removal of DBT by GNP is relatively predominant compare to both 2-MT and T removal. These results suggests that the GNPs have potential to use industrially for the adsorptive desulfurization process due to its high adsorptive capacities.

Chapter 6

Extractive Desulfurization Of Fuels Using Diglycol Based Deep Eutectic Solvents

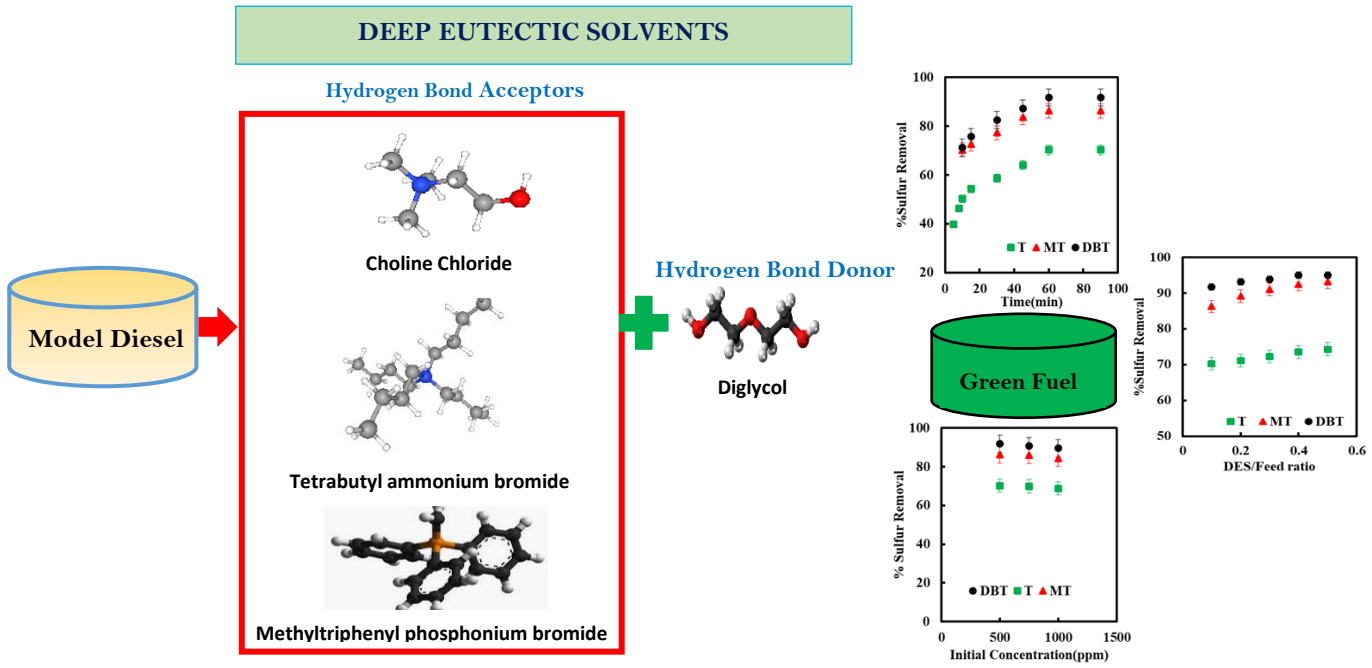

The content of this chapter has been published in

Divyam Jha, Mohd Belal Haider, Rakesh Kumar, Balathanigaimani Marriyappan Sivagnanam, " Extractive Desulfurization of Fuels using Diglycol based Deep Eutectic Solvents" Journal of Environmental Chemical Engineering 2020, 85,104182 .*https://doi.org/10.1016/j.jece.2020.104182.*

6.1 Introduction

Extractive Desulfurization (EDS) emerged as one of the plausible methods to remove heavy sulfur refractory compounds because of its low cost and high extraction efficiency[58]. However, the traditional organic solvents such as polyalkylene glycol, imidazolidinone used for desulfurization are volatile and toxic[71,103]. Therefore, there is a need to develop green solvents that can extract the heavy sulfur refractory compounds without causing much harm to the environment.

Ionic liquids (ILs) are widely regarded as green solvents and have shown the potential to remove heavy refractory sulfur compounds by extraction [22,58,211]. The ILs have low volatility, high thermal, and oxidative stability and were found to be thio-selective[212,213]. Extensive research has been done on the imidazolium, pyridinium, and phosphonium based ILs for EDS[52,107,214–216]. Nevertheless, ILs are difficult to prepare and require complex purification process, which drastically increase their price. In addition, ILs have biodegradable and bio-compatibility issues.

Recently, DESs have been developed using hydrogen bond donor (HBD) and hydrogen bond acceptor(HBA) resulting in compound with lower melting point compared to either of precursors [98,99]. The physicochemical properties of DESs are comparable to ILs these include low volatility, high thermal stability, non-corrosive behavior. DESs can be tailored made depending on the application and therefore commonly referred to as designer solvents. In recent years, DESs have found its applicability in various fields such as catalysis, electrochemistry, synthesis, gas separation application, denitrogenation of liquid fuel, etc[217–219]

The glycol, one of the prominent HBDs, based DESs have been generally used for EDS [76,220,221]. A series of ammonium-based DESs having glycol as HBD were synthesized to test thier extractive desulfurization capabilities [76]. It was reported that HBA has a greater influence on the extractive capability of DESs and the highest extraction capacity was achieved by tetra butyl ammonium chloride /polyethylene glycol based DESs. Similarly, six glycol-based DESs were used to study their removal capacities for T [222]. Further, it was reported that tetraethylene glycol-based DESs increases the DBT extraction efficiency with increasing number of extraction cycles [223]. Like glycol, the carboxylic acid-based DESs have been used as HBD for EDS and especially, tetra butyl ammonium bromide (TBAB)/formic acid-based DESs shows up to ~82% benzothiophene removal efficiency using in single-stage extraction [220]. Recently, researchers have shown that polyethylene glycol-based deep eutectic solvents are very effective in removing organosulfur compounds[221,224].

The researchers have studied the effect of metal halide ($FeCl_3$ and $ZnCl_2$) in DESs for EDS and found that up to ~70% extraction efficiency can be achieved for the case of DBT removal [225]. The π- π interaction present in the aromatic ring in arenium ion-based DESs containing toluene also gives a significant positive contribution for the deep removal of the refractory sulfur compounds, as reported elsewhere [226]. On the other hand, the HBA specific DESs such as choline chloride [78] as well as tetrabutylammonium chloride [226] based DESs have been prepared for EDS of various thio-compounds.

In this article, diglycol (DG) based DESs are synthesized and used for extractive desulfurization of refractory sulfur compounds. The single component extractive desulfurization studies were carried out for the separate removal of thiophene (T), 2-methylthiophene (2-MT) and dibenzothiophene (DBT) using three synthesized DESs namely

Choline chloride/DG, TBAB/DG & methyltriphenyl phosphonium bromide /DG. The influence of Time, DES/MF, and extraction temperature on sulfur extraction abilities of DESs were studied to find the best performing DES. Further, the critical property estimation and binary interaction were calculated for the extraction system using Aspen-Plus.

6.2 Experimental Methodology

6.2.1 Chemicals Used

Tetrabutyl ammonium bromide (TBAB) (≥ 99%), Choline Chloride (ChCl) (≥ 98%), diglycol (DG) (≥ 99%) and dibenzothiophene (DBT) (≥ 98%), were purchased from S D Fine-Chem Limited. Methyltriphenyl Phosphonium Bromide (MTPPhBr) (≥98 %) was purchased from Avras synthesis Pvt. Ltd. n-Heptane (≥ 99%), Thiophene (T) (≥ 99%) and 2-(Methyl)-thiophene (2-MT) (≥ 98%) were purchased from Alfa Aesar.

6.2.2 DESs Synthesis & Preparation of Model Fuels

The procedure for synthesis of DESs was similar as described by Abbott et.al.[98]. In general, DESs were synthesized by combining the fixed molar ratios of hydrogen bond donor (HBD) and hydrogen bond acceptor (HBA). The mixture was heated at 333.15 K for a period of 1 hours under constant agitation of 500 rpm until a homogenous colorless liquid was formed. The moisture present in DESs was removed by drying DES overnight at 323.15 K under vacuum. **Table 6.1** represents the DESs synthesized in this work with their molar compositions**.** DESs synthesized using ChCl, TBAB and MTPPhBr were named as DES 1, DES 2 and DES 3.

The model fuels (MFs) were prepared by adding 0.1982, 0.1370 and 0.1046 g of DBT, 2 –MT and T as purchased without any further purification into three different containers of 100 mL of n-heptane, the initial concentration of all MFs was maintained at 500 ppmw.

Table 6.1 Molar composition and Molecular weight of Deep Eutectic Solvents (DESs)

Hydrogen Bond Donor	Hydrogen Bond Acceptor	Molar Composition	Name	Molecular weight (g/mol)
Diglycol (DG)	Choline Chloride (ChCl)	ChCl /2DG	**DES1**	121.11
	Tetra butyl Ammonium Bromide (TBAB)	TBAB/ 4DG	**DES2**	178.202
	Methyltriphenylphosphonium Bromide (MTPPhBr)	MTPPhBr/4DG	**DES3**	158.80

6.2.3 Liquid–liquid extractive desulfurization

The EDS was carried out to check the sulfur removal capacity of DESs. In a typical experiment, DESs were added to MFs in a 50 mL Erlenmeyer flask. The Erlenmeyer flask containing bi-phasic mixture was then transferred to Orbital Incubator Shaker (BR Biochem make) for carrying out single component batch extraction experiments. All the experiments were conducted at ambient conditions and for 60 minutes. The samples were then removed and allowed to settle for 10 minutes. The extraction efficiency of the DESs is given by the equation

$$Extraction\ Efficiency(wt\ \%) = \frac{TS_1 - TS_2}{TS_1} \text{x } 100 \qquad \textbf{(6.1)}$$

Where TS_1 is the amount of sulfur present in the original feed and TS_2 is the amount of sulfur content present in the treated sample.

A possible desulfurization mechanism of extractive desulfurization is proposed in **Figure 6.1.** When DESs gets contacted by thiophenic sulfur compounds, some of them formed liquid clathrate, but others preferably form a complex.

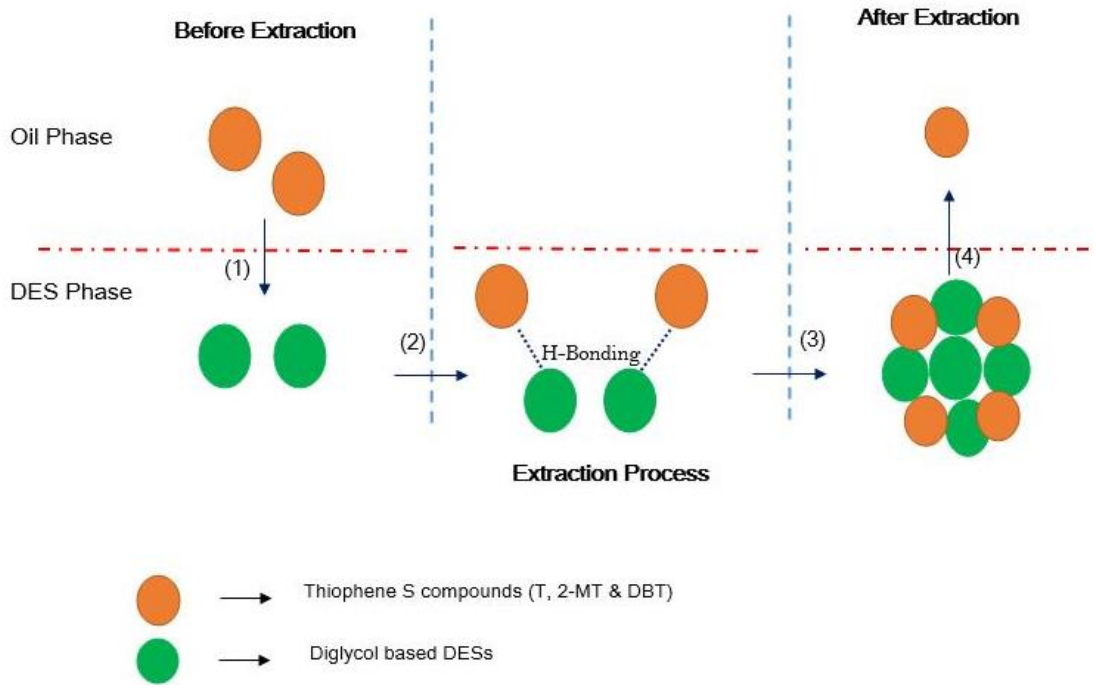

Figure 6.1 Process of extractive desulfurization

6.2.4 Analysis Methods

PerkinElmer Spectrum two spectrometer was used for the FTIR analysis of the synthesized DESs. Claurs 580 GC-FID (Perkin Elmer make) was used for desulfurization analysis using isopropanol as an internal indicator. Total chrome workstation was used for the graphical analysis of the GC-FID. The GC-FID operating conditions are presented in the **Table 6.2**.

^{1}HNMR spectra were recorded at 400 MHz on the Jeol spectrometer at 25 °C with eight scans. For HNMR analysis of hydrophobic DESs, 20 mg of DESs were weighed and added to 0.6 mL

of deuterated chloroform ($CDCl_3$). Before each analysis homogeneity of the mixture was assured.

Table 6.2 Operating Conditions of GC-FID.

Element	Characteristic
Column	Elite-1(PerkinElmer)
Oven	Helium as Carrier Gas; Temperature: 50 °C hold for 3 minutes then ramp @12 °C up to 300 °C
Injector	Injection:1µl;split ratio:1:85;temperature:320 °C
Detector	Type: FID; Temperature:350 °C

6.3 Results and Discussions

6.3.1 DESs Characterization

FTIR analysis for DESs:

The possible changes in DESs structures are studied using FTIR. As shown in **Figure 6.2** all synthesized DESs do not deviate significantly because of the same HBD used for their synthesis. The presence of –OH bond of diglycol is indicated between 3200-3600 cm^{-1} [228,229].It can be observed that –OH stretching of diglycol has been shifted from 3343 cm^{-1} to 3356, 3372 and 3401 cm^{-1} owing to the hydrogen bond formation. The presence of spectra around 3000-3400 cm^{-1} suggests O-H group convergence with N-H stretching. Similarly, P-H stretching is overlapped with C-H vibration in the range of 3000-2800 cm^{-1} [29]. This also matches well with previously reported data[230].

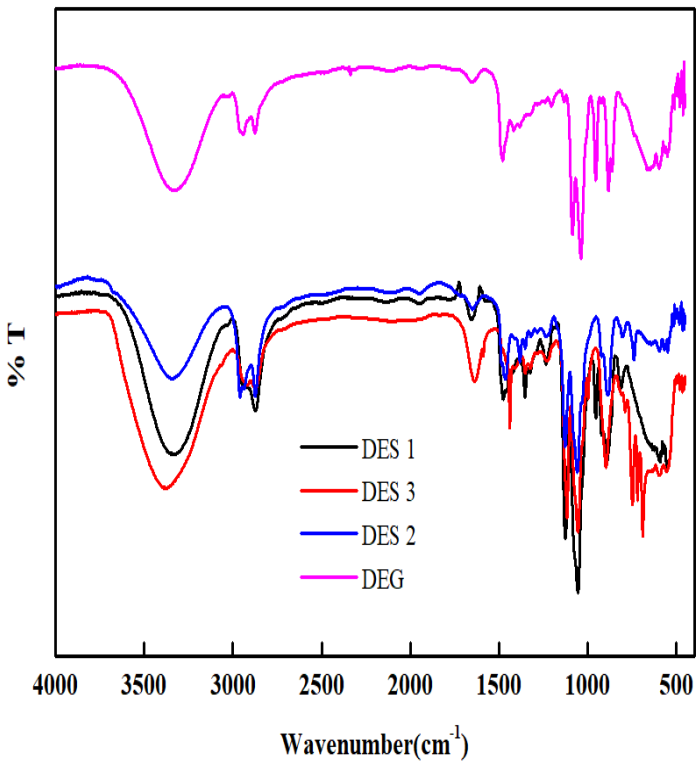

Figure 6.2 FTIR spectra of Diethylene Glycol and Deep Eutectic Solvents

Viscosity of synthesized DESs:

The viscosities of synthesized DESs were measured at different temperatures (293.15–333.15 K). As shown in **Figure 6.3** the viscosities of the DESs followed the order of DES 2 >DES 3>DES 1 for the same temperature. The higher viscosity of DESs is due to hydrogen bonding between HBD and HBA, and therefore lower free species mobility. The temperature dependence of the viscosity of synthesized DESs is shown in **Figure 6.3(a).** The viscosities of DESs decreases exponentially with increasing temperature. This could be attributed to the weakening of the hydrogen bond between HBD and HBA with increasing temperature, which promotes molecular movement and kinetic energy DES 2 has the highest viscosity of 202.19 cP at 293.15K, whereas DES 1 has the lowest viscosity of 48.78 cP at 293. 15K.The higher

(a)

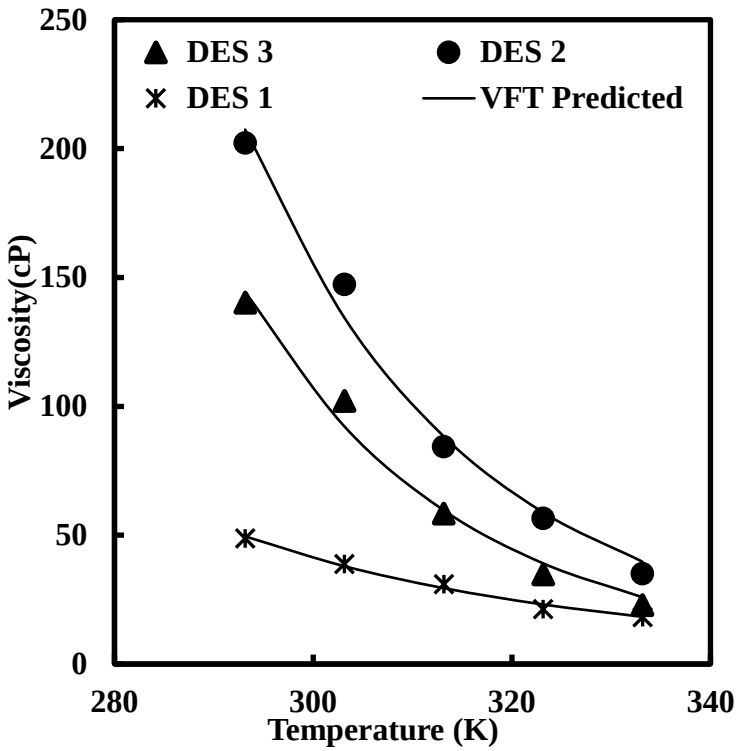

(b)

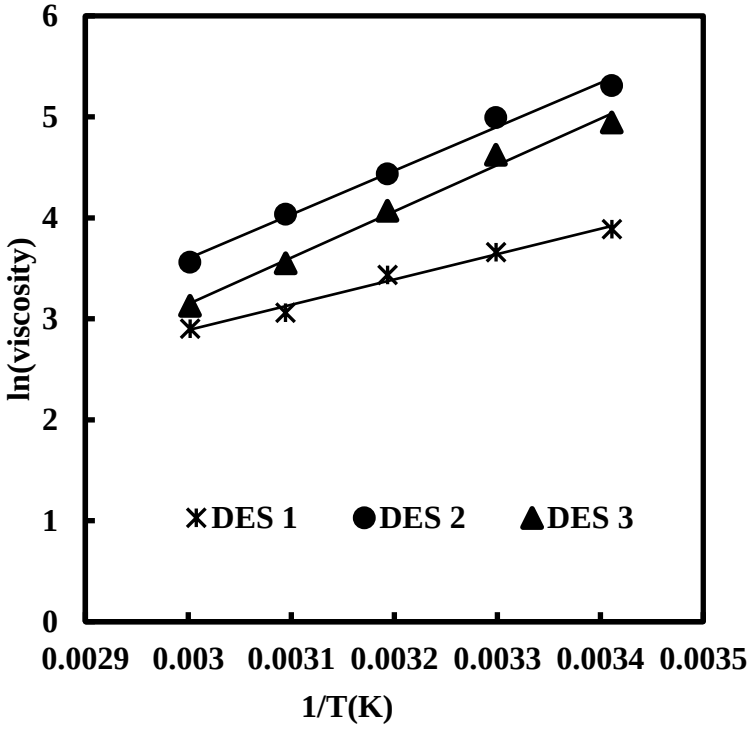

Figure 6.3 plot of viscosity vs temperature by **(a)** VFT equation **(b)** Arrhenius equation

viscosities dictate the presence of extensive hydrogen bonding between the starting materials. The viscosity is further modeled using Vogel-Fulcher-Tamman (VFT) equation[231].

$$\ln\left(\frac{\eta}{\eta_0}\right) = \frac{B}{T - T_0} \quad \textbf{(6.2)}$$

where ηviscosity in m.Pa S and T is the temperature in K, η_0 , B, and T_0 are constants. The corresponding values of empirical constant for their best fits are given in **Table 6.3.**

Table 6.3 Arrhenius and Vogel-Fulcher-Tamman parameters of DESs

	VFT Equation			**Arrhenius Equation**	
DES	**η_0 (m.PaS)**	**B (k)**	**T_0 (k)**	**$10^{-5}\eta_\infty$ (m.PaS)**	**E_η (kj/mol)**
DES 1	0.574	4745.8	124.43	973.43	20841.54
DES 2	1.09E-06	15287.6	295.53	7.98	36120.17
DES 3	1.93E-08	19282.5	357.38	2.45	38135.98

The Arrhenius equation, which was used for correlating viscosity dependence on temperature, is given below,

$$\ln\left(\frac{\eta}{\eta_\infty}\right) = \frac{E_\eta}{RT} \quad \textbf{(6.3)}$$

where E_η is the activation energy for viscous flow, R is gas constant and η_∞ is empirical constant. Fitting of lnη with 1/T is shown in **Figure 6.3(b)** and the empirical constant values are also listed in **Table 6.3.** As shown in Figure 2, both methods fitted well with the experimental data. The order of activation energy of DESs is DES 3 > DES 2> DES>1, which

means that the variation of DES 1's viscosity with the temperature is relatively less compared to the DES 2 and DES 3[232]**.**

6.3.2 Factors Affecting Desulfurization using DESs

Factors such as DES/ Feed mass ratios, extraction time, initial sulfur concentration and temperature are discussed in detail. The effect of extraction time for DES 1, DES 2 and DES 3 at constant temperature (30°C) and fixed DES/Feed ratio (0.1) is shown in **Figure 6.4**. It could be observed that the rate of sulfur removal was initially fast and after 60 minutes no further removal in impurities was observed for all three DESs, as the extraction system reaches the equilibrium state. In addition, this initial study also suggests that the extraction of heavier molecules e.g. Dibenzothiophene is more favored compared to lighter molecules e.g. thiophene. This is particularly favorable over the HDS process where more severity is required for a heavier molecule.

The effect of DES/Feed mass ratio is shown in **Figure 6.5** for DES1, DES2, and DES3, respectively**.** The experiments have been conducted at 30°C and for 60 minutes. As expected, the sulfur removal efficiency increases with an increasing DES/Feed ratio. Furthermore, the sulfur capacities of all three for all DESs were found as follows, DBT> 2-MT>T. This depicts the nature of the organo-sulfur compound has a considerable effect on the removal efficiency. 'The higher DBT extraction efficiency is attributed to higher electron density compared to 2-MT and thiophene [225,233].

The initial sulfur concentration in model oil is an important parameter to evaluate the extractive capacity of DESs. The sulfur removals with varied sulfur concentrations from 500 to 1000 ppm are listed in **Figure 6.6.** It can be seen that sulfur removal was not decreased

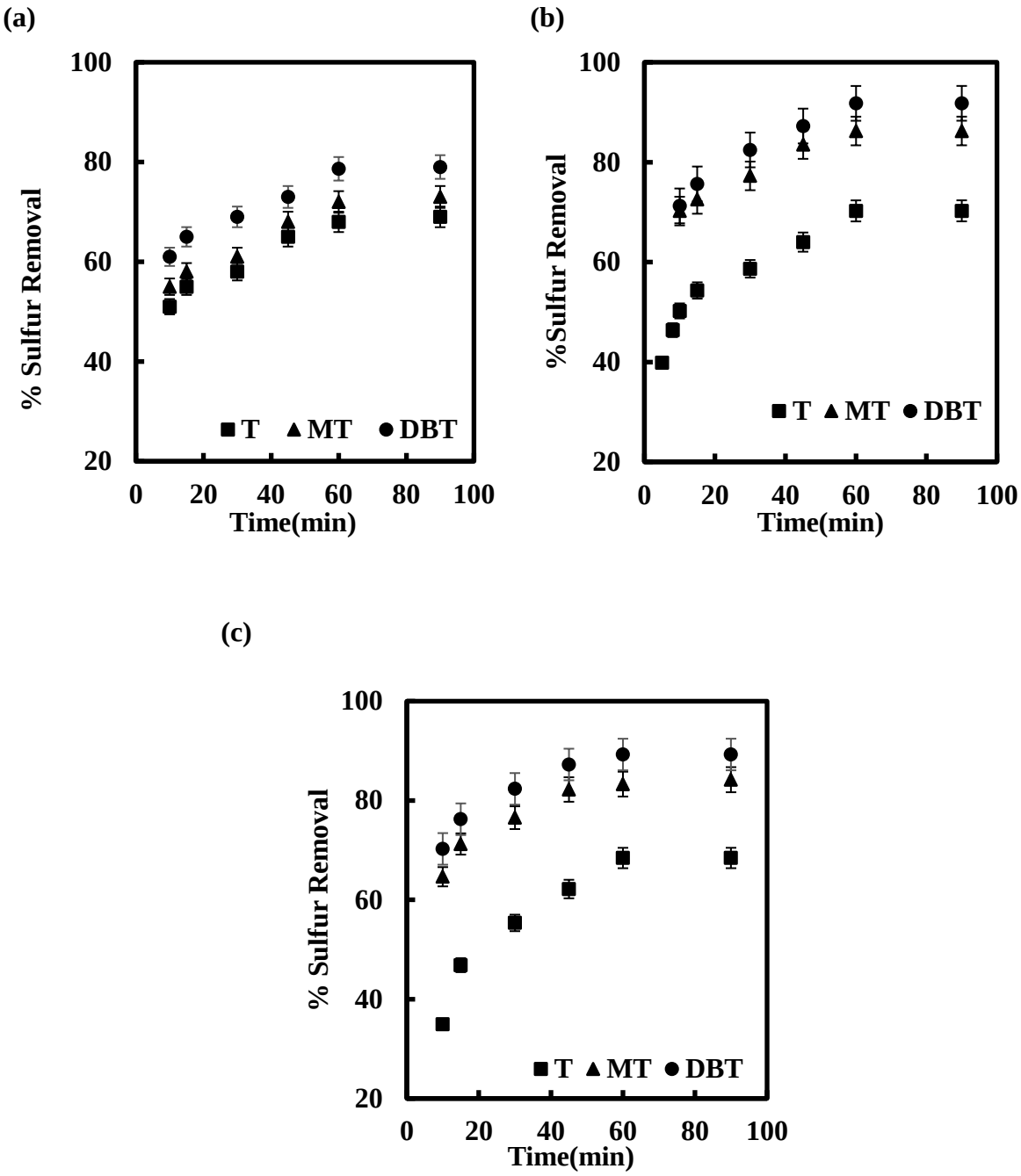

Figure 6.4 Effect of time on sulfur extraction using **(a)** DES1 **(b)** DES 2 & **(c)** DES 3 (Temperature = 30°C, DES/Feed Ratio 0.1, initial sulfur concentration = 500 ppm)

significantly. Therefore, it can be deduced that the extractive ability of the DESs was not be affected by the initial concentration. Therefore, the synthesized DESs can be applied to the desulfurization of more fuels.

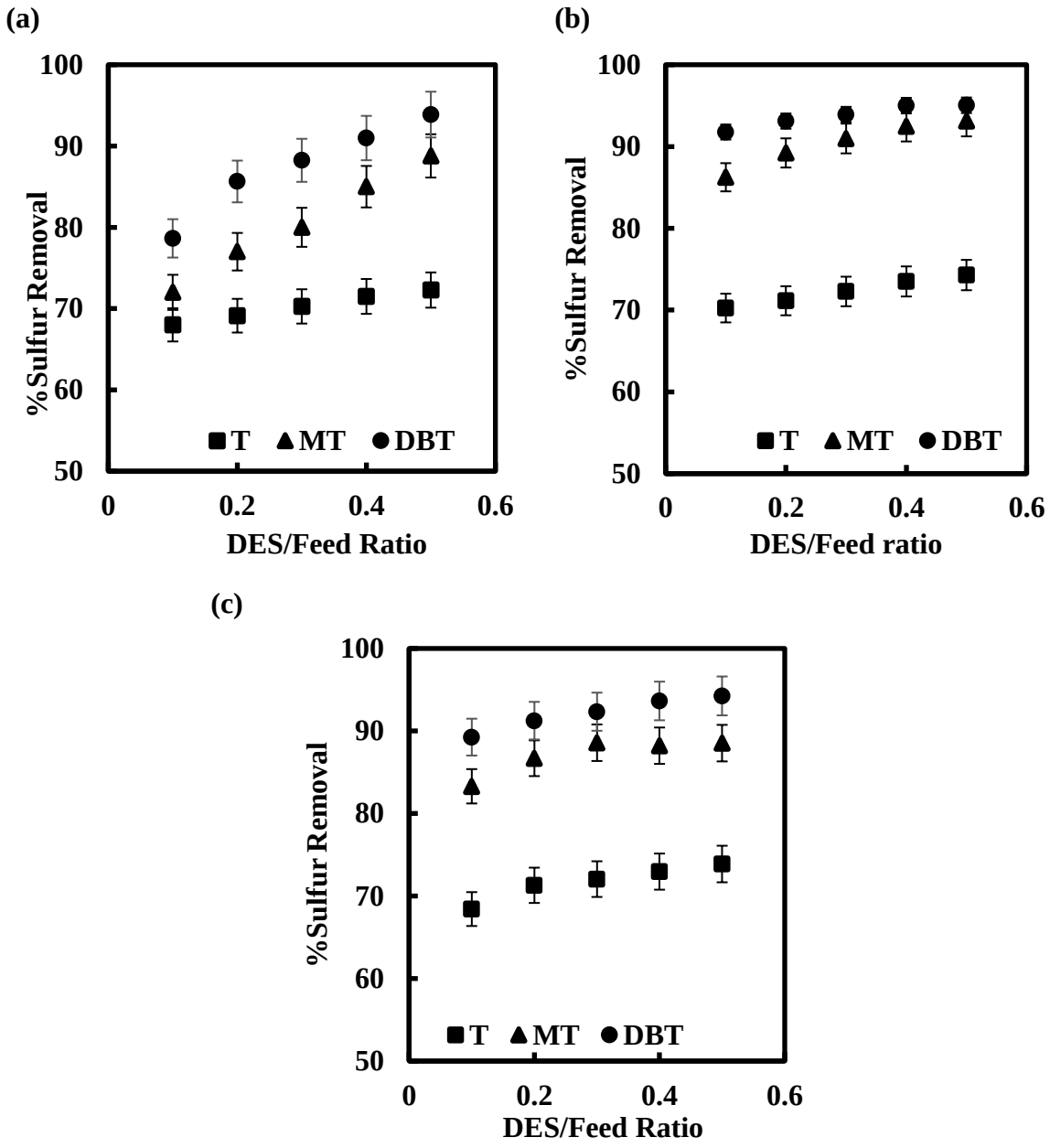

Figure 6.5 Effect of DESs/Feed ratio on % Sulfur removal using **(a)** DES1 **(b)** DES2 & **(c)**DES 3 (Temperature = 30°C, Time =60 min, initial sulfur concentration = 500 ppm)

To see the effect of temperature on extraction efficiency, the temperature was varied from 30 to 60 °C under similar experimental conditions i.e. DES/Feed ratio of 0.1, for 60 min and initial sulfur concentration of 500 ppm. As shown in **Figure 6.7**. It can be observed that the extraction efficiency of DESs marginally increases with increasing temperature. In general,

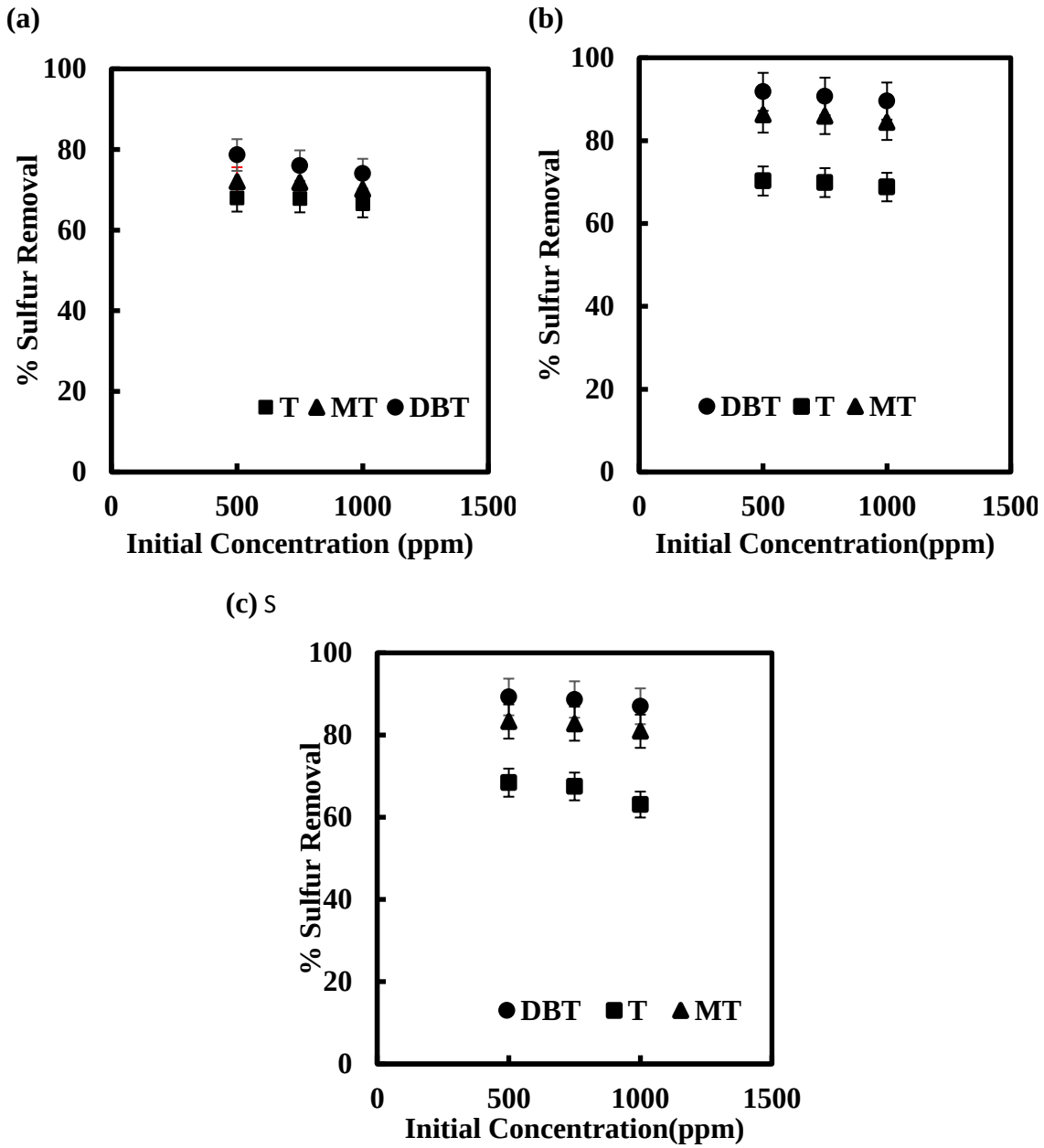

Figure 6.6 Effect of the initial sulfur concentration on % Sulfur removal using **(a)** DES1 **b)** DES 2 & **(c)** DES 3 (Temperature = 30°C, DES/Feed Ratio=0.1, Time= 60 min)

solubility increases with the temperature and therefore better interaction between MFs and DES, which subsequently results into higher extraction efficiency.

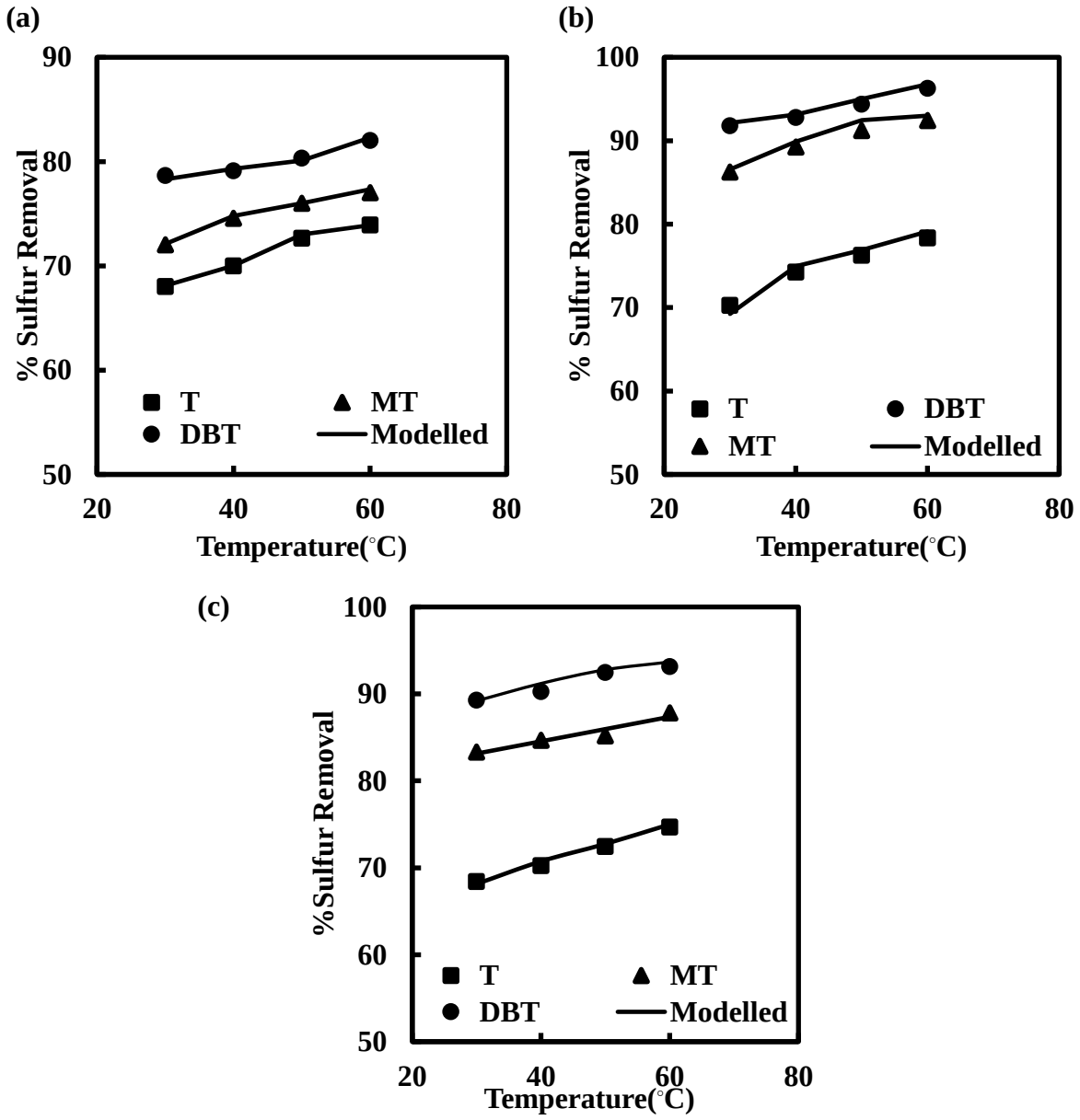

Figure 6.7 Experiment and NRTL predicted % Sulfur removal at different temperatures using **(a)** DES1 **(b)** DES2 & **(c)** DES 3 (initial sulfur concentration = 500 ppm, DES/Feed Ratio 0.1, Time= 60 min)

The effect of different HBAs on the sulfur removal capacity for DES/Feed ratio 0.1 from MFs is shown in **Figure 6.8** DBT removal efficiency of different DESs was found as follows, DES 2 > DES 3 > DES 1.

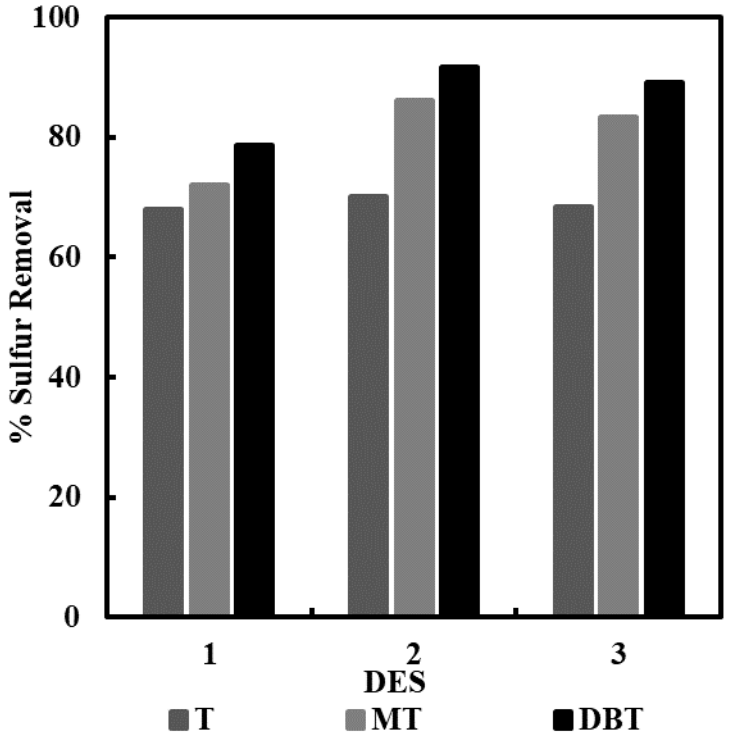

Figure 6.8. Comparison of different DESs (1, 2 &3) for sulfur removal efficiencies (Initial sulfur concentration = 500 ppm, DES/Feed Ratio= 0.1, Time= 60 min & Temperature=30°C)

The desulfurization yields of DES 1, 2 and 3 are 78.64%, 91.77% & 89.26% for DBT, 72.0, 86.24 & 83.30% for 2-MT, and 68.0, 70.25 & 68.42% for T, respectively. The highest removal of DBT by all DESs can be suitably explained by the electron density of the sulfur compounds, more the electron density on the S present in the organosulfur compound more extraction occurs. The increased efficiencies in DES 2 as well as DES 3 compared to DES 1 shows that increased free volume in both DES 2 and DES 3 due to their increased chain length, which

plays a critical role in this separation[234–236]. Similar behavior is also observed for 2-methylthiophene removal. However, in the case of thiophene removal, all three DESs have approximately same removal efficiency (~68%). This suggests that the thiophene interacts more with HBD of DES (i:e diglycol) rather than the HBAs of different DESs. However, the presence of HBAs also differs the S-removal capacity due to the formed H-bond between HBA and HBD. The sulfur present in the thiophene strongly interacts with the oxygen present in the HBD (DG), which is common for all three DESs, due to its electron-withdrawing property and hence all three DG based DESs show approximately same thiophene extraction efficiency [237].

Some desulfurization results of previously reported ILs from the literature were compared with the results of this work and presented in **Table 6.4.** This comparison studies clearly showed that the sulfur (DBT, 2-MT, and T) removal abilities of DES 2 is satisfactorily higher than some of the ILs. It can be concluded that the DES 2 is much more efficient for the extractive desulfurization. Further, the **Table 6.5** shows the sulfur removal capacities of various molecular solvent ILs and DESs.

Table 6.4 Comparison of Sulfur Extraction Efficiency between DES-2 and ILs

S compounds	Extractants	Initial Content (ppm)	S-Extractants : Feed ratio	Time (min)	Extraction yield (%)	References
DBT	DES-2	500	1:1	60	95.04	This work
DBT	$[C_4mim][BF_4]$	500	1:1	60	47	[15]
	$[Bmim]BF4_2$	747	0.2:1	30	12	[22]
2-MT	DES-2	500	1:1	60	93.10	This work
T	DES-2	500	1:1	60	74.21	This work
T	$[C_2mim][N(CN)_2]$	500	1:1	5	41.2	[238]
T	$[Bmim]Cl\text{-}Cu_2Cl_3$	680	0.2:1	30	99.6	[239]

6.3.3 Modelling

6.3.3.1 Critical Properties Estimation

For estimating pure component property two modeling approaches have been established. In the first approach, DESs precursor is individually modeled whereas in the second approach DESs ae considered as a pseudo pure component[240]. In this work first approach was followed i:e DESs are composed of diglycol (HBD) and quaternary ammonium and/or phosphonium salt (HBA) therefore their single component properties were first investigated using “modified Lydersen−Joback−Reid” (LJR) method[241]. The detail about the modified

Table 6.5 Comparison of Sulfur Extraction Efficiencies of molecular solvents, ILs and DESs.

S.No.	Extractant	% Sulfur removal	Reference
1.	Polyethylene glycol	76	[20]
2.	Dimethyl Sulfoxide	78	[242]
3.	ChCl/Pr	64.9	[243]
4.	DES-T	89.64	[79]
5.	[Bmim]Cl-$AlCl_3$[1]	45.0	[226]
6.	[Bmim]BF_4[2]	12.0	[226]
7.	MTPPBr/TetEG	47.0	[223]
8.	MTPPhBr/DG	89.26	This work
9.	TBAB/HCOOH	80.4	[220]
10.	N-butyl-N-methylimidazolium hydrogen sulfate ([BMIm]HSO_4)	100.0	[244]
11.	N-methyl-pyrrolidonium phosphate ([Hnmp]H_2PO_4)	99.8	[245]
12.	Protic ionic liquid (PIL), [Hnmp]HCOO	99	[246]

LJR method is reported in our previous work[229]. In general, the following equations were used to calculate individual properties;

$$T_b = 198.2 + \sum n_i \, \Delta T_{bMi} \tag{6.4}$$

$$T_c = \frac{T_b}{0.5703 + 1.0121 \sum n_i \, \Delta T_{Mi} - (\sum n_i \, \Delta T_{Mi})^2} \tag{6.5}$$

$$P_c = \frac{M}{0.2573 + (\sum n_i \, \Delta P_{Mi})^2} \tag{6.6}$$

$$V_c = 6.75 + \sum n_i \, \Delta V_{Mi} \tag{6.7}$$

where n_i represents the number of the appearance of i^{th} group, M represents molecular weight (g/mol) of the molecule. ΔT_{bM}, ΔT_M, ΔP_C, and ΔV_M represents group contribution of individual atoms present in the molecule to their boiling point (K), and respective critical properties. To predict the properties of the mixture, Lee-Kesler[247] mixing rule was used using equations below;

$$T_{CM} = \frac{1}{V_{CM}^{1/4}} \sum_i \sum_j x_i x_j V_{C_{ij}}^{1/4} T_{C_{ij}} \tag{6.8}$$

Where

$$T_{C_{ij}} = k_{ij} * \left(T_{C_i} * T_{C_j}\right)^{1/2} \tag{6.9}$$

$$V_{C_{ij}} = \frac{1}{8}\left(V_{C_i}^{1/3} + V_{C_j}^{1/3}\right)^3 \tag{6.10}$$

$$V_{CM} = \sum_i \sum_j x_i x_j V_{C_{ij}} \tag{6.11}$$

And

$$P_{CM} = \frac{(0.2905 - .085 \, \omega_{CM}) R T_{CM}}{V_{CM}} \tag{6.12}$$

where

$$\omega_M = \sum_I x_i \omega_i \tag{6.13}$$

T_{CM}(K), P_{CM}(bar), V_{CM} (cm^3/mol) represent respective critical properties of DESs. x_i, $\omega_{M,}$and k_{ij} represent mole fraction, acentric factor, and binary interaction parameter of DESs. The value k_{ij} depends upon the polarity of compounds[247]. Here, k_{ij} value is assumed to be 1 because of absence of any experimental data.

6.3.3.2 Non-Random Two Liquids

For modelling, the liquid-liquid equilibria PC-SAFT and NRTL model has been widely used[248–250]**.** In this work, the NRTL method was used for the modeling of liquid-liquid equilibria of MDF and DESs system The NRTL equation is:

$$ln\gamma_i = \frac{\sum_j x_j \tau_{ji} G_{ji}}{\sum_k x_k G_{ki}} + \sum_j \frac{x_j G_{ji}}{\sum_k x_k G_{ki}} \left(\tau_{ij} - \frac{\sum_m x_m \tau_{mj} G_{mj}}{\sum_k x_k G_{kj}} \right) \quad \textbf{(6.14)}$$

where

$$G_{ij} = \exp\left(-\alpha_{ij}\tau_{ji}\right) \quad \textbf{(6.15)}$$

$$\tau_{ji} = a_{ij} + \frac{b_{ij}}{T} + e_{ij}\ln(T) + f_{ij}T \quad \textbf{(6.16)}$$

$$\alpha_{ij} = c_{ij} + d_{ij}(T - 273.15) \quad \textbf{(6.17)}$$

$$\tau_{ii} = 0 \quad \textbf{(6.18)}$$

$$G_{ii} = 1 \quad \textbf{(6.19)}$$

Where a_{ij},b_{ij},e_{ij} and $f_{ij}$are interaction parameter.

The DESs critical properties are evaluated as discussed in section 3.1 and are listed in **Table 6.6**.

Table 6.6 Estimated critical properties and density of DESs at 298.15 K and at 0.1 MPa.

DESs	T_C (K)	V_C (cc/mol)	P_C (bar)	ω	Density calculated (kg/m^3)	Density experimental (kg/m^3)	Absolute percentage error
DES1	654.26	352.94	32.84	0.945	1199.6	1232.6	2.68
DES2	750.24	420.62	31.45	0.956	1242.0	1208.7	2.75
DES3	712.32	528.73	23.52	0.981	1172.2	1075.4	8.59

The result shows that estimated density deviates from experimental density. This is because critical properties were estimated considering DESs precursor molecule only. Further, the NRTL method was used for the modeling of liquid-liquid equilibria of the MF and DESs systems. DESs were assumed to be non-volatile and are non-dissociating compounds. The experimental data modeled well with the NRTL thermodynamic model and the obtained binary interaction parameters are shown in **Tables 6.7, 6.8,** and **6.9**.

Table 6.7 Binary interaction parameters for DES1 system

Component i	T	Heptane	T	DES1	Heptane	DES1	Heptane
Component j	DES1	DES1	Heptane	2-MT	2-MT	DBT	DBT
a_{ij}	22.917	3.597	5.098	-1.030	1.823	-23.380	9.314
a_{ji}	-0.355	9.354	7.951	0.471	5.274	-1.020	5.717
b_{ij}	3694.823	525.612	1751.994	0	0	9382.143	0
b_{ji}	2675.884	-445.015	485.860	0	0	3899.071	0
c_{ij}	0.300	0.300	0.300	0.300	0.300	0.300	0.300

Table 6.8 Binary interaction parameters for DES2 system

Component i	T	T	Heptane	Heptane	DBT	Heptane	DES2
Component j	DES2	Heptane	DES2	DBT	DES2	2-MT	2-MT
a_{ij}	14.806	7.622	4.399	11.027	-4.411	-2.355	8.373
a_{ji}	-1.868	7.488	3.538	10.801	-1.795	1.328	-15.301
b_{ij}	5893.016	1202.404	1318.911	-2554.85	1919.626	3482.049	-1794.050
b_{ji}	2810.245	440.544	1660.327	119.081	0	-760.077	4667.625
c_{ij}	0.300	0.300	0.300	0.300	0.300	0.300	0.300

Table 6.9 Binary interaction parameters for DES3 system

Component i	2-MT	2-MT	DES 3	DES 3	Thiophene	DES 3	Heptane
Component j	DES 3	Heptane	Heptane	Thiophene	Heptane	DBT	DBT
a_{ij}	-0.110	2.891	3.780	-12.401	7.627	-1.559	10.624
a_{ji}	4.427	10.072	8.369	15.858	0.269	-1.338	1.472
b_{ij}	396.158	-361.143	1735.981	6057.143	1192.882	2841.551	137.614
b_{ji}	1983.066	1231.160	39.796	6281.479	2652.012	1845.399	-190.464
c_{ij}	0.300	0.300	0.300	0.300	0.300	0.300	0.300

This also suggests that the intra-molecule interaction in DES is different from the inter-molecule interaction between DES and the sulfur compounds due to the presence of strong electronegative atoms in organo-sulfur compounds[220,237,251].

6.4 Conclusion

The extractive desulfurization of MFs having DBT, 2-MT, and T as sulfur compounds were successfully investigated using diglycol based DESs. All synthesized DESs are effective in extractive desulfurization. Among different synthesized DESs, TBAB/4DG showed the highest removal capacity of sulfur compounds. The effect of different parameters such as extraction time, DES ratio, and the temperature was also investigated. The result indicated that DES/ MF ratio has a significant effect compared to the other variables such as extraction time and temperature. The DESs used in this study showed higher extraction efficiency for DBT (>90%) and lower extraction efficiency for thiophene (~68%). The thermodynamic modeling showed that non-random two liquid (NRTL) model best fit the extraction of sulfur compounds.

Overall Conclusions And Recommendations

This research is focused on the desulfurization of sulfur refractory compounds from model diesel oil by adsorptive and extractive approaches. Mainly, carbon-based materials M-CNT, M-CNF, PMACs as well as GNP, were used for adsorptive desulfurization. Further, the possibilities of utilizing DESs for sulfur removal have also been explored. The results showed that adsorptive desulfurization using carbon materials as well as extractive desulfurization using DESs have the potential to replace the conventional hydrodesulfurization method for sulfur removal.

The preliminary study indicates that the M-CNT and M-CNF possess a significant adsorptive capacity for the removal of DBT from MDF. M-CNT showed a greater capacity to adsorb the DBT compare to that of M-CNF mainly due to its high surface area and pore size. The adsorption of DBT on M-CNT generally is spontaneous, exothermic process and has less randomness at the interface.

The textural characteristics of adsorbents significantly affect the adsorption behavior. Thus, the DBT adsorption capacity of PMACs have been studied. The study shows that the desulfurization ability of PMAC 1/3 exhibits better performance compared to PMAC 1/4. The higher desulfurization capabilities of PMAC 1/3 have a direct correspondence with the better micro-porosity. The results suggest that the Mongolian based activated carbon have the potential to be used in the industry for the adsorptive desulfurization process due to its high adsorptive capacities.

The observation of breakthrough behavior for the continuous adsorption process is vital. In consequence, the adsorption of model diesel fuels containing sulfur compounds over GNP was conducted in both batch and continuous adsorption modes for single and multicomponent feed. The individual study of DBT, 2-MT & T removal by GNP from the batch studies showed that the removal capacity of GNP follows the order DBT>2-MT> T. Investigation of continuous desulfurization study shows that the adsorption breakthrough curve strongly depends on the bed height, flow rate & initial S-compounds concentration.

The extractive desulfurization of MFs having DBT, 2-MT, and T as sulfur compounds were successfully investigated using Diglycol based DESs. All synthesized DESs are effective in extractive desulfurization. Among different synthesized DESs, TBAB/4DG showed the highest removal capacity of sulfur compounds. The DESs used in this study showed higher extraction efficiency for DBT and lower extraction efficiency for Thiophene. The thermodynamic modelling showed that the NRTL model best fit the extraction of sulfur compounds.

Future recommendation

The sulfur removal using carbon-based adsorbents and deep eutectic solvents is limited to laboratory scale only and the commercialization of this process have not still explored by various researchers, Although adsorbents and extractant have shown significant sulfur removal capacity. Based on the results obtained in this work for model diesel oil, it is recommended to explore the adsorption behavior of the carbon-based adsorbents and DESs for the removal of sulfur compounds from commercial diesel oil. This will provide essential data for modelling the physical adsorption and extraction processes.

The development of an acceptable regeneration/solvent recovery methodology for the sorbent/extractant is value learning. Considering the cyclic adsorption/extraction requirement, the detailed analysis of multiple regeneration/recovery cycles need to be thoroughly explored.

References

[1] Y. Sano, K. Sugahara, K.H. Choi, Y. Korai, I. Mochida, Two-step adsorption process for deep desulfurization of diesel oil, Fuel. 84 (2005) 903–910.

[2] R.. Verma, Fundamentals of hydro-processing from Indian oil publication.

[3] S. Steiner, J. Czerwinski, P. Comte, N. V Heeb, A. Mayer, A. Petri-fink, B. Rothen-rutishauser, Effects of an iron-based fuel-borne catalyst and a diesel particle filter on exhaust toxicity in lung cells in vitro, (2014).

[4] G. Lemasters, L. Levin, D.I. Bernstein, S.D.L. Iv, J.E. Lockey, J. Burkle, G.K.K. Hershey, K. Brunst, P.H. Ryan, Secondhand Smoke and Traffic Exhaust Confer Opposing Risks for Asthma in Normal and Overweight Children, 23 (2015) 32–36.

[5] H. Tong, A.G. Rappold, M. Caughey, A.L. Hinderliter, D.W. Graff, J.H. Berntsen, W.E. Cascio, R.B. Devlin, J.M. Samet, Cardiovascular effects caused by increasing concentrations of diesel exhaust in middle-aged healthy GSTM1 null human volunteers, 8378 (2014) 319–326.

[6] N.L.J. Gense, Riemersma, C. Such, L. Ntziachristos, TNO report: Euro VI technologies and costs for Heavy Duty vehicles The expert panels summary of stakeholders responses, (2006) 30–34.

[7] S. Chaudhuri, Bharat Emission Standards" Alter. Fuels Pros & Cons.

[8] S.H. S Salvi, Is diesel exhaust a cause for increasing allergies ?, 29 (2000) 4–8.

[9] E. Kowsari, Recent Advances in the Science and Technology of Desulfurization of Diesel Fuel Using Ionic Liquids, (2009).

[10] J. Zhang, D. Zhao, J. Wang, L. Yang, Photocatalytic oxidation of dibenzothiophene using TiO2/bamboo charcoal, J. Mater. Sci. 44 (2009) 3112–3117.

[11] A. Stanislaus, A. Marafi, M.S. Rana, Recent advances in the science and technology of ultra low sulfur diesel (ULSD) production, Catal. Today. 153 (2010) 1–68.

[12] S. Otsuki, T. Nonaka, N. Takashima, W. Qian, A. Ishihara, T. Imai, T. Kabe, Oxidative Desulfurization of Light Gas Oil and Vacuum Gas Oil by Oxidation and Solvent Extraction, Energy and Fuels. 14 (2000) 1232–1239.

[13] H. Mei, B.W. Mei, T.F. Yen, A new method for obtaining ultra-low sulfur diesel fuel via ultrasound assisted oxidative desulfurization, Fuel. 82 (2003) 405–414.

[14] P.S. Tam, J.R. Kittrell, J.W. Eldridge, Desulfurization of Fuel Oil by Oxidation and Extraction. 1. Enhancement of Extraction Oil Yield, Ind. Eng. Chem. Res. 29 (1990) 321–324.

[15] J.D. Holbrey, I. López-Martin, G. Rothenberg, K.R. Seddon, G. Silvero, X. Zheng, Desulfurisation of oils using ionic liquids: Selection of cationic and anionic components to enhance extraction efficiency, Green Chem. 10 (2008) 87–92.

[16] P. De Filippis, M. Scarsella, Oxidative Desulfurization: Oxidation Reactivity of Sulfur Compounds in Different Organic Matrixes, Energy and Fuels. 17 (2003) 1452–1455.

[17] A.B. Martin, A. Alcon, V.E. Santos, F. Garcia-Ochoa, Production of a biocatalyst of Pseudomonas putida CECT5279 for dibenzothiophene (DBT) biodesulfurization for different media compositions, Energy and Fuels. 18 (2004) 851–857.

[18] T. Macpherson, C.W. Greer, E. Zhou, A.M. Jones, G. Wisse, P.C.K. Lau, B. Sankey, M.J. Grossman, J. Hawari, Application of SPME/GC-MS to characterize metabolites in the biodesulfurizadon of organosulfur model compounds in bitumen, Environ. Sci. Technol. 32 (1998) 421–426.

[19] † and Z. Conrad Zhang Shuguang Zhang, Qinglin Zhang, Extractive desulfurization and denitrogenation of fuels using ionic liquids, Ind. Eng. Chem. Res. 43 (2004) 614–622.

[20] E. Kianpour, S. Azizian, Polyethylene glycol as a green solvent for effective extractive desulfurization of liquid fuel at ambient conditions, Fuel. 137 (2014) 36–40.

[21] H. Zhao, G.A. Baker, D. V. Wagle, S. Ravula, Q. Zhang, Tuning task-specific ionic liquids for the extractive desulfurization of liquid fuel, ACS Sustain. Chem. Eng. 4 (2016) 4771–4780.

[22] S. Zhang, Q. Zhang, Z.C. Zhang, Extractive Desulfurization and Denitrogenation of Fuels Using Ionic Liquids, Ind. Eng. Chem. Res. 43 (2004) 614–622.

[23] J.H. Kim, X. Ma, A. Zhou, C. Song, Ultra-deep desulfurization and denitrogenation of diesel fuel by selective adsorption over three different adsorbents: A study on adsorptive selectivity and mechanism, Catal. Today. 111 (2006) 74–83.

[24] A.J. Hernández-Maldonado, R.T. Yang, Desulfurization of commercial liquid fuels by selective adsorption via π-complexation with Cu(I)-Y zeolite, Ind. Eng. Chem. Res. 42 (2003) 3103–3110.

[25] J. Xiong, L. Yang, Y. Chao, J. Pang, P. Wu, M. Zhang, W. Zhu, H. Li, A large number of low coordinated atoms in boron nitride for outstanding adsorptive desulfurization performance, Green Chem. 18 (2016) 3040–3047.

[26] D.D. Whitehurst, T. Isoda, I. Mochida, Present State of the Art and Future Challenges in the Hydrodesulfurization of Polyaromatic Sulfur Compounds, Adv. Catal. 42 (1998) 345–471.

[27] I. V Babich, J.A. Moulijn, 03/02171 Science and technology of novel processes for deep desulfurization of oil refinery streams: a review Babich, I. V. and Moulijn, J. A. Fuel, 2003, 82, (6), 607–631, Fuel Energy Abstr. 44 (2003) 362.

[28] J.R. Gallagher, E.S. Olson, D.C. Stanley, Microbial desulfurization of dibenzothiophene: A sulfur-specific pathway, FEMS Microbiol. Lett. 107 (1993) 31–35.

[29] J. Calzada, M.T. Zamarro, A. Alcón, V.E. Santos, E. Díaz, J.L. García, F. Garcia-Ochoa, Analysis of dibenzothiophene desulfurization in a recombinant pseudomonas putida

strain, Appl. Environ. Microbiol. 75 (2009) 875–877.

[30] I. Martinez, V.E. Santos, A. Alcon, F. Garcia-Ochoa, Enhancement of the biodesulfurization capacity of Pseudomonas putida CECT5279 by co-substrate addition, Process Biochem. 50 (2015) 119–124.

[31] E. Gomez, V.E. Santos, A. Alcon, F. Garcia-Ochoa, Oxygen transport rate on Rhodococcus erythropolis cultures: Effect on growth and BDS capability, Chem. Eng. Sci. 61 (2006) 4595–4604.

[32] G.- Ochoa, , "Influence of oxygen uptake rate on Rhodococcus erythropolis growth rate and biodesulfurization capacity:limit on the fluid dynamic conditions" ECCE9/ECAB2

[33] F. Garcia-Ochoa, S. Escobar, E. Gomez, Specific oxygen uptake rate as indicator of cell response of Rhodococcus erythropolis cultures to shear effects, Chem. Eng. Sci. 122 (2015) 491–499.

[34] F. Davoodi-Dehaghani, M. Vosoughi, A.A. Ziaee, Biodesulfurization of dibenzothiophene by a newly isolated Rhodococcus erythropolis strain, Bioresour. Technol. 101 (2010) 1102–1105.

[35] I.B.W. Gunam, Y. Yaku, M. Hirano, K. Yamamura, F. Tomita, T. Sone, K. Asano, Biodesulfurization of alkylated forms of dibenzothiophene and benzothiophene by Sphingomonas subarctica T7b, J. Biosci. Bioeng. 101 (2006) 322–327.

[36] M.K. Lee, J.D. Senius, M.J. Grossman, Sulfur-specific microbial desulfurization of sterically hindered analogs of dibenzothiophene, Appl. Environ. Microbiol. 61 (1995) 4362–4366.

[37] S. Velu, X. Ma, C. Song, Selective adsorption for removing sulfur from jet fuel over zeolite-based adsorbents, Ind. Eng. Chem. Res. 42 (2003) 5293–5304.

[38] L. Alves, S.M. Paixão, Enhancement of dibenzothiophene desulfurization by Gordonia alkanivorans strain 1B using sugar beet molasses as alternative carbon source, Appl. Biochem. Biotechnol. 172 (2014) 3297–3305.

[39] M. Seredych, J. Lison, U. Jans, T.J. Bandosz, Textural and chemical factors affecting adsorption capacity of activated carbon in highly efficient desulfurization of diesel fuel, Carbon N. Y. 47 (2009) 2491–2500.

[40] J.G. Park, C.H. Ko, K.B. Yi, J.H. Park, S.S. Han, S.H. Cho, J.N. Kim, Reactive adsorption of sulfur compounds in diesel on nickel supported on mesoporous silica, Appl. Catal. B Environ. 81 (2008) 244–250.

[41] J.. Mulva, "Performing today preparing for tomorrow" sustainable development report -baseline, (2005) .

[42] K.S. Triantafyllidis, E.A. Deliyanni, Desulfurization of diesel fuels: Adsorption of 4,6-DMDBT on different origin and surface chemistry nanoporous activated carbons, Chem. Eng. J. 236 (2014) 406–414.

[43] S. a Kauffman, N.P. Group, Nature Publishing Group, Group. 224 (1969) 177–178.

[44] G.G. Tibbetts, M.L. Lake, K.L. Strong, B.P. Rice, A review of the fabrication and properties of vapor-grown carbon nanofiber/polymer composites, Compos. Sci. Technol. 67 (2007) 1709–1718.

[45] S. Bigdeli, S. Fatemi, Fast carbon nanofiber growth on the surface of activated carbon by microwave irradiation: A modified nano-adsorbent for deep desulfurization of liquid fuels, Chem. Eng. J. 269 (2015) 306–315.

[46] S. Kim, B. Bajaj, C.K. Byun, S.J. Kwon, H.I. Joh, K.B. Yi, S. Lee, Preparation of flexible zinc oxide/carbon nanofiber webs for mid-temperature desulfurization, Appl. Surf. Sci. 320 (2014) 218–224.

[47] A. Deneuve, K. Wang, I. Janowska, K. Chizari, D. Edouard, O. Ersen, M.J. Ledoux, C. Pham-Huu, Bucky paper with improved mechanical stability made from vertically aligned carbon nanotubes for desulfurization process, Appl. Catal. A Gen. 400 (2011) 230–237.

[48] W. Zhang, H. Zhang, J. Xiao, Z. Zhao, M. Yu, Z. Li, Carbon nanotube catalysts for oxidative desulfurization of a model diesel fuel using molecular oxygen, Green Chem. 16 (2014) 211–220.

[49] J. Goering, U. Burghaus, Adsorption kinetics of thiophene on single-walled carbon nanotubes (CNTs), Chem. Phys. Lett. 447 (2007) 121–126.

[50] T.H.T. Vu, T.T.T. Nguyen, P.H.T. Nguyen, M.H. Do, H.T. Au, T.B. Nguyen, D.L. Nguyen, J.S. Park, Fabrication of photocatalytic composite of multi-walled carbon nanotubes/TiO 2 and its application for desulfurization of diesel, Mater. Res. Bull. 47 (2012) 308–314.

[51] B.C. Gates, H. Topsøe, Reactivities in deep catalytic hydrodesulfurization: Challenges, opportunities, and the importance of 4-methyldibenzothiophene and 4,6-dimethyldibenzothiophene, Polyhedron. 16 (1997) 3213–3217.

[52] Y. Nie, C.X. Li, Z.H. Wang, Extractive desulfurization of fuel oil using alkylimidazole and its mixture with dialkylphosphate ionic liquids, Ind. Eng. Chem. Res. 46 (2007) 5108–5112.

[53] M.K. Hadj-Kali, Z. Salleh, E. Ali, R. Khan, M.A. Hashim, Separation of aromatic and aliphatic hydrocarbons using deep eutectic solvents: A critical review, Fluid Phase Equilib. 448 (2017) 152–167.

[54] G.W. Meindersma, A. Podt, A.B. De Haan, Selection of ionic liquids for the extraction of aromatic hydrocarbons from aromatic/aliphatic mixtures, Fuel Process. Technol. 87 (2005) 59–70.

[55] T.S. and J.P.M. I. Anugwom, P. Maki-Arvela, Ionic liquid assisted extraction of nitrogen and sulphur-containing air pollutants from model oil and regeneration of the spent ionic liquid, J.Environ. Prot., 2, (2011) 796.

[56] X. Jiang, Y. Nie, C. Li, Z. Wang, Imidazolium-based alkylphosphate ionic liquids - A potential solvent for extractive desulfurization of fuel, Fuel. 87 (2008) 79–84.

[57] 3 and Dejan Macut2 Beata GabriT, 1 Aleksandra Sander, 2 Marina Cvjetko Bubalo, Extraction of S- and N-Compounds from the Mixture of Hydrocarbons by Ionic Liquids as Selective Solvents, 2013 (2013) 1–10.

[58] J. Ranke, S. Stolte, R. Störmann, J. Aming, B. Jastorff, Design of sustainable chemical products - The example of ionic liquids, Chem. Rev. 107 (2007) 2183–2206.

[59] J.S. Wilkes, A short history of ionic liquids - From molten salts to neoteric solvents, Green Chem. 4 (2002) 73–80.

[60] S. Zhu, R. Chen, Y.W. U, Q. Chen, X. Zhang, Z. Yu, A mini-review on greenness of ionic liquids, Chem. Biochem. Eng. Q. 23 (2009) 207–211.

[61] H. Niedermeyer, J.P. Hallett, I.J. Villar-Garcia, P.A. Hunt, T. Welton, Mixtures of ionic liquids, Chem. Soc. Rev. 41 (2012) 7780–7802.

[62] R.N. Das, K. Roy, Advances in QSPR/QSTR models of ionic liquids for the design of greener solvents of the future, Mol. Divers. 17 (2013) 151–196.

[63] M. Francisco, A. Arce, A. Soto, Fluid Phase Equilibria Ionic liquids on desulfurization of fuel oils, 294 (2010) 39–48.

[64] B. Rodríguez-cabo, H. Rodríguez, E. Rodil, A. Arce, A. Soto, Extractive and oxidative-extractive desulfurization of fuels with ionic liquids, 117 (2014) 882–889.

[65] B. Rodríguez-cabo, A. Arce, A. Soto, Fluid Phase Equilibria Desulfurization of fuels by liquid – liquid extraction with 1-ethyl-3-methylimidazolium ionic liquids, Fluid Phase Equilib. 356 (2013) 126–135.

[66] F.T. Li, B. Wu, R.H. Liu, X.J. Wang, L.J. Chen, D.S. Zhao, An inexpensive N-methyl-2-pyrrolidone-based ionic liquid as efficient extractant and catalyst for desulfurization of dibenzothiophene, Chem. Eng. J. 274 (2015) 192–199.

[67] X. Lu, L. Yue, M. Hu, Q. Cao, L. Xu, Y. Guo, S. Hu, W. Fang, Piperazinium-based ionic liquids with lactate anion for extractive desulfurization of fuels, Energy and Fuels. 28 (2014) 1774–1780.

[68] S.A. Dharaskar, K.L. Wasewar, M.N. Varma, D.Z. Shende, K.K. Tadi, C.K. Yoo, Synthesis, characterization, and application of novel trihexyl tetradecyl phosphonium bis (2,4,4-trimethylpentyl) phosphinate for extractive desulfurization of liquid fuel, Fuel Process. Technol. 123 (2014) 1–10.

[69] C. Shu, T. Sun, H. Zhang, J. Jia, Z. Lou, A novel process for gasoline desulfurization based on extraction with ionic liquids and reduction by sodium borohydride, Fuel. 121 (2014) 72–78.

[70] W. Jiang, W. Zhu, H. Li, X. Wang, S. Yin, Y. Chang, H. Li, Temperature-responsive ionic liquid extraction and separation of the aromatic sulfur compounds, Fuel. 140 (2015) 590–596.

[71] S.A. Dharaskar, K.L. Wasewar, M.N. Varma, D.Z. Shende, C.K. Yoo, Extractive desulfurization of liquid fuels by energy efficient green thiazolium based ionic liquids,

Ind. Eng. Chem. Res. 53 (2014) 19845–19854.

[72] H. Gao, S. Zeng, X. Liu, Y. Nie, X. Zhang, S. Zhang, Extractive desulfurization of fuel using N-butylpyridinium-based ionic liquids, RSC Adv. 5 (2015) 30234–30238.

[73] X. Chen, S. Yuan, A.A. Abdeltawab, S.S. Al-Deyab, J. Zhang, L. Yu, G. Yu, Extractive desulfurization and denitrogenation of fuels using functional acidic ionic liquids, Sep. Purif. Technol. 133 (2014) 187–193.

[74] H. Gao, S. Zeng, H. He, H. Dong, Y. Nie, X. Zhang, S. Zhang, Deep Desulfurization of Gasoline Fuel using FeCl3-Containing Lewis-Acidic Ionic Liquids, Sep. Sci. Technol. 49 (2014) 1208–1214.

[75] E. Kianpour, S. Azizian, M. Yarie, M.A. Zolfigol, M. Bayat, A task-specific phosphonium ionic liquid as an efficient extractant for green desulfurization of liquid fuel: An experimental and computational study, Chem. Eng. J. 295 (2016) 500–508.

[76] Z.Y. and Q.Z. Changping Li, Dan Li, a Shuangshuang Zou, a Zhuo Li, Jingmei Yin, a Ailing Wang,Yingna Cui, Extraction desulfurization process of fuels with ammonium based deep eutectic solvents, Green Chem., 2013,15, 2793-2799.

[77] W.S. Ahmed Rahma, F.S. Mjalli, T. Al-Wahaibi, A.A. Al-Hashmi, Polymeric-based deep eutectic solvents for effective extractive desulfurization of liquid fuel at ambient conditions, Chem. Eng. Res. Des. 120 (2017) 271–283.

[78] Z.S. Gano, F.S. Mjalli, T. Al-Wahaibi, Y. Al-Wahaibi, I.M. Alnashef, Solubility of thiophene and dibenzothiophene in anhydrous FeCl3- and ZnCl2-based deep eutectic solvents, Ind. Eng. Chem. Res. 53 (2014) 6815–6823.

[79] X. dong Tang, Y. fen Zhang, J. jing Li, Y. qiang Zhu, D. yong Qing, Y. xin Deng, Deep Extractive Desulfurization with Arenium Ion Deep Eutectic Solvents, Ind. Eng. Chem. Res. 54 (2015) 4625–4632.

[80] H.F. Mohd Zaid, F.K. Chong, M.I. Abdul Mutalib, Photooxidative-extractive deep desulfurization of diesel using Cu-Fe/TiO_2 and eutectic ionic liquid, Fuel. 156 (2015) 54–62.

[81] A. Sander, M. Rogošić, A. Slivar, B. Žuteg, Separation of Hydrocarbons by Means of Liquid-Liquid Extraction with Deep Eutectic Solvents, Solvent Extr. Ion Exch. 34 (2016) 86–98.

[82] Z.S. Gano, F.S. Mjalli, T. Al-Wahaibi, Y. Al-Wahaibi, I.M. AlNashef, Extractive desulfurization of liquid fuel with FeCl<inf>3</inf>-based deep eutectic solvents: Experimental design and optimization by central-composite design, Chem. Eng. Process. Process Intensif. 93 (2015) 10–20.

[83] H. Lü, P. Li, C. Deng, W. Ren, S. Wang, P. Liu, H. Zhang, Deep catalytic oxidative desulfurization (ODS) of dibenzothiophene (DBT) with oxalate-based deep eutectic solvents (DESs), Chem. Commun. 51 (2015) 10703–10706.

[84] J. Yin, J. Wang, Z. Li, D. Li, G. Yang, Y. Cui, A. Wang, C. Li, Deep desulfurization of

fuels based on an oxidation/extraction process with acidic deep eutectic solvents, Green Chem. 17 (2015) 4552–4559.

[85] H. Zhao, S. Xia, P. Ma, Use of ionic liquids as “green” solvents for extractions, J. Chem. Technol. Biotechnol. 80 (2005) 1089–1096.

[86] T. Welton, Room-Temperature Ionic Liquids . Solvents for Synthesis and Catalysis Room-Temperature Ionic Liquids . Solvents for Synthesis and Catalysis, Chem. Rev. 99 (1999) 2071–2084.

[87] a G.M. and L.I. Carlo Pretti, a Cinzia Chiappe, b Daniela Pieraccini, b Michela Gregori, a Francesca Abramo, Acute toxicity of ionic liquids to the zebrafish (Danio rerio), Green Chem. 8 (2006) 238–240.

[88] M. Matsumoto, K. Mochiduki, K. Fukunishi, K. Kondo, Extraction of organic acids using imidazolium-based ionic liquids and their toxicity to Lactobacillus rhamnosus, Sep. Purif. Technol. 40 (2004) 97–101.

[89] A.O. Diallo, C. Len, A.B. Morgan, G. Marlair, Revisiting physico-chemical hazards of ionic liquids, Sep. Purif. Technol. 97 (2012) 228–234.

[90] F.S.M.S.A.-H. S.Gano, Ionic liquids analogues based on potassium carbonate, Thermochim. Acta. 590 (2014) 138–144.

[91] F.S. Mjalli, J. Naser, B. Jibril, V. Alizadeh, Z. Gano, Tetrabutylammonium chloride based ionic liquid analogues and their physical properties, J. Chem. Eng. Data. 59 (2014) 2242–2251.

[92] M.A. Kareem, F.S. Mjalli, M.A. Hashim, I.M. Alnashef, Phosphonium-based ionic liquids analogues and their physical properties, J. Chem. Eng. Data. 55 (2010) 4632–4637.

[93] F. Lima, J. Gouvenaux, L.C. Branco, A.J.D. Silvestre, I.M. Marrucho, Towards a sulfur clean fuel: Deep extraction of thiophene and dibenzothiophene using polyethylene glycol-based deep eutectic solvents, Fuel. 234 (2018) 414–421.

[94] M. Rogošić, K.Z. Kučan, Deep eutectic solvents based on choline chloride and ethylene glycol as media for extractive denitrification/desulfurization/dearomatization of motor fuels, J. Ind. Eng. Chem. (2018).

[95] A. Paiva, R. Craveiro, I. Aroso, M. Martins, R.L. Reis, A.R.C. Duarte, Natural deep eutectic solvents–solvents for the 21st century, ACS Sustain. Chem. Eng. 2 (2014) 1063–1071.

[96] S.E.E. Warrag, N.R. Rodriguez, I.M. Nashef, M.V.S. Annaland, J.I. Siepmann, M.C. Kroon, C.J. Peters, Separation of Thiophene from Aliphatic Hydrocarbons Using Tetrahexylammonium-Based Deep Eutectic Solvents as Extracting Agents, (2017).

[97] F.R. Moghadam, S. Azizian, E. Kianpour, M. Yarie, M. Bayat, M.A. Zolfigol, Green fuel through green route by using a task-specific and neutral phosphonium ionic liquid: A joint experimental and theoretical study, Chem. Eng. J. 309 (2017) 480–488.

[98] A.P. Abbott, D. Boothby, G. Capper, D.L. Davies, R.K. Rasheed, Deep Eutectic Solvents formed between choline chloride and carboxylic acids: Versatile alternatives to ionic liquids, J. Am. Chem. Soc. 126 (2004) 9142–9147.

[99] A.P. Abbott, G. Capper, D.L. Davies, R.K. Rasheed, V. Tambyrajah, Novel solvent properties of choline chloride/urea mixtures, Chem. Commun. 9 (2003) 70–71.

[100] Q. Zhang, K. De Oliveira Vigier, S. Royer, F. Jérôme, Deep eutectic solvents: Syntheses, properties and applications, Chem. Soc. Rev. 41 (2012) 7108–7146.

[101] M. Armand, hiroyuki ohno and bruno scrosati , Frank endres, douglas r. macFarlane, Ionic, ionic-liquid materials for the electrochemical challenges of the future, Nat. Mater. 8 (2009) 621–629.

[102] S. Zhu, Y. Wu, Q. Chen, Z. Yu, C. Wang, S. Jin, Y. Ding, G. Wu, Dissolution of cellulose with ionic liquids and its application: A mini-review, Green Chem. 8 (2006) 325–327.

[103] R. Abro, A.A. Abdeltawab, S.S. Al-Deyab, G. Yu, A.B. Qazi, S. Gao, X. Chen, A review of extractive desulfurization of fuel oils using ionic liquids, RSC Adv. 4 (2014) 35302–35317.

[104] R. Martínez-Palou, R. Luque, Applications of ionic liquids in the removal of contaminants from refinery feedstocks: An industrial perspective, Energy Environ. Sci. 7 (2014) 2414–2447.

[105] P.S. Kulkarni, C.A.M. Afonso, Deep desulfurization of diesel fuel using ionic liquids: Current status and future challenges, Green Chem. 12 (2010) 1139–1149.

[106] W. Ding, W. Zhu, J. Xiong, L. Yang, A. Wei, M. Zhang, H. Li, Novel heterogeneous iron-based redox ionic liquid supported on SBA-15 for deep oxidative desulfurization of fuels, Chem. Eng. J. 266 (2015) 213–221.

[107] A. Bösmann, L. Datsevich, A. Jess, A. Lauter, C. Schmitz, P. Wasserscheid, Deep desulfurization of diesel fuel by extraction with ionic liquids, Chem. Commun. 23 (2001) 2494–2495.

[108] A.R. Ferreira, L.A. Neves, J.C. Ribeiro, F.M. Lopes, J.A.P. Coutinho, I.M. Coelhoso, J.G. Crespo, Removal of thiols from model jet-fuel streams assisted by ionic liquid membrane extraction, Chem. Eng. J. 256 (2014) 144–154.

[109] X.J. Wang, F.T. Li, J.X. Liu, C.G. Kou, Y. Zhao, Y.J. Hao, D. Zhao, Preparation of TiO2 in ionic liquid via microwave radiation and in situ photocatalytic oxidative desulfurization of diesel oil, Energy and Fuels. 26 (2012) 6777–6782.

[110] G. Yu, S. Lu, H. Chen, Z. Zhu, Diesel fuel desulfurization with hydrogen peroxide promoted by formic acid and catalyzed by activated carbon, Carbon N. Y. 43 (2005) 2285–2294.

[111] H. Lü, S. Wang, C. Deng, W. Ren, B. Guo, Oxidative desulfurization of model diesel via dual activation by a protic ionic liquid, J. Hazard. Mater. 279 (2014) 220–225.

[112] Y. Nie, C. Li, A. Sun, H. Meng, Z. Wang, Extractive desulfurization of gasoline using imidazolium-based phosphoric ionic liquids, Energy and Fuels. 20 (2006) 2083–2087.

[113] L.N.N.. S. N.L.J Gense, "Euro VI technologies and costs for Heavy Duty vehicles" The expert panels, 2006.

[114] A. Jess, J. Eber, DEEP DESULFURIZATION OF OIL REFINERY STREAMS Electrochemical Society Proceedings Volume 2004-24, 582 (2004) 572–582.

[115] F.H. Yang, R.T., Hernandez-Maldonado, A.J., Yang, Desulfurization of transportation fuels with zeolites under ambient conditions, Science 301 (2003) 48109.

[116] D. Jha, M.B. Haider, R. Kumar, M.S. Balathanigaimani, Extractive desulfurization of dibenzothiophene using phosphonium-based ionic liquid: Modeling of batch extraction experimental data and simulation of continuous extraction process, Chem. Eng. Res. Des. 111 (2016).

[117] N.M. Mubarak, J.N. Sahu, E.C. Abdullah, N.S. Jayakumar, P. Ganesan, Single stage production of carbon nanotubes using microwave technology, Diam. Relat. Mater. 48 (2014) 52–59.

[118] N.M. Mubarak, E.C. Abdullah, J.N. Sahu, N.S. Jayakumar, P. Ganesan, Mass production of carbon nanofibers using microwave technology, J. Nanosci. Nanotechnol. 15 (2015) 9571–9577.

[119] K.Y. Foo, B.H. Hameed, Insights into the modeling of adsorption isotherm systems, Chem. Eng. J. 156 (2010) 2–10.

[120] C. Sentorun-Shalaby, S.K. Saha, X. Ma, C. Song, Mesoporous-molecular-sieve-supported nickel sorbents for adsorptive desulfurization of commercial ultra-low-sulfur diesel fuel, Appl. Catal. B Environ. 101 (2011) 718–726.

[121] C. Marín-Rosas, L.F. Ramírez-Verduzco, F.R. Murrieta-Guevara, G. Hernández-Tapia, L.M. Rodríguez-Otal, Desulfurization of low sulfur diesel by adsorption using activated carbon: Adsorption isotherms, Ind. Eng. Chem. Res. 49 (2010) 4372–4376.

[122] S. Lagergren, About the Theory of So-Called Adsorption of Soluble Substances, 24 (1898).

[123] M. Ishaq, S. Sultan, I. Ahmad, H. Ullah, M. Yaseen, A. Amir, Adsorptive desulfurization of model oil using untreated, acid activated and magnetite nanoparticle loaded bentonite as adsorbent, J. Saudi Chem. Soc. 21 (2017) 143–151.

[124] Y.S. Ho, G. McKay, Comparative sorption kinetic studies of dye and aromatic compounds onto fly ash, J. Environ. Sci. Heal. - Part A Toxic/Hazardous Subst. Environ. Eng. 34 (1999) 1179–1204.

[125] R. Aravindhan, J.R. Rao, B.U. Nair, Removal of basic yellow dye from aqueous solution by sorption on green alga Caulerpa scalpelliformis, J. Hazard. Mater. 142 (2007) 68–76.

[126] M.J.K. Ahmed, M. Ahmaruzzaman, Adsorptive desulfurization of feed diesel using

chemically impregnated coconut coir waste, Int. J. Environ. Sci. Technol. 12 (2015) 2847–2856.

[127] J.C. Weber Jr, W.J., Morris, Kinetics of adsorption on carbon from solution,. Sanit. Eng. Div., ASCE , 89,(1963) 31 – 59.

[128] L.S.M. G. E. BOYD, A.W. Adamson, The Exchange Adsorption of Ions from Aqueous Solutions by Organic Zeolites II Kinetics, J. Am. Chem. Soc. 69, (1947) 2836–2848.

[129] S. Kumar, V.C. Srivastava, R.P. Badoni, Studies on adsorptive desulfurization by zirconia based adsorbents, Fuel. 90 (2011) 3209–3216.

[130] R.N. Fallah, S. Azizian, G. Reggers, R. Carleer, S. Schreurs, J. Ahenach, V. Meynen, J. Yperman, Effect of aromatics on the adsorption of thiophenic sulfur compounds from model diesel fuel by activated carbon cloth, Fuel Process. Technol. 119 (2014) 278–285.

[131] J. Xiao, G. Bian, W. Zhang, Z. Li, Adsorption of dibenzothiophene on Ag/Cu/Fe-supported activated carbons prepared by ultrasonic-assisted impregnation, J. Chem. Eng. Data. 55 (2010) 5818–5823.

[132] Y. Shi, X. Zhang, G. Liu, Activated Carbons Derived from Hydrothermally Carbonized Sucrose: Remarkable Adsorbents for Adsorptive Desulfurization, ACS Sustain. Chem. Eng. 3 (2015) 2237–2246.

[133] T.A. Saleh, K.O. Sulaiman, S.A. AL-Hammadi, H. Dafalla, G.I. Danmaliki, Adsorptive desulfurization of thiophene, benzothiophene and dibenzothiophene over activated carbon manganese oxide nanocomposite: with column system evaluation, J. Clean. Prod. 154 (2017) 401–412.

[134] E.S. Moosavi, S.A. Dastgheib, R. Karimzadeh, Adsorption of thiophenic compounds from model diesel fuel using copper and nickel impregnated activated carbons, Energies. 5 (2012) 4233–4250.

[135] S. Kumagai, H. Ishizawa, Y. Toida, Influence of solvent type on dibenzothiophene adsorption onto activated carbon fiber and granular coconut-shell activated carbon, Fuel. 89 (2010) 365–371.

[136] A. Srivastav, V.C. Srivastava, Adsorptive desulfurization by activated alumina, J. Hazard. Mater. 170 (2009) 1133–1140.

[137] A.E. Ofomaja, Intraparticle diffusion process for lead(II) biosorption onto mansonia wood sawdust, Bioresour. Technol. 101 (2010) 5868–5876.

[138] F.C. Wu, R.L. Tseng, R.S. Juang, Initial behavior of intraparticle diffusion model used in the description of adsorption kinetics, Chem. Eng. J. 153 (2009) 1–8.

[139] I. Guerrero-Coronilla, L. Morales-Barrera, E. Cristiani-Urbina, Kinetic, isotherm and thermodynamic studies of amaranth dye biosorption from aqueous solution onto water hyacinth leaves, J. Environ. Manage. 152 (2015) 99–108.

[140] A.A. Ismaiel, M.K. Aroua, R. Yusoff, Palm shell activated carbon impregnated with

task-specific ionic-liquids as a novel adsorbent for the removal of mercury from contaminated water, Chem. Eng. J. 225 (2013) 306–314.

[141] M.A. and Y.O. mehmet dogan, Adsorption of Methylene Blue From Aqueous Solution Onto Perlite, Water. Air. Soil Pollut. 120 (2000) 229–248.

[142] G. McKay, M.S. Otterburn, J.A. Aga, Fuller's earth and fired clay as adsorbents for dyestuffs - Equilibrium and rate studies, Water. Air. Soil Pollut. 24 (1985) 307–322.

[143] E. Bulut, M. Özacar, I.A. Şengil, Adsorption of malachite green onto bentonite: Equilibrium and kinetic studies and process design, Microporous Mesoporous Mater. 115 (2008) 234–246.

[144] J. Weitkamp, M. Schwark, S. Ernst, Removal of Thiophene Impurities from Benzene, J. Chem. Soc. Chem. Commun. (1991) 1133–1134.

[145] S.H.D. Lee, R. Kumar, M. Krumpelt, Sulfur removal from diesel fuel-contaminated methanol, Sep. Purif. Technol. 26 (2002) 247–258.

[146] X. Ma, L. Sun, C. Song, A new approach to deep desulfurization of gasoline, diesel fuel and jet fuel by selective adsorption for ultra-clean fuels and for fuel cell applications, Catal. Today. 77 (2002) 107–116.

[147] A.J. Hernández-Maldonado, S.D. Stamatis, R.T. Yang, A.Z. He, W. Cannella, New Sorbents for Desulfurization of Diesel Fuels via π Complexation: Layered Beds and Regeneration, Ind. Eng. Chem. Res. 43 (2004) 769–776.

[148] and H.L. Wangliang Li, Qingfen Liu, Jianmin Xing, Hongshuai Gao, Xiaochao Xiong, Yuguang Li, Xin Li, High-Efficiency Desulfurization by Adsorption with Mesoporous Aluminosilicates Wangliang, 60 (2014) 3263–3268.

[149] C. Yu, J.S. Qiu, Y.F. Sun, X.H. Li, G. Chen, Z. Bin Zhao, Adsorption removal of thiophene and dibenzothiophene from oils with activated carbon as adsorbent: Effect of surface chemistry, J. Porous Mater. 15 (2008) 151–157.

[150] H.J. Jeon, C.H. Ko, S.H. Kim, J.N. Kim, Removal of refractory sulfur compounds in diesel using activated carbon with controlled porosity, Energy and Fuels. 23 (2009) 2537–2543. https://doi.org/10.1021/ef801050k.

[151] M. Muzic, K. Sertic-Bionda, Z. Gomzi, Kinetic and statistical studies of adsorptive desulfurization of diesel fuel on commercial activated carbons, Chem. Eng. Technol. 31 (2008) 355–364.

[152] Y. Wang, R.T. Yang, Desulfurization of liquid fuels by adsorption on carbon-based sorbents and ultrasound-assisted sorbent regeneration, Langmuir. 23 (2007) 3825–3831.

[153] J. Wen, X. Han, H. Lin, Y. Zheng, W. Chu, A critical study on the adsorption of heterocyclic sulfur and nitrogen compounds by activated carbon: Equilibrium, kinetics and thermodynamics, Chem. Eng. J. 164 (2010) 29–36.

[154] V. Selvavathi, V. Chidambaram, A. Meenakshisundaram, B. Sairam, B. Sivasankar, Adsorptive desulfurization of diesel on activated carbon and nickel supported systems,

Catal. Today. 141 (2009) 99–102.

[155] C. Song, X. Ma, New design approaches to ultra-clean diesel fuels by deep desulfurization and deep dearomatization, Appl. Catal. B Environ. 41 (2003) 207–238.

[156] X. Ma, S. Velu, J.H. Kim, C. Song, Deep desulfurization of gasoline by selective adsorption over solid adsorbents and impact of analytical methods on ppm-level sulfur quantification for fuel cell applications, Appl. Catal. B Environ. 56 (2005) 137–147.

[157] A. Zhou, X. Ma, C. Song, Liquid-phase adsorption of multi-ring thiophenic sulfur compounds on carbon materials with different surface properties, J. Phys. Chem. B. 110 (2006) 4699–4707.

[158] J. Bu, G. Loh, C.G. Gwie, S. Dewiyanti, M. Tasrif, A. Borgna, Desulfurization of diesel fuels by selective adsorption on activated carbons: Competitive adsorption of polycyclic aromatic sulfur heterocycles and polycyclic aromatic hydrocarbons, Chem. Eng. J. 166 (2011) 207–217.

[159] N. Byamba-Ochir, W.G. Shim, M.S. Balathanigaimani, H. Moon, High density Mongolian anthracite based porous carbon monoliths for methane storage by adsorption, Appl. Energy. 190 (2017) 257–265.

[160] H.C. Lee, N. Byamba-Ochir, W.G. Shim, M.S. Balathanigaimani, H. Moon, High-performance super capacitors based on activated anthracite with controlled porosity, J. Power Sources. 275 (2015) 668–674.

[161] B. Davis, Effect of pP % on Crystal Phase of Zd32 Precipitated from Solution and Calcined at 600 ° C, 14 (1984) 1983.

[162] Jolly SC., Meat extract. In: Official standardized and recommendation methods of analysis. The Society for Analytical Chemistry; 1963, p. 130., (1963) 1963.

[163] H.S. Bamufleh, Adsorption of Dibenzothiophene (DBT) on Activated Carbon from Dates' Stones Using Phosphoric Acid (H 3 PO 4), JKAU Eng. Sci. 22 (2011) 89–105.

[164] M.K. Nazal, M. Khaled, M.A. Atieh, I.H. Aljundi, G.A. Oweimreen, A.M. Abulkibash, The nature and kinetics of the adsorption of dibenzothiophene in model diesel fuel on carbonaceous materials loaded with aluminum oxide particles, Arab. J. Chem. (2015).

[165] J. Hu, Advanced Materials and Structural Engineering, (2016).

[166] J.N. Jaubert, F. Mutelet, VLE predictions with the Peng-Robinson equation of state and temperature dependent kij calculated through a group contribution method, Fluid Phase Equilib. 224 (2004) 285–304.

[167] D. Jha, N.M. Mubarak, M.B. Haider, R. Kumar, M.S. Balathanigaimani, J.N. Sahu, Adsorptive removal of dibenzothiophene from diesel fuel using microwave synthesized carbon nanomaterials, Fuel. 244 (2019) 132–139.

[168] T.A. Saleh, G.I. Danmaliki, Adsorptive desulfurization of dibenzothiophene from fuels by rubber tyres-derived carbons: Kinetics and isotherms evaluation, Process Saf. Environ. Prot. 102 (2016) 9–19.

[169] Y. Yang, H. Lu, P. Ying, Z. Jiang, C. Li, Selective dibenzothiophene adsorption on modified activated carbons, Carbon N. Y. 45 (2007) 3042–3044.

[170] J. Cheng, S. Jin, R. Zhang, X. Shao, M. Jin, Enhanced adsorption selectivity of dibenzothiophene on ordered mesoporous carbon-silica nanocomposites via copper modification, Microporous Mesoporous Mater. 212 (2015) 137–145.

[171] S. Haji, C. Erkey, Removal of Dibenzothiophene from Model Diesel by Adsorption on Carbon Aerogels for Fuel Cell Applications, Ind. Eng. Chem. Res. 42 (2003) 6933–6937.

[172] M. Fayazi, M.A. Taher, D. Afzali, A. Mostafavi, Removal of dibenzothiophene using activated carbon/γ-Fe2O3 nano-composite: Kinetic and thermodynamic investigation of the removal process, Anal. Bioanal. Chem. Res. 2 (2015) 73-84.

[173] N. Farzin Nejad, E. Shams, M.K. Amini, J.C. Bennett, Synthesis of magnetic mesoporous carbon and its application for adsorption of dibenzothiophene, Fuel Process. Technol. 106 (2013) 376–384.

[174] Y. Zhang, Y. Yang, H. Han, M. Yang, L. Wang, Y. Zhang, Z. Jiang, C. Li, Ultra-deep desulfurization via reactive adsorption on Ni/ZnO: The effect of ZnO particle size on the adsorption performance, Appl. Catal. B Environ. 119–120 (2012) 13–19.

[175] J.A. Ritter, S.J. Bhadra, A.D. Ebner, On the use of the dual-process langmuir model for correlating unary equilibria and predicting mixed-gas adsorption equilibria, Langmuir. 27 (2011) 4700–4712.

[176] I. Langmuir, Equação de Langmuir, 345 (1918).

[177] N.J. Nsami, M.J. Ketcha, The adsorption efficiency of chemically prepared activated carbon from cola nut shells by ZnCl2 on methylene blue, J. Chem. 2013 (2013).

[178] W. Zhao, J. Zhu, W. Wei, L. Ma, J. Zhu, J. Xie, Comparative study of modified/non-modified aluminum and silica aerogels for anionic dye adsorption performance, RSC Adv. 8 (2018) 29129–29140.

[179] S. Suresh, V.C. Srivastava, I.M. Mishra, Studies of adsorption kinetics and regeneration of aniline, phenol, 4-chlorophenol and 4-nitrophenol by activated carbon, Chem. Ind. Chem. Eng. Q. 19 (2012) 195–212.

[180] B. Crittenden, W.J. Thomas, Adsorption Technology and Design, Technology. (1998) 288.

[181] S. Mikhail, T. Zaki, L. Khalil, Desulfurization by an economically adsorption technique, Appl. Catal. A Gen. 227 (2002) 265–278.

[182] A. Ibrahim, S. Ben Xian, Z. Wei, Desulfurization of FCC gas oil by solvent extraction, photooxidation, and oxidizing agents, Pet. Sci. Technol. 22 (2004) 287–301.

[183] G. Shan, H. Liu, J. Xing, G. Zhang, K. Wang, Separation of Polycyclic Aromatic Compounds from Model Gasoline by Magnetic Alumina Sorbent Based on π-Complexation, Ind. Eng. Chem. Res. 43 (2004) 758–761.

[184] M. Ahmadi, M. Mohammadian, M.R. Khosravi-nikou, Experimental , kinetic , and thermodynamic studies of adsorptive desulfurization and denitrogenation of model fuels using novel mesoporous materials, J. Hazard. Mater. 374 (2019) 129–139.

[185] M. Mohammadian, M. Reza, K. Nikou, Model fuel desulfurization and denitrogenation using copper and cerium modified mesoporous material (MSU - S) through adsorption process, Clean Technol. Environ. Policy. (2017).

[186] J. Sasanipour, A. Shariati, M. Aghajani, Dibenzothiophene removal from model fuel using an acid treated activated carbon, Pet. Sci. Technol. 35 (2018) 2066–2073.

[187] M. Mohammadian, M. Ahmadi, M.R. Khosravi-, Adsorptive desulfurization and denitrogenation of model fuel by mesoporous adsorbents (MSU-S and, Pet. Sci. Technol. 35 (2017) 608–614.

[188] M. Montazerolghaem, A. Rahimi, F. Seyedeyn-Azad, Equilibrium and kinetic modeling of adsorptive sulfur removal from gasoline by synthesized Ce-Y zeolite, Appl. Surf. Sci. 257 (2010) 603–609.

[189] M. Ahmadi, B. Anvaripour, M.R. Khosravi-nikou, Journal of Environmental Chemical Engineering Selective denitrogenation of model fuel through iron and chromium modi fi ed microporous materials (MSU-S), J. Environ. Chem. Eng. 5 (2017) 849–860.

[190] L. Ban, P. Liu, C. Ma, B. Dai, Deep extractive desulfurization of diesel fuels by FeCl 3 / ionic liquids, Chinese Chem. Lett. 24 (2013) 755–758.

[191] S. Rashidi, M.R. Khosravi Nikou, B. Anvaripour, Adsorptive desulfurization and denitrogenation of model fuel using HPW and NiO-HPW modified aluminosilicate mesostructures, Microporous Mesoporous Mater. 211 (2015) 134–141.

[192] S. Wang, H. Sun, H.M. Ang, M.O. Tadé, Adsorptive remediation of environmental pollutants using novel graphene-based nanomaterials, Chem. Eng. J. 226 (2013) 336–347.

[193] X. Yuan, Y. Wang, J. Wang, C. Zhou, Q. Tang, X. Rao, Calcined graphene/MgAl-layered double hydroxides for enhanced Cr(VI) removal, Chem. Eng. J. 221 (2013) 204–213.

[194] H. Wang, X. Yuan, Y. Wu, H. Huang, G. Zeng, Y. Liu, X. Wang, N. Lin, Y. Qi, Adsorption characteristics and behaviors of graphene oxide for Zn(II) removal from aqueous solution, Appl. Surf. Sci. 279 (2013) 432–440.

[195] L. Ai, J. Jiang, Removal of methylene blue from aqueous solution with self-assembled cylindrical graphene-carbon nanotube hybrid, Chem. Eng. J. 192 (2012) 156–163.

[196] L.A. Al-Khateeb, S. Almotiry, M.A. Salam, Adsorption of pharmaceutical pollutants onto graphene nanoplatelets, Chem. Eng. J. 248 (2014) 191–199.

[197] and Z.Y. Kun Guo, Minfen Gu, Carbon Nanocatalysts for Aquathermolysis of Heavy Crude Oil: Insights into Thiophene Hydrodesulfurization, The Energy Conundrum. (2018) 119–190.

[198] H.A. Al-jamimi, A. Bagudu, A. Saleh, An intelligent approach for the modeling and experimental optimization of molecular hydrodesulfurization over AlMoCoBi catalyst, 278 (2019) 376–384.

[199] T.A. Saleh, S.A. Al-hammadi, A.M. Al-amer, Effect of Boron on the Efficiency of MoCo catalysts Supported on Alumina for the Hydrodesulfurization of Liquid Fuels, Process Saf. Environ. Prot. (2018).

[200] S.A. Al-hammadi, A. Al-amer, T.A. Saleh, Alumina-carbon nanofiber composite as a support for MoCo catalysts in hydrodesulfurization reactions, Chem. Eng. J. (2018).

[201] P. Taylor, T.A. Saleh, Desalination and Water Treatment Nanocomposite of carbon nanotubes / silica nanoparticles and their use for adsorption of Pb (II): from surface properties to sorption mechanism, (2015) 37–41.

[202] I.W.A. Publishing, W. Supply, Mercury sorption by silica / carbon nanotubes and silica / activated carbon : a comparison study Taw fi k A . Saleh, (2015) 892–903.

[203] T.A. Saleh, Isotherm , kinetic , and thermodynamic studies on Hg (II) adsorption from aqueous solution by silica- multiwall carbon nanotubes, (2015) 16721–16731.

[204] M. Chen, Y. Ding, Y. Liu, N. Wang, B. Yang, L. Ma, Adsorptive desulfurization of thiophene from the model fuels onto graphite oxide/metal-organic framework composites, Pet. Sci. Technol. 36 (2018) 141–147.

[205] M.J. Jaycock, G.D. Parfitt, Chemistry of Interfaces, 85 (1981) 718.

[206] S. Murzin, D., Chemical kinetics 1st Edition.

[207] M.L. Samaniego, M.D.G. De Luna, D.C. Ong, M.W. Wan, M.C. Lu, Isotherm and Thermodynamic Studies on the Removal of Sulfur from Diesel Fuel by Mixing-Assisted Oxidative-Adsorptive Desulfurization Technology, Energy and Fuels. 33 (2019) 1098–1105.

[208] B.R. Fox, B.L. Brinich, J.L. Male, R.L. Hubbard, M.N. Siddiqui, T.A. Saleh, D.R. Tyler, Enhanced oxidative desulfurization in a film-shear reactor, Fuel. 156 (2015) 142–147.

[209] J. Goel, K. Kadirvelu, C. Rajagopal, V.K. Garg, Removal of lead(II) by adsorption using treated granular activated carbon: Batch and column studies, J. Hazard. Mater. 125 (2005) 211–220.

[210] D.C.K.Ko, J.F.Porter, G.Mckay, Fixed Bed Studies for the Sorption of Metal Ions onto Peat, Process Saf Environ Prot, 81 (2003) 78–86.

[211] M.D. Joshi, J.L. Anderson, Recent advances of ionic liquids in separation science and mass spectrometry, RSC Adv. 2 (2012) 5470.

[212] P. Liu, J.-W. Hao, L.-P. Mo, Z.-H. Zhang, Recent advances in the application of deep eutectic solvents as sustainable media as well as catalysts in organic reactions, RSC Adv. 5 (2015) 48675–48704.

[213] Z. Lei, B. Chen, Y.M. Koo, D.R. Macfarlane, Introduction: Ionic Liquids, Chem. Rev.

117 (2017) 6633–6635.

[214] P.W. Jochen Eßer, A. Jess, Deep desulfurization of oil by extraction with ionic liquids, Green Chem. 6 (2004) 316–322.

[215] D. Jha, M.B. Haider, R. Kumar, M.S. Balathanigaimani, Extractive desulfurization of dibenzothiophene using phosphonium-based ionic liquid: Modeling of batch extraction experimental data and simulation of continuous extraction process, Chem. Eng. Res. Des. 111 (2016) 218–222.

[216] H. Zhao, G.A. Baker, D. V. Wagle, S. Ravula, Q. Zhang, Tuning task-specific ionic liquids for the extractive desulfurization of liquid fuel, ACS Sustain. Chem. Eng. 4 (2016) 4771–4780.

[217] Q. Zhang, K. De Oliveira Vigier, S. Royer, F. Jèrôme, Deep eutectic solvents: syntheses, properties and applications, Chem. Soc. Rev. 41 (2012) 7108–7146.

[218] E.L. Smith, A.P. Abbott, K.S. Ryder, Deep Eutectic Solvents (DESs) and Their Applications, Chem. Rev. 114, (2012) 11060–11082.

[219] M.C. Ali, R. Liu, J. Chen, T. Cai, H. Zhang, Z. Li, H. Zhai, H. Qiu, New deep eutectic solvents composed of crown ether, hydroxide and polyethylene glycol for extraction of non-basic N-compounds, Chinese Chem. Lett. 30 (2019) 871–874.

[220] J.J. Li, H. Xiao, X.D. Tang, M. Zhou, Green Carboxylic Acid-Based Deep Eutectic Solvents as Solvents for Extractive Desulfurization, Energy and Fuels. 30 (2016) 5411–5418.

[221] F. Lima, M. Dave, A.J.D. Silvestre, L.C. Branco, I.M. Marrucho, Concurrent Desulfurization and Denitrogenation of Fuels Using Deep Eutectic Solvents, ACS Sustain. Chem. Eng. 7 (2019) 11341–11349.

[222] S.E.E. Warrag, C.J. Peters, M.C. Kroon, Deep eutectic solvents for highly efficient separations in oil and gas industries, Curr. Opin. Green Sustain. Chem. 5 (2017) 55–60.

[223] N. Sudhir, P. Yadav, B.R. Nautiyal, R. Singh, H. Rastogi, H. Chauhan, Extractive desulfurization of fuel with methyltriphenyl phosphonium bromide- tetraethylene glycol-based eutectic solvents, Sep. Sci. Technol. 00 (2019) 1–10.

[224] J. Gao, S. Zhu, Y. Dai, C. Xiong, C. Li, W. Yang, X. Jiang, Performance and mechanism for extractive desulfurization of fuel oil using modified polyethylene glycol, Fuel. 233 (2018) 704–713.

[225] Z.S. Gano, F.S. Mjalli, T. Al-Wahaibi, Y. Al-Wahaibi, I.M. Alnashef, Solubility of thiophene and dibenzothiophene in anhydrous FeCl3- and ZnCl2-based deep eutectic solvents, Ind. Eng. Chem. Res. 53 (2014) 6815–6823.

[226] X. dong Tang, Y. fen Zhang, J. jing Li, Y. qiang Zhu, D. yong Qing, Y. xin Deng, Deep Extractive Desulfurization with Arenium Ion Deep Eutectic Solvents, Ind. Eng. Chem. Res. 54 (2015) 4625–4632.

[227] M.B. Haider, D. Jha, B. Marriyappan Sivagnanam, R. Kumar, Modelling and simulation

of CO_2 removal from shale gas using deep eutectic solvents, J. Environ. Chem. Eng. 7 (2019) 102747.

[228] H. Ghaedi, M. Ayoub, S. Sufian, B. Lal, Y. Uemura, Thermal stability and FT-IR analysis of Phosphonium-based deep eutectic solvents with different hydrogen bond donors, J. Mol. Liq. 242 (2017) 395–403.

[229] M.B. Haider, D. Jha, B.M. Sivagnanam, R. Kumar, Thermodynamic and Kinetic Studies of CO 2 Capture by Glycol and 2 Amine-Based Deep Eutectic Solvents, 63 (2018) 2671–2680.

[230] R.K. Ibrahim, M. Hayyan, M.A. Alsaadi, S. Ibrahim, A. Hayyan, M.A. Hashim, Diethylene glycol based deep eutectic solvents and their physical properties, Stud. Univ. Babeș-Bolyai Chem. 62 (2017) 433–450.

[231] J.N. Al-Dawsari, A. Bessadok-Jemai, I. Wazeer, S. Mokraoui, M.A. AlMansour, M.K. Hadj-Kali, Fitting of experimental viscosity to temperature data for deep eutectic solvents, J. Mol. Liq. 310 (2020) 2–4.

[232] M.K. Alomar, M. Hayyan, M.A. Alsaadi, S. Akib, A. Hayyan, M.A. Hashim, Glycerol-based deep eutectic solvents: Physical properties, J. Mol. Liq. 215 (2016) 98–103.

[233] W.N.A.W. Mokhtar, W.A.W.A. Bakar, R. Ali, A.A.A. Kadir, Deep desulfurization of model diesel by extraction with N,N-dimethylformamide: Optimization by Box-Behnken design, J. Taiwan Inst. Chem. Eng. 45 (2014) 1542–1548.

[234] D. Chandran, M. Khalid, R. Walvekar, N.M. Mubarak, S. Dharaskar, W.Y. Wong, T.C.S.M. Gupta, Deep eutectic solvents for extraction-desulphurization: A review, J. Mol. Liq. 275 (2019) 312–322.

[235] D. V. Wagle, H. Zhao, C.A. Deakyne, G.A. Baker, Quantum Chemical Evaluation of Deep Eutectic Solvents for the Extractive Desulfurization of Fuel, ACS Sustain. Chem. Eng. 6 (2018) 7525–7531.

[236] W. Jiang, H. Li, C. Wang, W. Liu, T. Guo, H. Liu, W. Zhu, H. Li, Synthesis of Ionic-Liquid-Based Deep Eutectic Solvents for Extractive Desulfurization of Fuel, Energy and Fuels. 30 (2016) 8164–8170.

[237] M.K. Hadj-Kali, S. Mulyono, H.F. Hizaddin, I. Wazeer, L. El-Blidi, E. Ali, M.A. Hashim, I.M. AlNashef, Removal of Thiophene from Mixtures with n-Heptane by Selective Extraction Using Deep Eutectic Solvents, Ind. Eng. Chem. Res. 55 (2016) 8415–8423.

[238] G. Yu, X. Li, X. Liu, C. Asumana, X. Chen, Deep Desulfurization of Fuel Oils Using Low-Viscosity 1-Ethyl-3-methylimidazolium Dicyanamide Ionic Liquid - Industrial & Engineering Chemistry Research (ACS Publications), (2011) 2236–2244.

[239] C. Huang, B. Chen, J. Zhang, Z. Liu, Y. LI, Desulfurization of gasoline by extraction with new ionic liquids, Energy and Fuels. 18 (2004) 1862–1864.

[240] C.H.J.T. Dietz, A. Erve, M.C. Kroon, M. Van Sint, F. Gallucci, C. Held, Fluid Phase

Equilibria Thermodynamic properties of hydrophobic deep eutectic solvents and solubility of water and HMF in them : Measurements and PC-SAFT modeling, Fluid Phase Equilib. 489 (2019) 75–82.

[241] J.O. Valderrama, R.E. Rojas, Critical Properties of Ionic Liquids. Revisited, Ind. {&} Eng. Chem. Res. 48 (2009) 6890–6900.

[242] S. Singh, V.C. Srivastava, S. Gautam, Oxidative-Extractive Desulfurization of Liquid Fuel by Dimethyl Sulfoxide and $ZnCl_2$ Based Ionic Liquid, Int. J. Chem. React. Eng. 14 (2016) 539–545.

[243] K.H. Almashjary, M. Khalid, S. Dharaskar, P. Jagadish, R. Walvekar, T.C.S.M. Gupta, Optimisation of extractive desulfurization using Choline Chloride-based deep eutectic solvents, Fuel. 234 (2018) 1388–1400.

[244] M. Wang, Q. Wu, H.S. Li, Y. Zhao, Q.Z. Jiao, Oxidative desulfurization of dibenzothiophene catalyzed by polyoxometalate-based ionic liquid, Adv. Mater. Res. 1033–1034 (2014) 65–69.

[245] D.S. Zhao, Z.M. Sun, F.T. Li, H.D. Shan, Optimization of oxidative desulfurization of dibenzothiophen using acidic ionic liquid as catalytic solvent, Ranliao Huaxue Xuebao/Journal Fuel Chem. Technol. 37 (2009) 194–198.

[246] Z. Ren, L. Wei, Z. Zhou, F. Zhang, W. Liu, Extractive Desulfurization of Model Oil with Protic Ionic Liquids, Energy and Fuels. 32 (2018) 9172–9181.

[247] S.D. Labinov, J.R. Sand, An analytical method of predicting Lee-Kesler-Ploecker equation-of-state binary interaction coefficients, Int. J. Thermophys. 16 (1995) 1393–1411.

[248] C.H.J.T. Dietz, F. Gallucci, M.V.S. Annaland, C. Held, M.C. Kroon, 110th Anniversary: Distribution Coefficients of Furfural and 5-Hydroxymethylfurfural in Hydrophobic Deep Eutectic Solvent + Water Systems: Experiments and Perturbed-Chain Statistical Associating Fluid Theory Predictions, Ind. Eng. Chem. Res. 58 (2019) 4240–4247.

[249] A. Samarov, I. Prikhodko, N. Shner, G. Sadowski, C. Held, A. Toikka, Liquid − Liquid Equilibria for Separation of Alcohols from Esters Using Deep Eutectic Solvents Based on Choline Chloride: Experimental Study and Thermodynamic Modeling, (2019).

[250] S.E.E. Warrag, C. Pototzki, N.R. Rodriguez, M. Van Sint, M.C. Kroon, C. Held, G. Sadowski, C.J. Peters, Fluid Phase Equilibria Oil desulfurization using deep eutectic solvents as sustainable and economical extractants via liquid-liquid extraction : Experimental and PC-SAFT predictions, Fluid Phase Equilib. 467 (2018) 33–44.

[251] H. Renon, J.M. Prausnitz, Local compositions in thermodynamic excess functions for liquid mixtures, AIChE J. 14 (1968) 135–144.

Appendix-A: Sample calculation for Model diesel fuel preparation:

A.1. Calculation for model fuel preparation:

- Concentration of sulfur present in Dibenzothiophene(C_S) is given by

$$C_S = \frac{\text{molecular weight of sulfur}}{\text{molecular weight of thiophene}} * 100$$

Atomic weight of sulfur = 32

Molecular weight of Dibenzothiophene ($C_{12}H_8S$) = 184.26g/mol

Mass % of 'S'in Dibenzothiophene (DBT) molecule= [32.065/ (184.26)] ×100

=17.330%

Material balance:

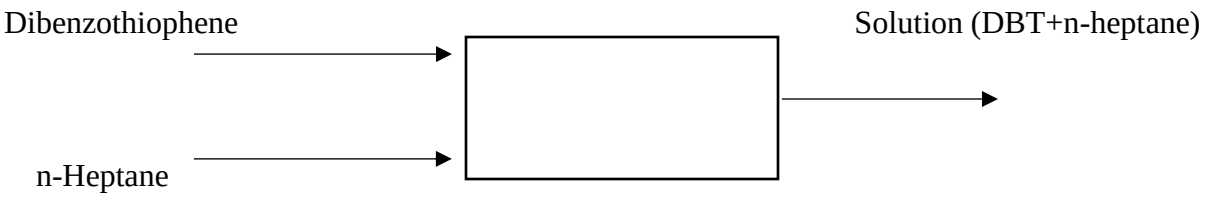

Solution=DBT+ n-Heptane

Concentration of Sulfur× DBT = Concentration Of sulfur× Solution

A.1.1 Model Diesel fuel (MDF) Preparation:

n-heptane + Dibenzothiophene (DBT) (250 ppm sulfur concentration

Amount of sulfur present in Dibenzothiophene is = 17.33%

Amount of sulfur in DBT= (17.33/100) ×10^6 = 17.33 ×10^4 ppmw (Parts per million weight)

By material balance:

Amount of DBT× (17.331×0^4) = Amount of solution× (250)

(Amount of DBT/Amount of solution) = [250/ (17.33×10^4)]

Mass Fraction Amount in ppmw

Procedure:

Amount of n-heptane taken = 100 ml

Density of n-heptane = 0.683 g/ml

Amount of n-heptane (g) = (100×0.683) = 68.3 g

Mass % of DBT= [250/ (17.33×10^4)]*100

=0.1442 mass%

0.1442= [x/ (68.3+x)] ×100

= (0.1442×68.3) + (0.1442x) =100x

9.84886 = (100-0.1442) x

9.84886 = 99.8558x

x = 0.098630 g

Amount of DBT should be added to make solution 250 ppm sulfur concentration in 100 ml n-heptane = 0.098630g

n-heptane = 100 ml Dibenzothiophene = 0.098630g

A. 1.2. Calibration Curve for DBT (Dibenzothiophene) and n-heptane: Four Samples were prepared for four different concentration of DBT in constant amount of n-heptane taking amount of DBT 10, 25, 50 and 75 mg in constant volume of 20 ml n-heptane for each sample are given in **Table.A.1.1.**Calculation sulfur concentration of given samples were done as same as **Section A. 1.1.**For each amount of Sulfur concentration, different ratio of area were

generated in GC-FID. The graph has been plotted between Areas (DBT/n-heptane) ratio and sulfur concentration (ppmw).

The X-axis is sulfur concentration in ppmw and Y-axis is the ratio of areas.Trendline was generated for the plot of sulfur concentration vs. of ratio of areas (Area of Sulfur compound/Area of n-heptane). Hence, further sulfur concentration were obtaining by calculation of x value from the trend-line equation.

Equation of Trend-line, y=7E-06x+0.0003

$$\text{Sulfur concentration (ppmw)} = \frac{[(\text{Area of Sulfur compound/Area of n-heptane})-(0.0003)]}{7E\text{-}06}$$

A typical chromatograph of GC-FID is showing the retention time of n-heptane and DBT as shown in the **Fig A. 1.1.** The calibration curve of DBT for different concentrations is shown in **Fig A. 1.2.**

Table A. 1.1 Sulfur concentrations for GC calibration

S.No.	Mass of DBT	Calculated Sulfur in ppmw
1.	0.01	126
2.	0.025	316
3.	0.050	632
4.	0.075	946

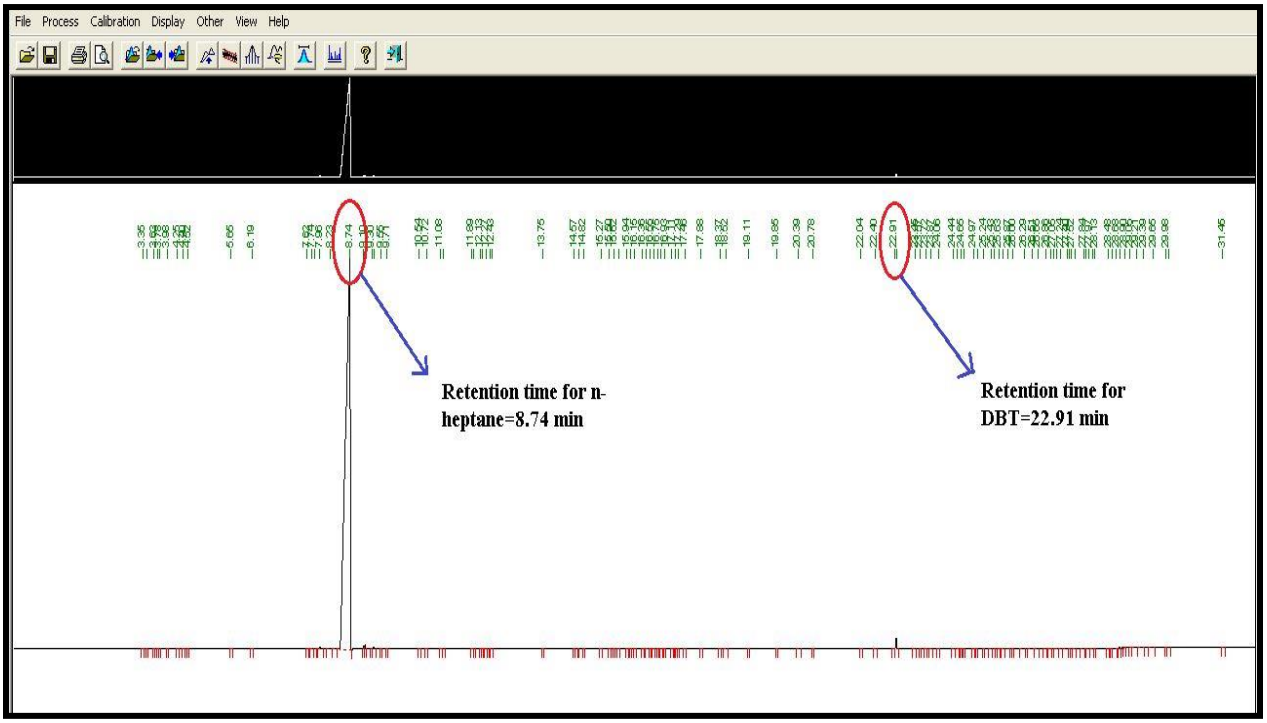

Fig. A. 1.1 Chromatogram of FID for (n-heptane+DBT)

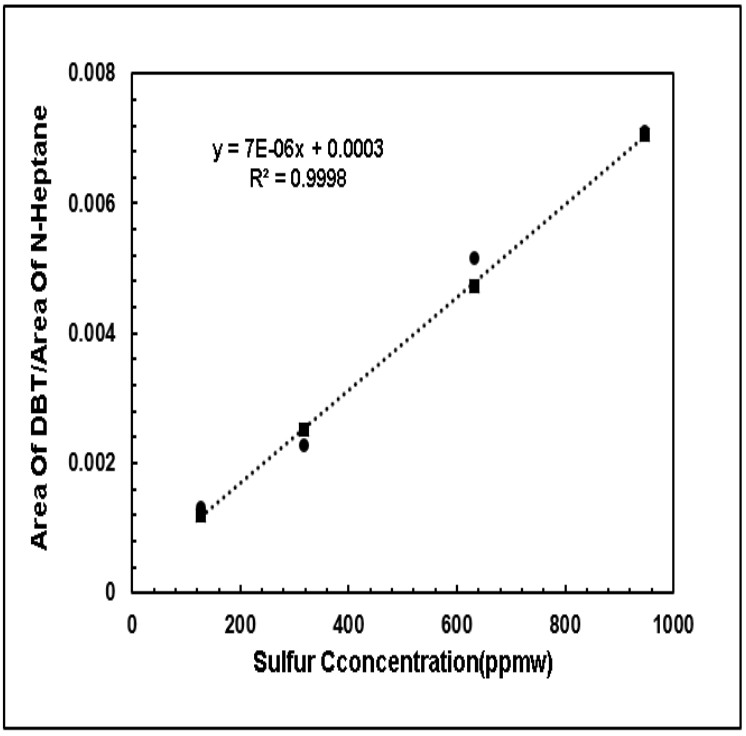

Fig. A. 1.2 Calibration curve for GC Analysis for Dibenzothiophene

Appendix-B: Supplementary information for Chapter 6

Table B.6.1 Comparison of melting point and viscosity of DESs and diethylene glycol.

	Viscosity(cP)	Melting Point (K)
DEG	21.756	261.80
DES1	38.8958	258.51
DES2	147.327	243.23
DES3	102.094	245.17

Table B.6.2 Standard Deviation Error Analysis of Experimental and Modelled.

	T	2MT	DBT
DES1	0.4134	0.2686	0.6555
DES2	0.9393	0.5584	0.8262
DES3	0.9740	1.1229	0.7734

Table B.6.3 Summary of extractive desulfurization.

DES	DES/Feed	S-compound	Sulfur in oil containing aromatics (wt%)× 10^{-3}
Chcl/DG	0.1	DBT	0.62
		2-MT	0.56
		T	0.49
	0.2	DBT	0.41
		2-MT	0.46
		T	0.47
	0.3	DBT	0.34
		2-MT	0.40
		T	0.45
	0.4	DBT	0.26
		2-MT	0.30
		T	0.44
	0.5	DBT	0.18
		2-MT	0.22
		T	0.42
TBAB/DG	0.1	DBT	0.24
		2-MT	0.28
		T	0.45
	0.2	DBT	0.20
		2-MT	0.22
		T	0.44
	0.3	DBT	0.18
		2-MT	0.18
		T	0.42
	0.4	DBT	0.14
		2-MT	0.15
		T	0.41
	0.5	DBT	0.14
		2-MT	0.14
		T	0.39
MTPPBr/DG	0.1	DBT	0.31
		2-MT	0.33
		T	0.48
	0.2	DBT	0.25
		2-MT	0.27
		T	0.44
	0.3	DBT	0.22
		2-MT	0.23
		T	0.43
	0.4	DBT	0.18
		2-MT	0.24
		T	0.41
	0.5	DBT	0.17
		2-MT	0.23
		T	0.40

Table B.6.4 Sulfur removal efficiencies of various extractants.

Extractants	**V_{extrac}/V_{feed}**	**Sulfur Removal (%)**	**Reference**
Diethylene Glycol(DEG)	1:3	19.3	[5]
[BMMOR][Br]/ DEG	1:3	21.00	[5]
ChCl/DG	1:3	88.24	This chapter
TBAB/DG	1:3	93.91	This chapter
MTPPhBr/DG	1:3	92.34	This chapter
TBAB/EG	1:4	16.08	[6]
MTPPBr/EG	1:4	21.42	[6]
TBAB/TrEG	1:4	20.67	[6]

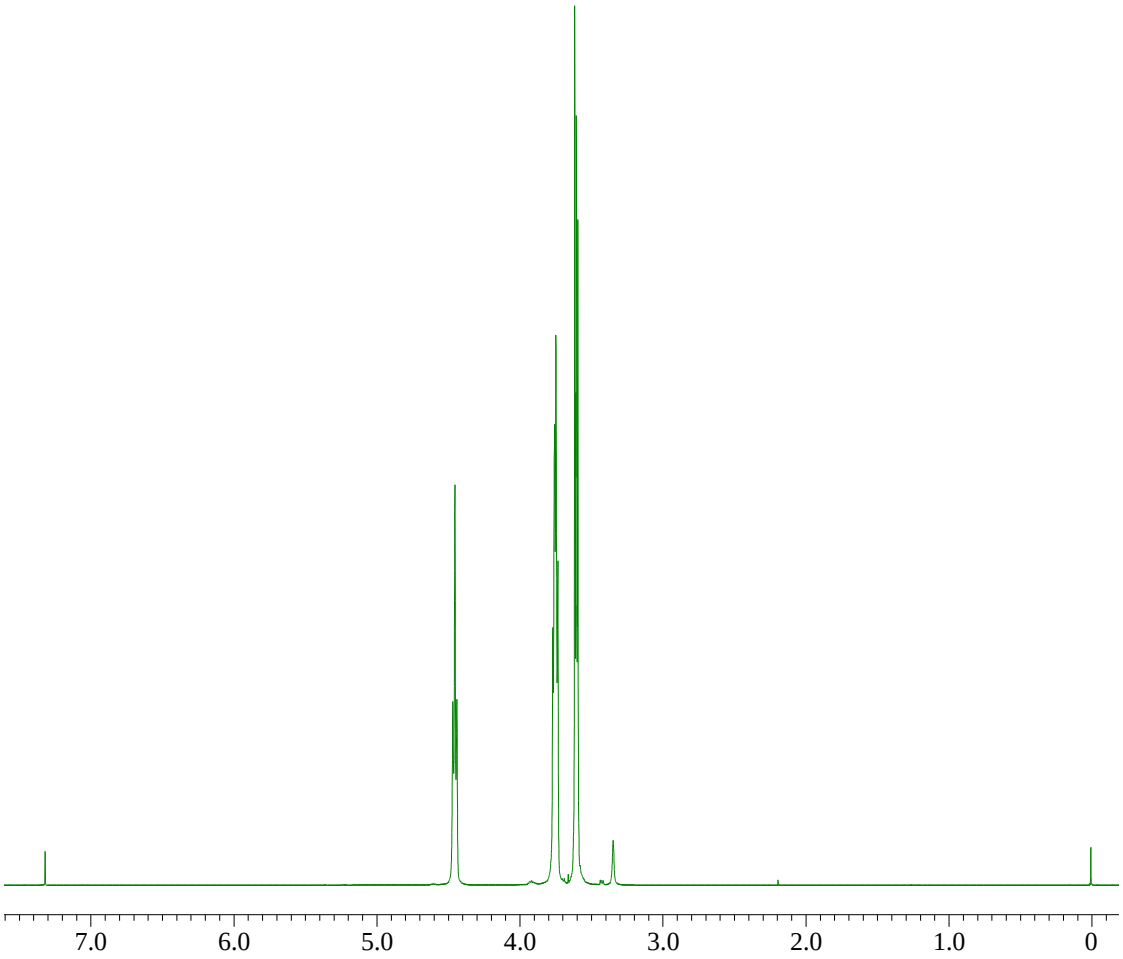

Figure B.6.1 HNMR Spectra of diethylene glycol

Figure B.6.2 HNMR Spectra of DES3

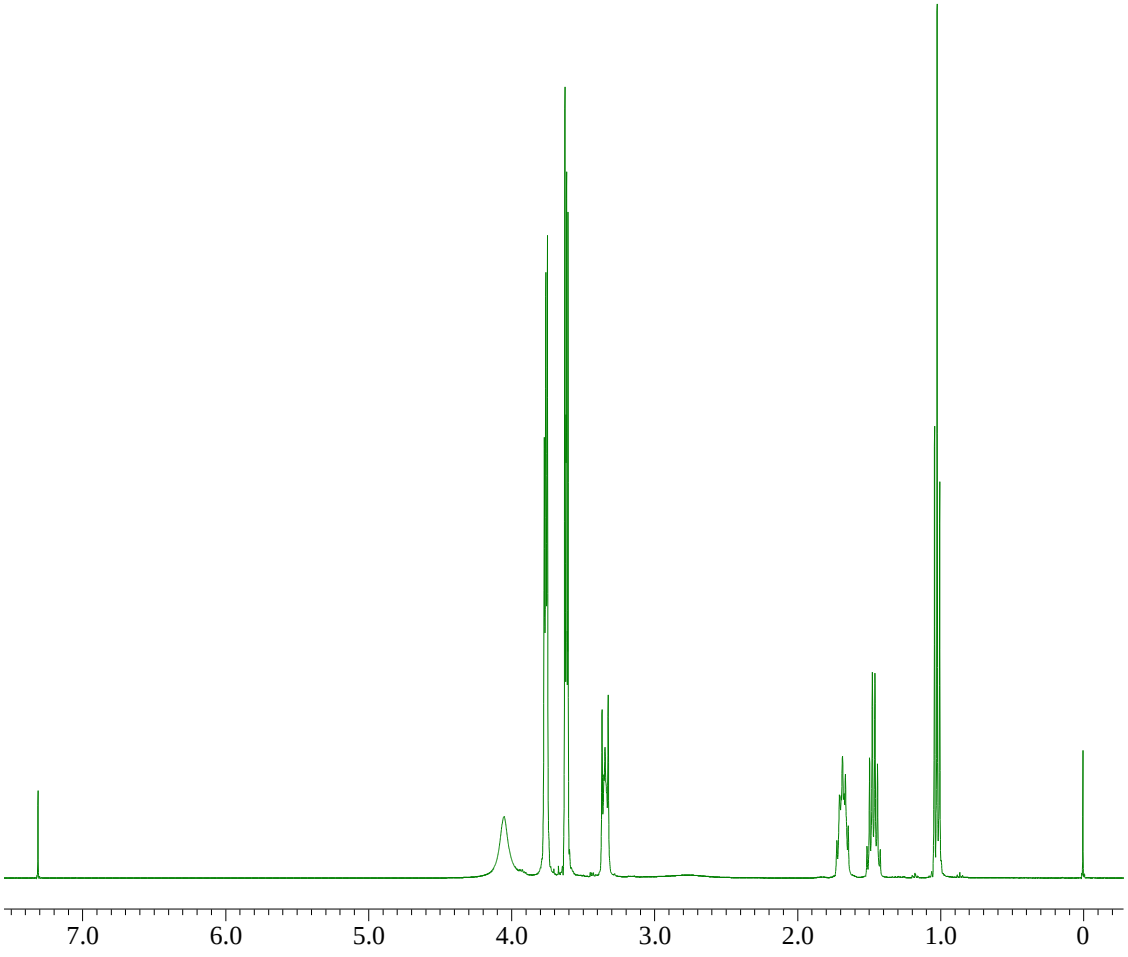

Figure B.6.3 HNMR Spectra of DES2

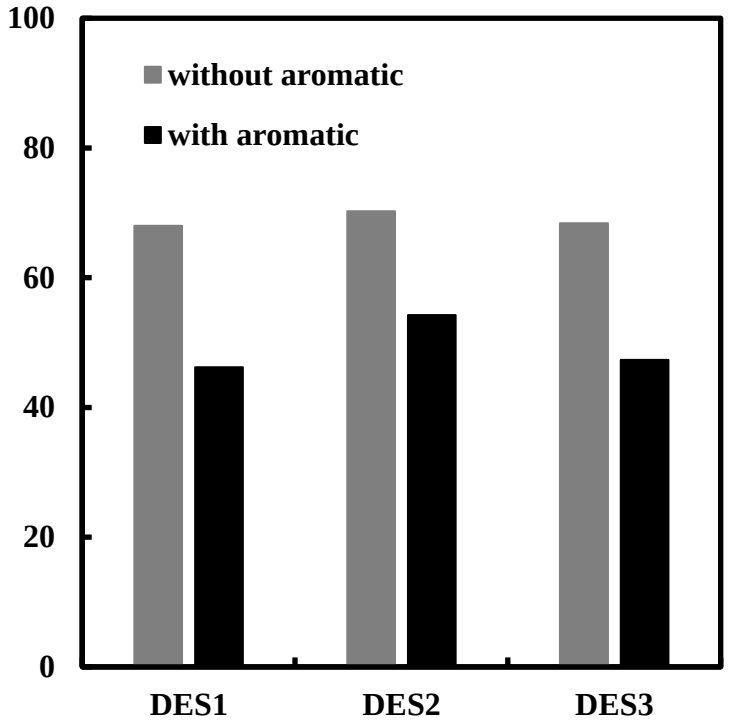

Figure B.6.4 Effect of aromatic addition on the thiophene removal using different DESs

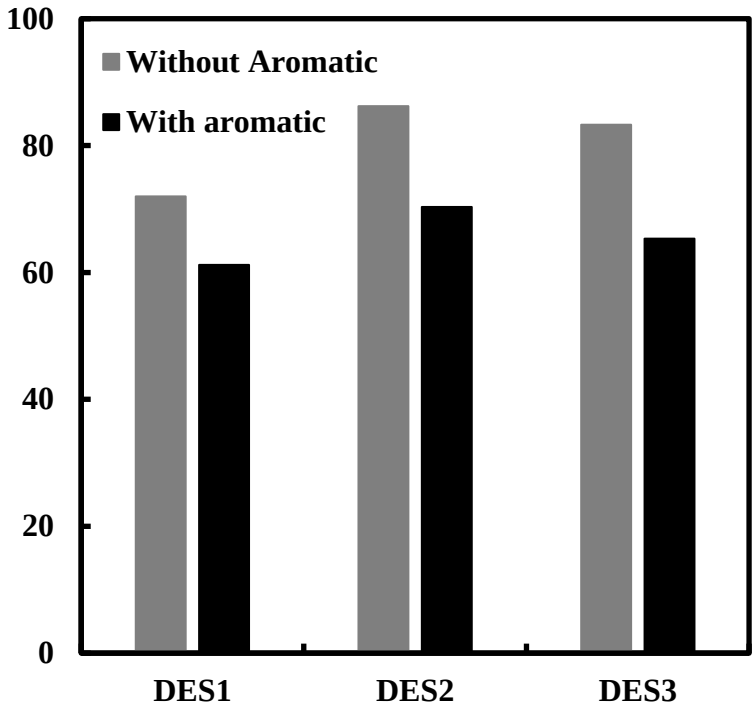

Figure B.6.5 Effect of aromatic addition on the 2-methylthiophene removal using different DESs

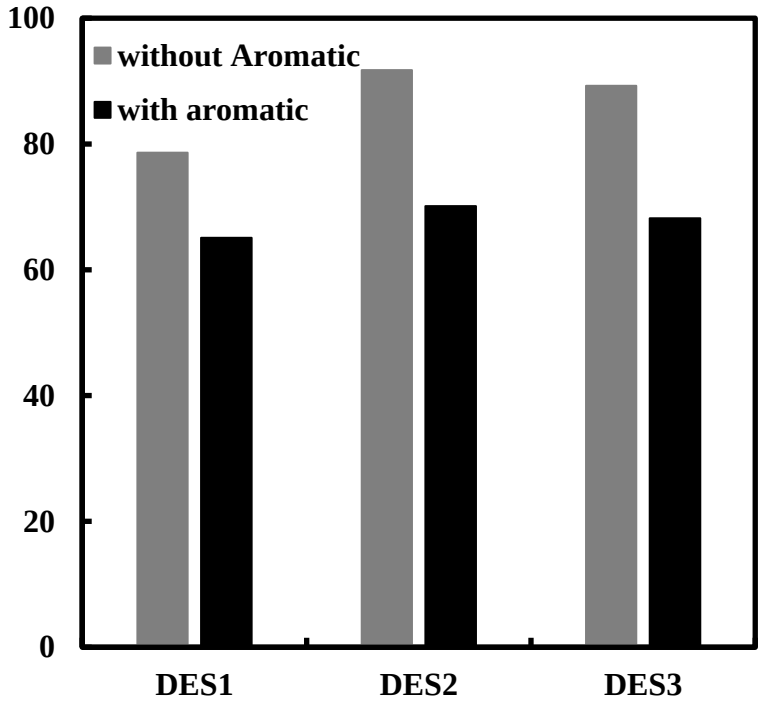

Figure B.6.6 Effect of aromatic addition on the Dibenzothiophene removal using different DESs

Research Publications

1.Mohd Belal Haider, Manas Dwivedi, **Divyam Jha**, Rakesh Kumar, M.S.Balathanigaimani, "Azeotropic Separation of Isopropanol-water using Natural Hydrophobic Deep Eutectic Solvents", *Journal of Environmental Chemical Engineering*, **2021.**9,1, 104786. **IF : 4.30**

2.Divyam Jha, Mohd Belal Haider, Rakesh Kumar, Balathanigaimani Marriyappan Sivagnanam, " Extractive Desulfurization of Fuels using Diglycol based Deep Eutectic Solvents", *Journal of Environmental Chemical Engineering*, **2020**. 8, 5, 104182. **IF: 4.30**

3.Divyam Jha, Mohd. Belal Haider, Rakesh Kumar, M.S. Balathanigaimani, "Recent Advancements in Extractive Desulfurization using Ionic Liquids & Deep Eutectic Solvents: A Short Review", *Fluid Phase Equilibria,* **2020.** (Submitted after revision). **IF : 2.83**

4.Divyam Jha, Mohd Belal Haider, Rakesh Kumar, Wang Geun Shim, Balathanigaimani Marriyappan Sivagnanam, "Batch and Continuous Adsorptive Desulfurization of Model Diesel Fuels Using Graphene Nanoplatelets". *Journal of Chemical & Engineering Data*, **2020**, 65, 4, 2120–2132**. IF:2.19**

5. Divyam Jha, Mohd Belal Haider, Rakesh Kumar, Narandalai Byamba-Ochir, Wang Geun Shim, Balathanigaimani Marriyappan Sivagnanam, and Hee Moon, "Enhanced Adsorptive

Desulfurization Using Mongolian Anthracite-Based Activated Carbon", *ACS Omega*, **2019**, 4, 20844−20853. **IF: 2.58**

6. Mohd Belal Haider, **Divyam Jha**, Rakesh Kumar, M.S Balathanigaimani, "Ternary Hydrophobic Deep Eutectic Solvents for CO_2 capture", *International Journal of Greenhouse Gas Control*, **2019**,102839. **IF: 3.63**

7. Divyam Jha, N.M. Mubarak, Mohd Belal Haider, M. S. Balathanigaimani, J.N.Sahu. "Adsorptive Removal of Dibenzothiophene from Model Diesel Fuel using Microwave synthesized Carbon Nanotube (M-CNT) and Carbon Nanofiber(M-CNF)",*Fuel*,**2019**,244,132-139. **IF: 5.57**

8. Mohd Belal Haider, **Divyam Jha**, M.S Balathanigaimani, Rakesh Kumar, "Modelling and simulation of CO_2 removal from shale gas using deep eutectic solvents", *Journal of Environmental Chemical Engineering*, **2019**, 102747. **IF: 4.30**

9. Mohd Belal Haider, **Divyam Jha**, M.S Balathanigaimani, Rakesh Kumar, "Thermodynamic and Kinetic Studies of CO_2 Capture by Glycol and Amine-Based Deep Eutectic Solvents, *Journal of Chemical Engineering Data*, **2018**,63, 2671-2680. **IF: 2.19**

10. M.S. Balathanigaimani, Mohd Belal Haider, **Divyam Jha**, Rakesh Kumar, Seung Jae Lee,Wang Geun Shim, Ho Kyong Shon, Sang Chai Kim, and Hee Moon, "Nanostructured Biomass Based Carbon Materials from Beer Lees for Hydrogen Storage", *Journal of Nanoscience and Nanotechnology*, **2018**,18, 2196-2199. **IF: 1.35**

11. Divyam Jha, Md. Belal Haider, Rakesh Kumar, M.S Balathanigaimani, "Extractive desulfurization of Dibenzothiophene using phosphonium-based ionic liquid: modelling of batch extraction experimental data and simulation of continuous extraction process using Aspen Plus", *Chemical Engineering Research &Design,* Volume 111, (**2016**) Pages 218–222. **IF: 3.35**

Conferences:

1. **Divyam Jha,** M.S. Balathanigaimani, "Adsorptive Desulfurization diesel fuel using microwave synthesized carbon nanomaterials","SEFCO-2019" 9–11 May 2019, ***CSIR-IIP,*** Dehradun.

2. **Divyam Jha**, M.S. Balathanigaimani, "Adsorptive removal of dibenzothiophene from diesel fuel using microwave synthesized carbon nanomaterials", 3rd Research Scholar's Day, 13th April 2019, ***RGIPT***, Jais, India.

3. **Divyam Jha**, Md. Belal Haider, Rakesh Kumar, M. S. Balathanigaimani, Extractive Removal of Dibenzothiophene from Model Diesel Fuel, International Conference on 'Energy Innovations - Today and Tomorrow' ,***HP Green R&D Center,Bengaluru.***14-15th October 2016.